QUANTUM PROJECT: MODELLING OF THE DREDGE AND DISPOSAL PROGRAMME

Final: 10th Oct 2009

Prepared for:
Sinclair Knight Merz

Document control form

Document draft	Originated by	Edit & review	Authorized for release by	Date
Draft 1 - for internal review Q1 and Q2	Jo Garcia-Webb Brett Wallace Murray Burling Scott Langtry	Scott Langtry	Scott Langtry	19/5/2009
Draft 2 - for internal review with Q3 details	Jo Garcia-Webb Brett Wallace Scott Langtry	Scott Langtry	Scott Langtry	27/5/2009
Draft 3 Issued for client review		Jo Garcia-Webb Brett Wallace Scott Langtry	Scott Langtry	24/6/2009
Draft 4 after external review		Brett Wallace Scott Langtry	Scott Langtry	12/8/2009
Draft 5		Brett Wallace	Scott Langtry	14/9/2009
Final		SKM Scott Langtry	Scott Langtry	8/10/2009

Document name: Quantum dredge and disposal modelling Final Report.

APASA Project Manager: Scott Langtry

DISCLAIMER:

This document contains confidential information that is intended only for use by the client and is not for public circulation, publication, nor any third party use without the approval of the client.

Readers should understand that modelling is predictive in nature and while this report is based on information from sources that Asia-Pacific ASA Pty Ltd. considers reliable, the accuracy and completeness of said information cannot be guaranteed. Therefore, Asia-Pacific ASA Pty Ltd., its directors, and employees accept no liability for the result of any action taken or not taken on the basis of the information given in this report, nor for any negligent misstatements, errors, and omissions. This report was compiled with consideration for the specified client's objectives, situation, and needs. Those acting upon such information without first consulting Asia-Pacific ASA Pty Ltd., do so entirely at their own risk.

Contents

Figures

Tables

EXECUTIVE SUMMARY

BHP Billiton Iron Ore is proposing to dredge new shipping channels and berths to access cargo loaded from Port Hedland. The shipping channels would access the wharf extending approximately 6 km from shore. Under this option, approximately 54 Million m^3 of surface sediment and bedrock would need to be removed and deposited to spoil grounds. It has been proposed that the dredging activities would be completed over a number of stages.

Quantum 1 ($\approx$22 Mm^3) – Berth and wharf pocket, eastern departure and swing basins, departure link channel

Quantum 2 ($\approx$25 Mm^3) – Western departure and swing basins, link and new departure channel

Quantum 3 ($\approx$7 Mm^3) – extensions to the berth and wharf pockets, expansion of departure and swing basins and widening of departure channel

Asia Pacific ASA (APASA) were commissioned to undertake numerical modelling of the operations based on a designated dredging plan, working method and timetable and with defined geotechnical specifications for the material to be moved.

Completion of the study required establishment and validation of detailed hydrodynamic and wave models for a region surrounding the proposed dredging and disposal areas. Analysis of measurements of circulation patterns affecting the area demonstrated there would be a net drift to the northeast at most times of the year in concert with a significant onshore-offshore tidal migration. A reversal of the net drift is indicated for a period during the winter months. This net drift is attributable to the synoptic wind patterns and the orientation of the coastline, The coastline parallels both the persistent westerly to south-westerly winds over the study area during summer and summer-winter transitional periods as well as the easterly winds that are prevalent during winter. Reversals of the residual current during winter were indicated to be weaker and of shorter durations in the observed current data. The hydrodynamic model established for the area faithfully reproduced both the shorter term tidal magnitudes and directions and the longer-term transport along the coast. Hence the sample current data generated for the study was considered suitably representative and accurate.

Similarly, the measured wave data indicate a dominant directional trend with 92% of waves originating from the northwest throughout the year, mostly as short wavelength wind-waves. The frequency of long-period swell waves that would exert significant mixing energy over the depths of water at the dredging and disposal areas is generally low, but these waves occur as periodic bursts lasting up to 5 days (although more frequently of shorter duration). The wave model established for the area showed faithful reproduction of the observed wave parameters across the full wave spectra and hence the sample wave data generated for the study was also considered suitably representative and accurate.

Collectively, the current and wave models are demonstrated to be fit for the purpose of representing ambient current and wave fields, as input to sediment fate modelling.

Relatively short period (30 day) simulations of disposal into alternative disposal areas indicated there would tend to be migration of a proportion of the finer components (clay and silt sized) outside the bounds of the disposal areas due initially to migration with the tide as

these particles tend to be jetted into the water column after the descending plume strikes the seabed. Fine sediments pushed into the water column will then undergo an extended sinking time. Finer components were also predicted to concentrate near the seabed and drift without depositing under the shear forces generated by local tidal currents. Ongoing resuspension and sedimentation was indicated over time, with sediments migrating with the net drift direction. Habitats up to 10-15 km to the northwest and southeast of the disposal grounds were predicted to receive elevated total suspended solids (TSS) and sedimentation as a result of these two related processes. A greater net drift was indicated for disposal into areas closer to shore than areas further offshore. Sediments also tended to migrate further inshore during the simulations for the most shoreward disposal sites, indicating a response to the onshore steering of tidal currents with approach to the land.

Simulations for the full dredging and disposal programme required information on the location and likely timing of the dredging and disposal activities; the type and production rates of the equipment that would be used, which will affect the sources of sediment suspension as well as their rates and durations. Information was also required on the expected particle-size distributions of the sediments that would be released. An indicative dredging and disposal plan was developed by BHP Billiton Iron Ore to inform the modelling specifications, based on a review of geotechnical information for the proposed dredging area and an assessment of dredger performance, capacities and likely work practices.

The indicative plan specified that dredging and placement of sediment for Quantum Stages 1 to 3 would be carried out using a large cutter-suction dredge (CSD) and large trailer-suction hopper dredge (TSHD). The dredging practice would involve dredging of unconsolidated sediment using the TSHD, which would overflow for part of each loading operation to maximise the sediment mass collected in each load. When the sediment load within the TSHD was maximised, the vessel would cease dredging and move to an offshore disposal where the sediment would be placed on the seabed through doors at the bottom of the hull. The CSD would fracture hard rock and discharge directly behind and onto the seabed for subsequent collection by a TSHD, using the operation described above. The indicative plan specified that disposal grounds would be positioned to the east and west of the dredging area. Under this plan, Quantum 1 and 2 would be dredged in sequence over 4 years. Quantum 3 would be delayed approximately 15 months after completing Quantum 2 and would take about 7 months to complete.

A sediment fate model (SSFATE) was configured to follow the specifications for the dredging activities as specified in the indicative dredging plan. This included specifications for the production rates, locations of operation, timing of operations and particle-size distributions for the sediments that are expected in the discharges. The model was applied to simulate the complete operation for all stages, hence the simulations spanned 5 years. Metocean conditions, inclusive of currents and waves, were represented by numerical modelling over a sample period of 10 years to capture variations at scales of hourly to inter-annual.

The sediment fate modelling estimated for both the shorter term processes of mixing, transport, sinking and deposition and the longer term processes of resuspension, dewatering and armouring that can affect the fate of finer sediments.

Measurement and modelling of the currents over the study area indicated that there is a strong onshore-offshore migration of the water column due to the tidal currents as well as a longshore drift that generates net migration to the east and north-east during late spring, summer and early autumn and a net migration west at other times. Measurements and modelling of the wave climate indicated that the area periodically receives long period (swell) waves that would penetrate to the seabed in the relatively shallow (5-15 m depth range) project area.

Based on the dredging plan, the dredging and disposal operations would release a proportion of relatively fine sediments (clay, silt and fine sand) that will be subject to the current and wave climate. The silt and clay size fractions are represented by the model as being susceptible to the prevailing levels of shear stress, with the result that plumes are expected to migrate and disperse as a benthic plume, undergoing cycles of settlement and resuspension due to the state of tide and the prevailing waves. The regular cycling of the tide (at a time scale of about 6 hours), in particular, was indicated to induce cycles of sedimentation and resuspension for a proportion of the finer sediments. While resuspended, the fine sediments are indicated to migrate, with a tendency to distribute near seabed. These migrations are predicted to be variable over seasonal and shorter time scales. A net migration to the east and northeast is indicated for the summer months while a net migration to the west is indicated for winter months. Flooding and ebbing tides are also predicted to spread the plumes in a generally onshore-offshore direction (southeast to northwest, respectively).

Heavier sediments and a proportion of the finer sediments are predicted to deposit around the dredging and disposal operations while finer sediments are predicted to deposit as thinner layers and for short durations over a wider area. Deposition rates were found to be subject to the tidal currents over regular cycles as well as the prevailing waves, with a more irregular frequency.

Sinclair Knight Merz (SKM) developed estimates of the temporal and spatial variability in natural TSS concentrations and sedimentation rates based on field measurements over time. TSS estimated from turbidity measurements at 1 m above bottom was compared to the reduction of light intensity within the zone 1-2 m above bottom. Estimates of the TSS concentrations required to suppress light levels to 25% and 50% of ambient light penetration were derived by SKM and used to derive TSS thresholds that would trigger these levels of light suppression. These triggers were supplied to APASA for comparison of the modelled estimates of TSS for dredge generated (i.e. above-background) concentrations. The thresholds were varied for different depth zones due to observed differences in the light levels, turbidity patterns and sedimentation that would affect benthic primary producers in each zone.

Based on defined thresholds, the modelled predictions for TSS concentrations indicated variable zones of potential influence and impact. These areas were predicted to vary seasonally and among stages of the operation. Hence the same areas were not always expected to experience light attenuation above the threshold levels for the threshold durations throughout the programme. The zone of potential influence was predicted to generally extend to the northeast of the operation, following the bathymetric contours of the inner shelf, during the 'dry' season (June to November). During the 'wet' season (December

to May), the zone of influence extended to the west of the operation. There was a central area around the operation where the seasonal zones of influence overlapped.

The zone of potential impact from TSS generated turbidity was reduced to a smaller and patchier area immediately around the dredging and disposal areas as well as isolated patches along the inshore margin where the coastal morphology acts as a trapping zone for fine sediments. Note that these zones are calculated from the estimates of turbidity and must be compared with the distribution of sensitive habitats and biota to judge the potential impact on these habitats.

The distributions for the zone of potential influence extended beyond the distance over which sediments are predicted to initially sink to the seabed given the expected PSD and water depths, indicating a strong influence of delayed deposition and ongoing resuspension of fine sediments, due to excessive turbulence generated by tidal currents and waves. Due to the extended duration of the operations that were simulated, these fine sediments are predicted to move over time to affect turbidity levels over a larger area. Simulations assumed that fine sediments generated from dredging would have relatively low cohesivity and, thus, are considered to be conservative in these predictions.

In contrast to TSS, thresholds developed for sediment deposition indicated that the predicted sediment loads would tend to exceed levels indicative of more extreme (95th percentile) natural sedimentation rates over more restricted areas arranged along the tidal axis around the sites of dredging and disposal. Beyond these areas, the deposition of finer sediments is not predicted to exceed these sedimentation thresholds.

The study area is indicated to be dispersive. Hence, fine sediments will tend to migrate alongshore and disperse to decreasing concentration over time rather than remain trapped. Simulations of the fate of sediments after completion of dredging and disposal operations indicated a reduction in TSS concentrations over time around the disposal and dredging areas, due to ongoing longshore dispersal of fine sediments to the northeast, in combination with a reduction of the resuspension rate of fine sediments from the bed. The reduction in the resuspension rate over time is attributed to the reduction in the supply of fine sediments in the surface layers of the deposited sediments. Burial and cementing processes are also likely to further reduce rates of resuspension of fine sediments from these deposits. A caveat on this suggestion is that the disposal areas are positioned in water depths shallow enough for storm swells to penetrate to the seabed. Hence, during the passage of storms, the heavier grain sizes will tend to be re-organised, exposing trapped fines to resuspension. Hence, resuspension of fines is likely to occur during the passage of storms. Such processes could occur for some time (multiple years).

1   INTRODUCTION

BHP Billiton Iron Ore proposes to expand their iron ore operations with a major upgrade known as Project Quantum. As part of the project, a new outer port, known as the Port Hedland Outer Harbour Development, will be developed on the coast near Port Hedland in the Pilbara region of Western Australia (Figure 1-1).

The Outer Harbour Development would involve dredging of a shipping berth, multiple turning circles surrounding the shipping berth, an entry/departure channel linking to the existing channel, a new departure channel bypassing the existing shipping channel and construction of a wharf and jetty. Based on an indicative dredging plan developed for the work, approximately 54 million cubic metres of sediment would be extracted and placed within two marine disposal areas.

Most of the sediment is expected to be dredged by a trailer suction hopper dredge (TSHD), which will transport collected sediment and place them into two defined disposal areas. A smaller proportion will be dredged by a cutter suction dredge (CSD), which would pump sediments directly back to the seabed from a submerged location at the rear of the dredger. The TSHD would then be used to collect the material cut by the CSD from within the dredging footprint.

The dredging programme is currently planned to be split into three stages (Quantum 1, 2 and 3), with the first two stages, each spanning approximately 2 years, occurring in sequence with no break between completion of Quantum 1 and commencement of Quantum 2. The third stage, Quantum 3, is expected to take approximately 7 months and would commence about 15 months after the completion of Quantum 2. Details of each stage are as follows:

Quantum 1: This includes dredging a wharf area and berth pockets, arrival and departure basins to the east of the pockets, and a 3.4 km entry/departure channel to link to the existing channel. The volume of material to be dredged and placed during this stage is ≈22 million cubic metres (refer to the red and green shaded areas in Figure 1-1).

Quantum 2: This involves dredging arrival and departure basins to the west of the berth pocket, a 9.2 km departure link channel and a new departure channel. The new departure channel will have a length of 34 km, however dredging is only required for a total length of 18 km at various sections along the channel. The volume dredged and placed during this stage is estimated as 25 million cubic metres (refer to the blue shaded areas in Figure 1-1).

Quantum 3: Additional wharf area and berth pockets will be dredged, along with arrival and departure basins to both the east and west of the new wharf area and berth pockets. The link channel will also be widened. Approximately 7 million cubic metres of material will be dredged and placed during this stage (refer to the yellow shaded areas in Figure 1-1).

Sinclair Knight Merz (SKM) are carrying out environmental impact studies and providing support to BHP Billiton Iron Ore to facilitate the environmental approvals process for the Quantum project. As part of this, Asia-Pacific Applied Science Associates (APASA) were commissioned to carry out modelling tasks that aim to quantify the magnitude, intensity, spatial distribution and duration of effects of the proposed dredging program, in terms of suspended sediment concentration and sedimentation rates.

This report is a summary of modelling methods and results based on the indicative dredging plan developed by BHP Billiton Iron Ore, which was based on an analysis of geotechnical data for the dredging area and expectations of the most effective dredging equipment and dredging methods.
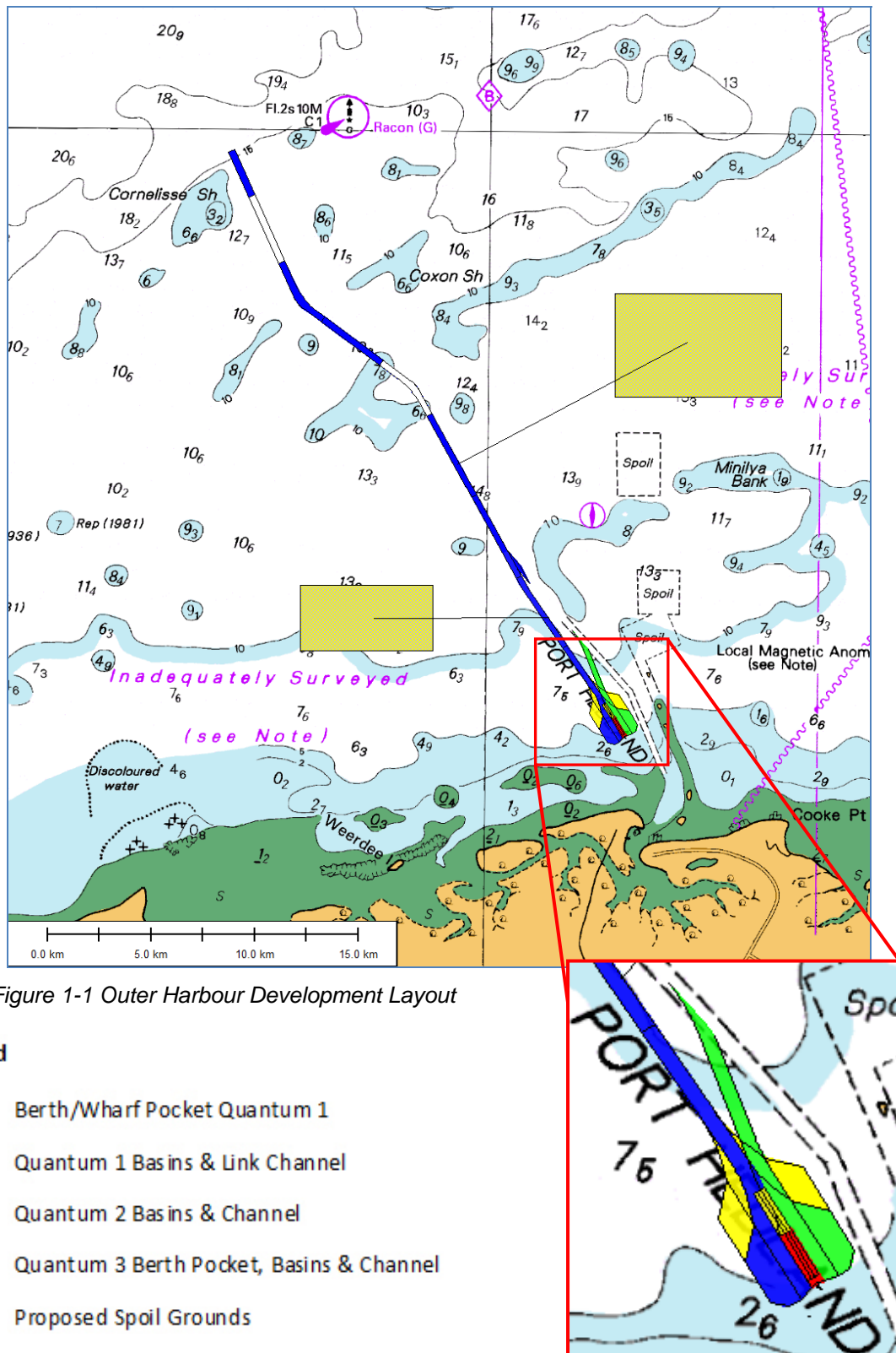
Figure 1-1 Outer Harbour Development Layout

Legend

■ Berth/Wharf Pocket Quantum 1

■ Quantum 1 Basins & Link Channel

■ Quantum 2 Basins & Channel

■ Quantum 3 Berth Pocket, Basins & Channel

▨ Proposed Spoil Grounds

2   SCOPE OF WORK

The following scope of work was undertaken, with the objective of estimating as accurately as possible, the likely outcomes of the proposed dredging and disposal programme, in terms of the distribution and concentration of the resulting sediment suspensions and sedimentation and, therefore, the potential for influence of or impact upon benthic primary producers and other components of the local habitat.

- Sourcing, analysing and selecting suitable wind and wave data for the hydrodynamic and wave models, respectively, to ensure that the data was representative of the central tendency and trends for the site. This effort concentrated on validating long term archives of wind and wave data that were available from modelled and measured sources against locally measured data. The data was also analysed for seasonal and interannual variations in wind and wave data in response to positive and negative Southern Oscillation Indices (SOI) – representing La Niña and El Niño years, respectively. The SOI represents the differential in surface air pressure between the eastern and western side of the Pacific Ocean, with effects upon the strength of the Pacific trade winds and sea temperatures.

- Sourcing tidal constituent data from authoritative global databases.

- Hydrodynamic and wave modelling

    o Set up of a high-resolution nested grid for the model domain, consistent for both the hydrodynamic and wave models. This grid encompassed the extensive intertidal foreshore and extended into the Port Hedland estuary.

    o Incorporating high-resolution Light Detection and Ranging (LIDAR) bathymetry and other bathymetric data to define the three-dimensional shape of the model domain.

    o Simulation of current and wave patterns for periods covering third-party measurements at the study site and validation by comparison to the measured data.

    o Production of a model hindcast of current and wave data, spanning 10 years, to allow for the inter-annual variation in the SOI.

    o Analysis of the hindcast to determine effects of the SOI, and hence selection of an appropriately representative span of coverage of the duration necessary for modelling of the full dredging and disposal programme (6 years).

- Sediment fate modelling to determine the likely outcomes of the proposed dredging programme in terms of the distributions of suspended sediments and sedimentation

    o Simulate all operations for all 3 stages of the proposed dredge programme using wave and hydrodynamic model output data that spanned both El Niño and La Niña years.

- o Calculation of cumulative suspended sediment concentrations (TSS) and sedimentation values due to all overlapping operations.

- o Generation of contour maps of TSS based on calculations of the median and more extreme concentrations (80th percentile) over bi-monthly stages of the operation.

- o Generation of contour maps of sedimentation based on calculations of the net sedimentation at bi-monthly stages of the operation.

- Post processing of the predicted concentrations for TSS and sedimentation to determine the likely size of effect of the proposed dredging programme, using exceedance of intensity, duration and frequency thresholds developed by SKM. The thresholds are calculated from temporal measurements at monitoring sites surrounding the dredging and disposal sites.

3   STUDY DATUM

Water depths and levels presented in this report are with respect to Mean Sea Level (MSL) unless otherwise stated and are in units of metres. Positions are satellite derived from the Global Positioning System using the GDA94 datum (MGA94 zone 50), unless stated otherwise. Position units are in latitude/longitude in decimal degrees. All units are in standard SI units.

4   MODELLING STRATEGY

The study has been undertaken to quantify the movement of suspended sediment generated by dredging during construction of the proposed Outer Harbour Development. The study involves using Lagrangian particle tracking models to track the fate of the sediment using forcing conditions specified by a wave model and three-dimensional, numerical, hydrodynamic model. The models enable the sediment dispersal patterns to be calculated under a range of forcing conditions, and for different construction scenarios.

The domain of the study needed to be sufficient to encompass the total area affected by the sediment plumes arising from the proposed dredging and disposal operations, to a distance where the concentrations might be significant. The total area affected not only included the initial extent of the sediment plume and deposition, but areas affected following the reworking of sediments, which occurs through resuspension and subsequent transport.

The domain of the study also needed to be large enough to properly capture the forcing effects of all relevant sediment transport mechanisms over the study area. In particular, the effect of wind energy transfer to the sea surface over long fetches, of the order of 10's km, was important for both wave and current generation.

The sediment transport model needed to account for the particle-size specific sinking, sedimentation and resuspension of sediments given the range of current and wave conditions indicated for the area, as derived by the hydrodynamic and wave models. This model also needed to account for the effects of sediment cohesion (i.e. clumping) on sinking rates of fine

particles and the effects of sedimentation history, burial and armouring on resuspension rates. The sediment model also needed to represent cumulative effects of multiple sources of suspended sediment over and beyond the duration of the full dredging and disposal programme, spanning longer than 5 years, in order to quantify the time-history of effects and the full footprint of the operation.

All of these requirements have been considered in developing optimal models for this study.

5   METOCEAN CHARACTERISTICS OF THE SITE

5.1   General Oceanography

The regional oceanographic system is tidally-dominated in the near shore waters, due to the large tidal range. The tidal range at Port Hedland is up to 7.5 m and the tide pattern is semi-diurnal (two tides per day). These drive oscillating tidal currents around 1 m/s, which can increase in the entrances of the numerous tidal creeks that have formed along the coastline. The tidal currents are typically aligned northwest-southeast but are steered in the shallows by local bathymetric contours. The ebb jets and flood sink flows related to the tidal creeks locally modify conditions near the entrances. Substantial areas of drying mudflats occur along the coastline, and the bathymetry is typically flat and shallow (e.g.) many kilometres from the shore.

The wind is the secondary forcing mechanism for local currents, and typically drives persistent, residual flows along the coastline. A slight dominance in the strength and persistence of W-NW winds during the spring and summer months typically results in a long term drift towards the east and north east, following the coastline. Weaker and less persistent current reversals occur during times of northerly and easterly winds during autumn and winter (UKHO, 2005).

Large scale currents, such as the Leeuwin Current, have little impact in the near shore region, being typically stronger and more coherent south of 22.5°S latitude (Godfrey and Ridgeway, 1985) and centred on the continental shelf (approximately 200 m isobath). This has important implications to the issue of interannual variability, as large scale currents are known to be strongly correlated to El Niño Southern Oscillation (ENSO) events.

Each of the important meteorological and oceanographic factors is discussed in further detail below.

5.2   Tides

Tides at Port Hedland are semi-diurnal (two highs and two lows per day) and macro-tidal with a mean spring tidal range of 5.5 m (ANTT, 2008). The tidal plane information is given in Table 5-1.

Table 5-1 Tidal planes at Port Hedland (after ANTT, 2008)

Tidal Plane	Elevation Above Datum (m)
HAT (Highest Astronomical Tide)	7.5
MHWS (Mean High Water Springs)	6.7
MHWN (Mean High Water Neaps)	4.6
MSL (Mean Sea Level)	3.9
MLWN (Mean Low Water Neaps)	3.3
MLWS (Mean Low Water Springs)	1.2
LAT (Lowest Astronomical Tide)	0.0

A typical tidal elevation time-series is shown in Figure 5-1. Note the transition from spring to neaps to springs again occurring at intervals of 14.5 days, approximately half the length of the lunar (synodic) cycle.
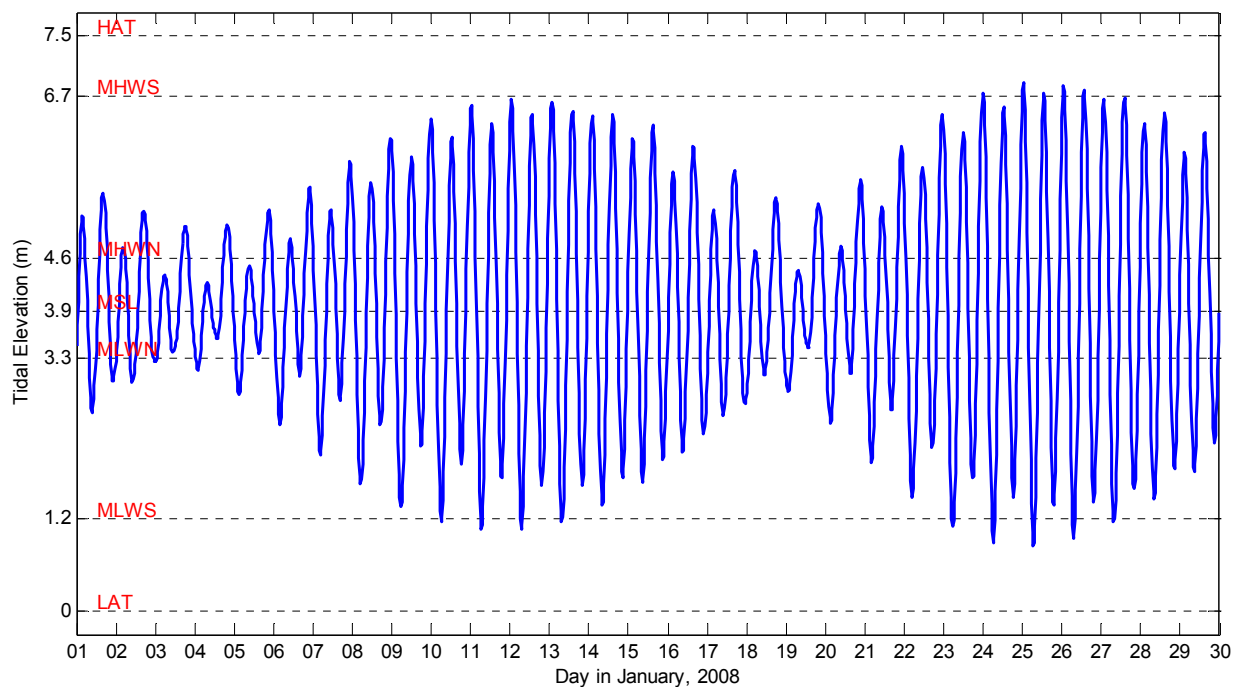
Figure 5-1 Typical tidal elevation time-series at Port Hedland. Period shown is 1 January 2008 to 30 January 2008 and elevation is shown as metres above datum, which is Lowest Astronomical Tide (LAT).

5.3   Wind

The climate of this region is monsoonal and seasonally controlled by the position of large high pressure cells, which pass from west to east across the Australian continent. These pressure systems result in summer prevailing winds from the north-west and south-west, swinging to cooler winter south-easterlies. The characteristics of these large high pressure cells are known to be affected by El Niño Southern Oscillation cycles.

Wind patterns are at their weakest and most variable during the transition periods between summer and winter around March and October. The transition period characteristics are due to the development of a low pressure system over central parts of the Australian continent. The area is also prone to tropical cyclones, mostly during the wet season. Under extreme cyclone conditions winds can reach 220 km/h. This region is impacted by El Niño Southern Oscillation cycles, resulting in a lower incidence of cyclones, as they form further east from where they ordinarily do, under non-El Niño (La Niña) conditions.

Figure 5-2 is a wind rose that shows the proportional occurrence of wind speed and direction around the compass, as the direction the wind is from. A joint frequency table of wind speed and directional occurrence from Bureau of Meteorology (BOM) data for Port Hedland Airport from 1995 to 2007 is included. Figure 5-3 shows seasonal wind roses from the full data set.

Port Hedland - 1995-2007
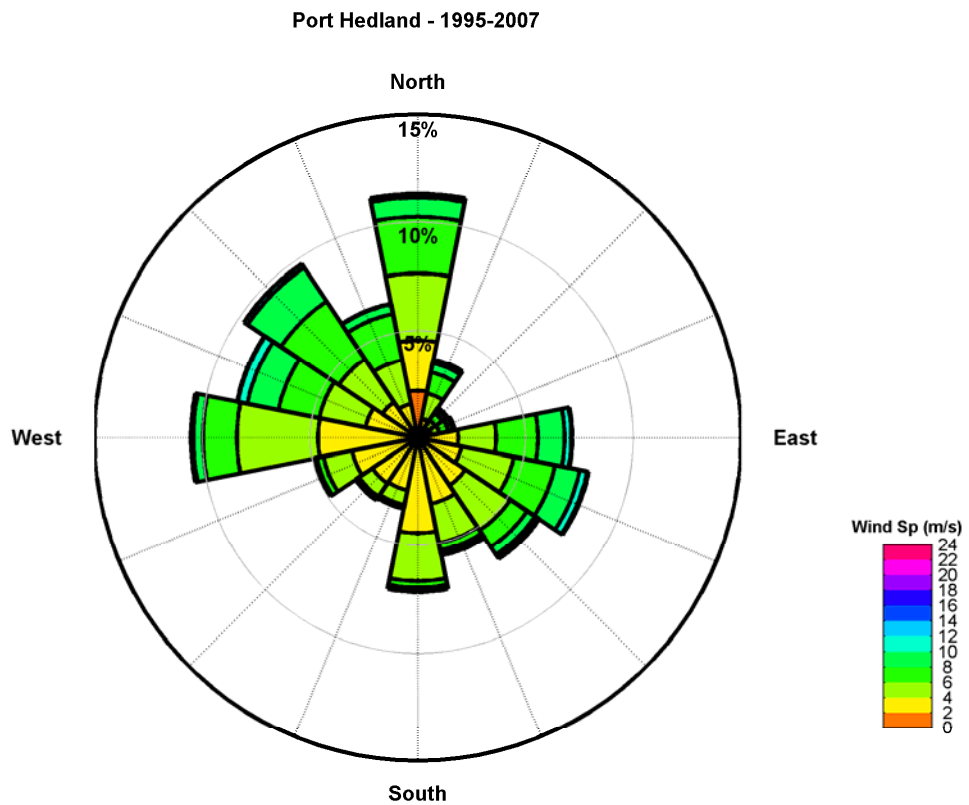
N=227022	N	NNE	NE	ENE	E	ESE	SE	SSE	S	SSW	SW	WSW	W	WNW	NW	NNW	Total	Cumul.
0–2	2.18	0.09	0.08	0.11	0.23	0.22	0.23	0.26	0.43	0.31	0.30	0.32	0.42	0.25	0.20	0.17	5.77	5.77
2–4	2.36	0.80	0.47	0.51	1.64	1.85	2.41	2.84	3.98	2.15	2.22	2.77	4.20	2.21	1.78	1.42	33.62	39.40
4–6	3.09	1.20	0.41	0.39	1.76	2.47	2.52	1.88	2.25	0.70	0.74	1.36	3.76	2.19	2.43	2.09	29.21	68.61
6–8	2.60	1.00	0.40	0.42	1.94	1.95	0.94	0.35	0.30	0.12	0.15	0.31	1.57	1.94	3.23	2.20	19.41	88.02
8–10	0.89	0.44	0.20	0.21	1.24	1.17	0.44	0.14	0.11	0.03	0.04	0.08	0.45	1.47	1.86	0.45	9.23	97.25
10–12	0.15	0.12	0.07	0.07	0.31	0.35	0.16	0.06	0.06	0.01	0.01	0.01	0.10	0.45	0.19	0.03	2.18	99.43
12–14	0.01	0.02	0.02	0.02	0.03	0.05	0.04	0.02	0.02	*	*	*	0.01	0.03	0.01	*	0.31	99.74
14–16	0.01	0.02	*	*	*	0.02	0.02	0.01	0.01	*	*	*	*	*	*	*	0.14	99.89
16–18	*	*	*	*	*	*	*	*	*	*	–	*	*	*	–	*	0.05	99.94
18–20	*	*	*	*	*	*	*	*	*	*	–	–	*	*	*	*	0.03	99.97
20–22	*	*	*	*	*	*	*	*	–	–	–	–	*	–	–	*	0.01	99.98
22–24	*	*	*	–	–	*	*	*	–	–	–	–	*	–	–	*	0.02	100.00
Total	11.29	3.71	1.67	1.75	7.16	8.08	6.77	5.59	7.17	3.34	3.47	4.86	10.52	8.55	9.69	6.36		
Cumul.	11.29	15.01	16.67	18.43	25.59	33.67	40.45	46.03	53.20	56.54	60.01	64.88	75.39	83.94	93.64	100.00		

* denotes values less than 0.01%   – denotes no records in bin

Figure 5-2   Wind rose (TOP) and Joint Frequency Table (BOTTOM) for wind data obtained from Bureau of Meteorology for Port Hedland Airport. Data has been converted to speeds in m/s at an elevation of 10m.The data period is 1 January 1995 to 31 December 2007, inclusive.
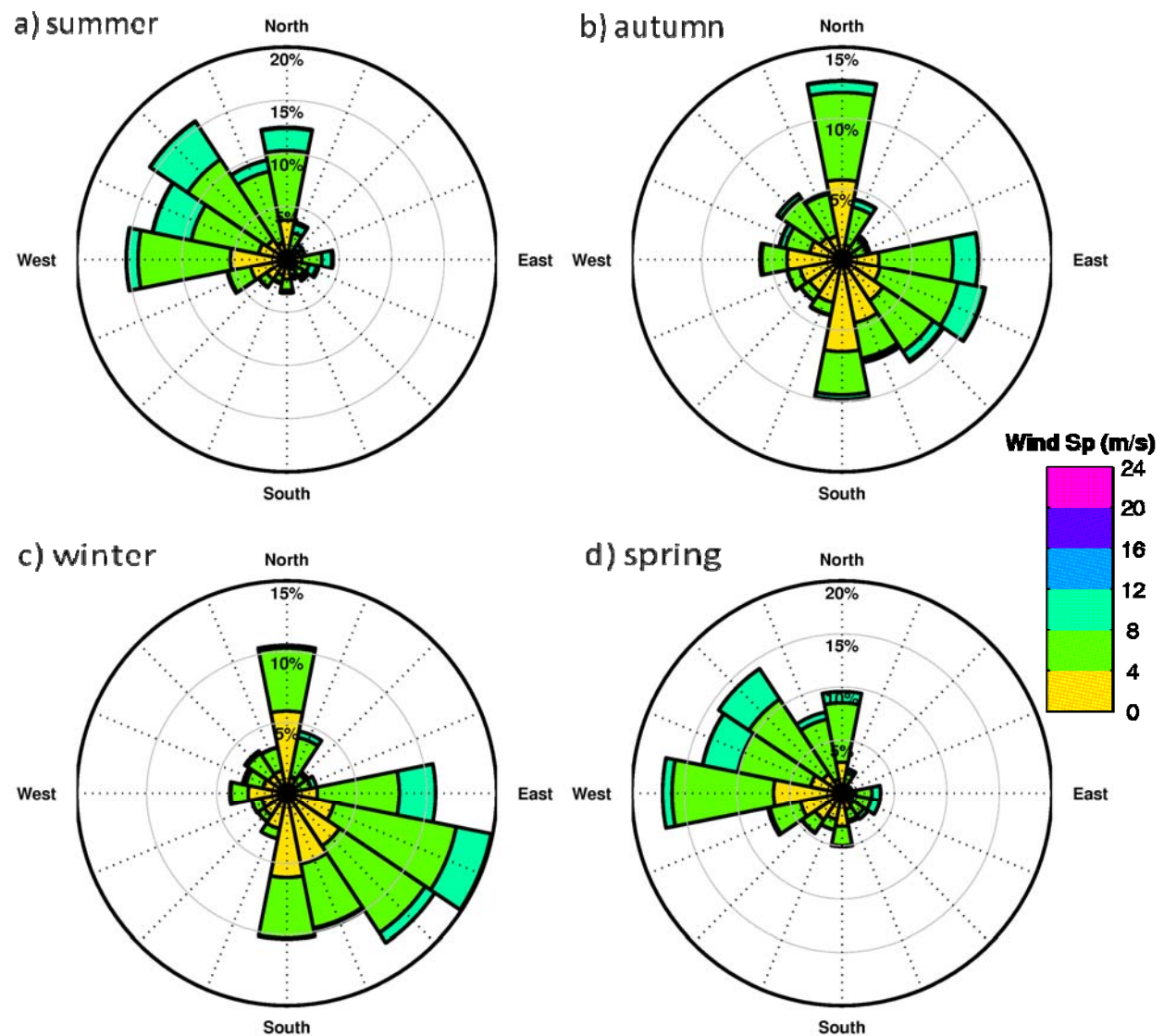
Figure 5-3 Seasonal wind roses derived from BOM data at Port Hedland Airport.

The data shows that there is a clear seasonal cycling in the wind fields, consistent with the monsoonal climate. In the warmer summer and spring months, the winds are consistently from the west to north quadrant (typically NW), while in the cooler months winds tend to be east to southerly (typically SE). The winds are important in driving mean or residual drift along the coastline near Port Hedland.

Median wind speeds are around 5 m/s and do not vary greatly from year to year (discussed further below with regard to an interannual analysis), but do vary seasonally, usually being greatest during the summer months (see Figure 5-4). The highest wind speeds occur during tropical cyclone events, which typically occur during November to March. Extreme winds are also associated with occasional winter storms.
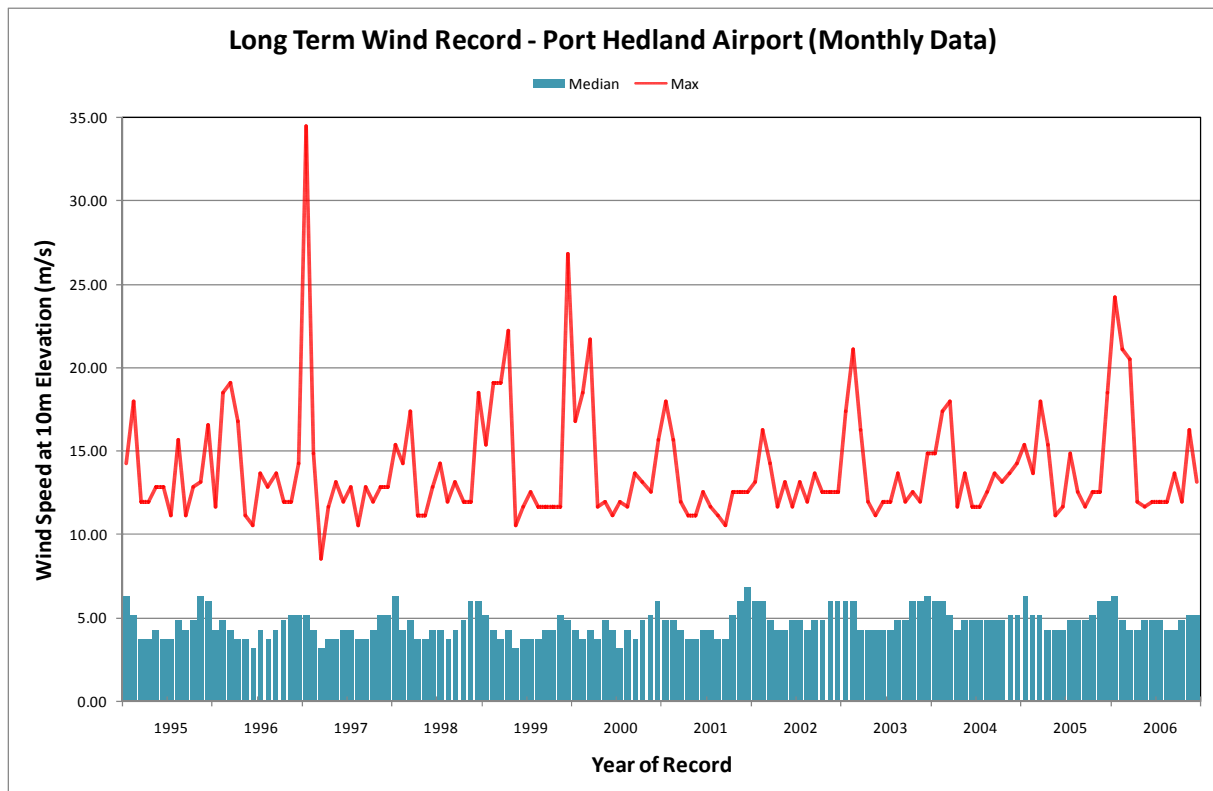
Figure 5-4 Monthly wind speed statistics for 1995-2006 at Port Hedland Airport. Monthly median shown by the blue bars, monthly maximum by the red line. Note the high maximums during the cyclone seasons (end of year, start of next year) and the relatively larger medians also during these months.

Extreme winds are generated by Tropical Cyclones that form in warm waters to the north of Western Australia. Cyclones have affected Port Hedland on average about once every two years, with seven severe (Category 3 or greater) cyclones recorded since 1910 (BOM, 2008). Wind gusts during these extreme events can exceed 170 km/h, with the highest recorded gust being more than 200 km/h during TC Joan in 1975 (Figure 5-5).

Cyclones may affect the sediment dispersion in two ways during this project:

- The onset of a cyclone will cause a cessation in dredging, thereby reducing the persistence of the dredge induced sediment plume.

- The large currents and possibly extreme waves may act to resuspend previously settled material, subsequently dispersing it over a larger region.

- Subsequent land flooding is likely to lead to a large scale sediment plume in the nearshore waters carried from onshore.

Based on the frequency of past cyclone activity, there is a probability of around 70% that a cyclone would affect the operational area during the 56 month dredging period. While dredging operations would be ceased prior to the approach of a cyclone, the extreme waves and currents set up by a cyclone would affect resuspension of dredged sediment deposits

and natural sediments alike. Cyclones have been observed to generate extreme levels of turbidity over the region due to suspension of seabed sediments and from terrestrial run-off. The duration of this influence is relatively short (multiple days to a few weeks). The sample current, wind and wave data used in the modelling were not filtered for cyclones and thus intense storm events have been included in the forcing data for resuspension of the dredged sediments, at the observed natural frequency of cyclone effects during the 10-year hind-cast sample period.
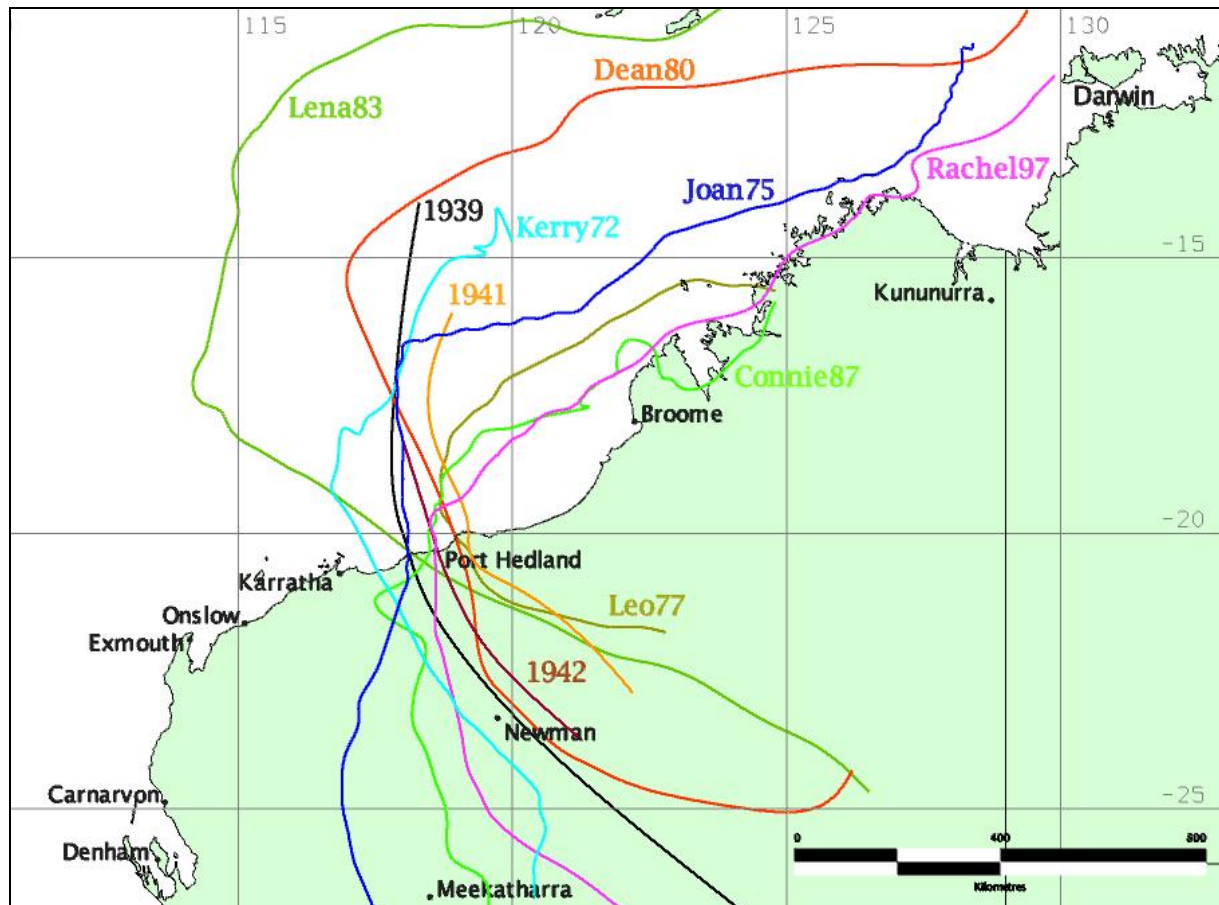
Figure 5-5 Tropical Cyclone tracks affecting Port Hedland – only notable events shown (source: BOM, 2008).

5.4 Currents

In terms of speeds, currents in the vicinity of Port Hedland are dominated by the tide. Tidal diamonds on the navigation charts show mid-tide currents (when currents are typically strongest) greater than 2 knots (approximately 1 m/s). A strong ebb tidal jet is expected from the harbour entrance due to the release of the large stored volume of water via the constricted opening.

Measured current data at three sites (see Table 5-2 and Figure 5-6) was made available by third parties for use in this study. All measurements were conducted using a Nortek AWAC Acoustic Doppler Current Profiler instrument. Specific Quantum project measurements (13 months duration) have been undertaken by Metocean Engineers, while the longer term

Beacon 15 data set (3 years duration), which is part of the operational system used by Port Hedland Port Authority, was provided by Tremarfon.

Summary data presentations for each of the data sets are shown in Figure 5-7 to Figure 5-9 for each of the three measurement sites.

Table 5-2 Summary of current measurement data available for this study

Site Name	Latitude	Longitude	Depth (m)	Start Date	End Date
Quantum Inshore	-20.2266	118.51055	12.5	15/12/07	03/02/09
Quantum Offshore	-20.1313	118.3982	18	15/12/07	03/02/09
Beacon 15	-20.1733	118.5082	14-15m	1/7/04	30/6/07
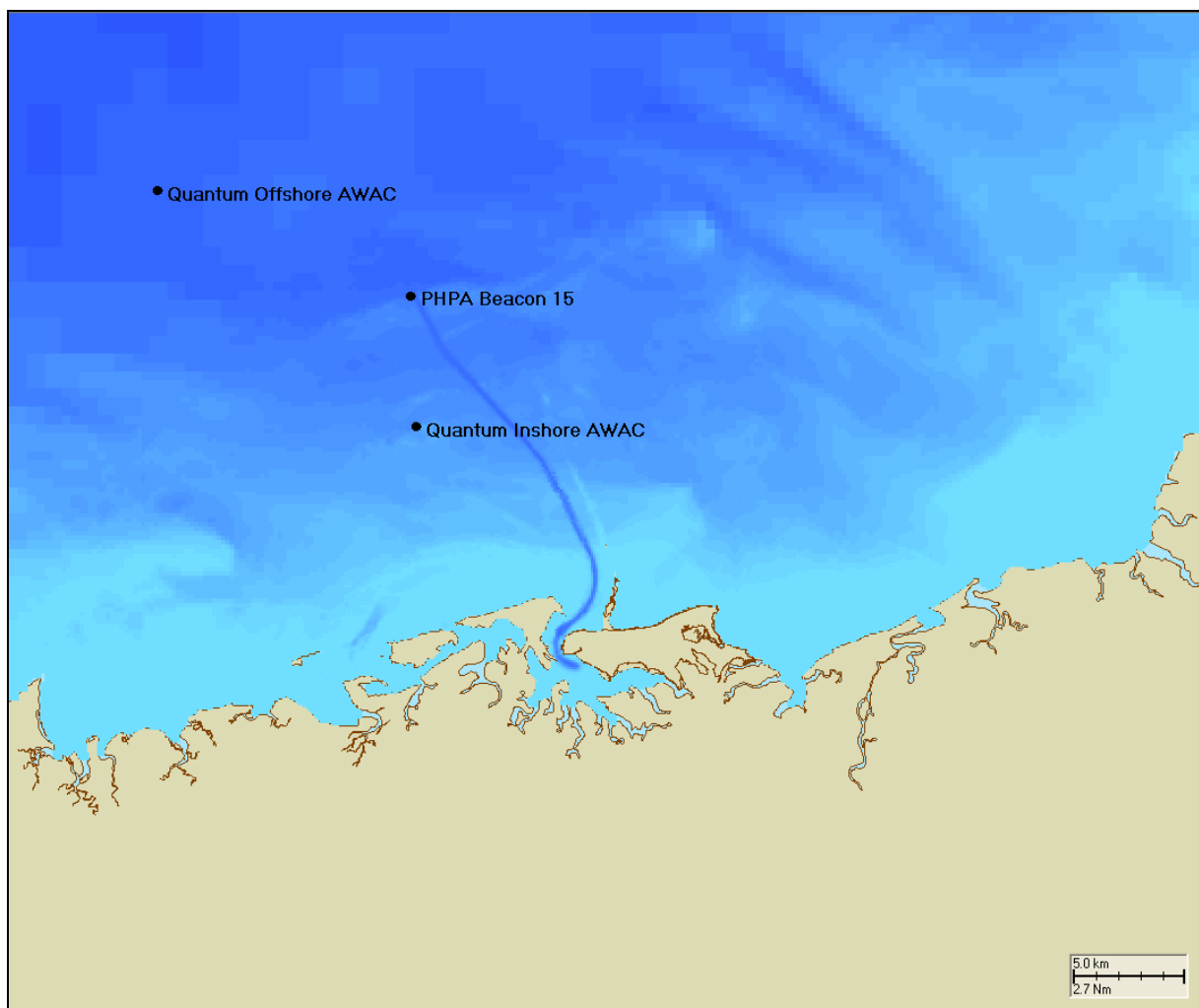
Figure 5-6 Relative locations of the three current measurement locations used in this study. Note the shipping channel defined by the clear blue line representing the locally deeper area.

Current Speed and Dir'n Rose for Quantum Inshore AWAC (mid-depth), Dec-2007 to Feb-2009
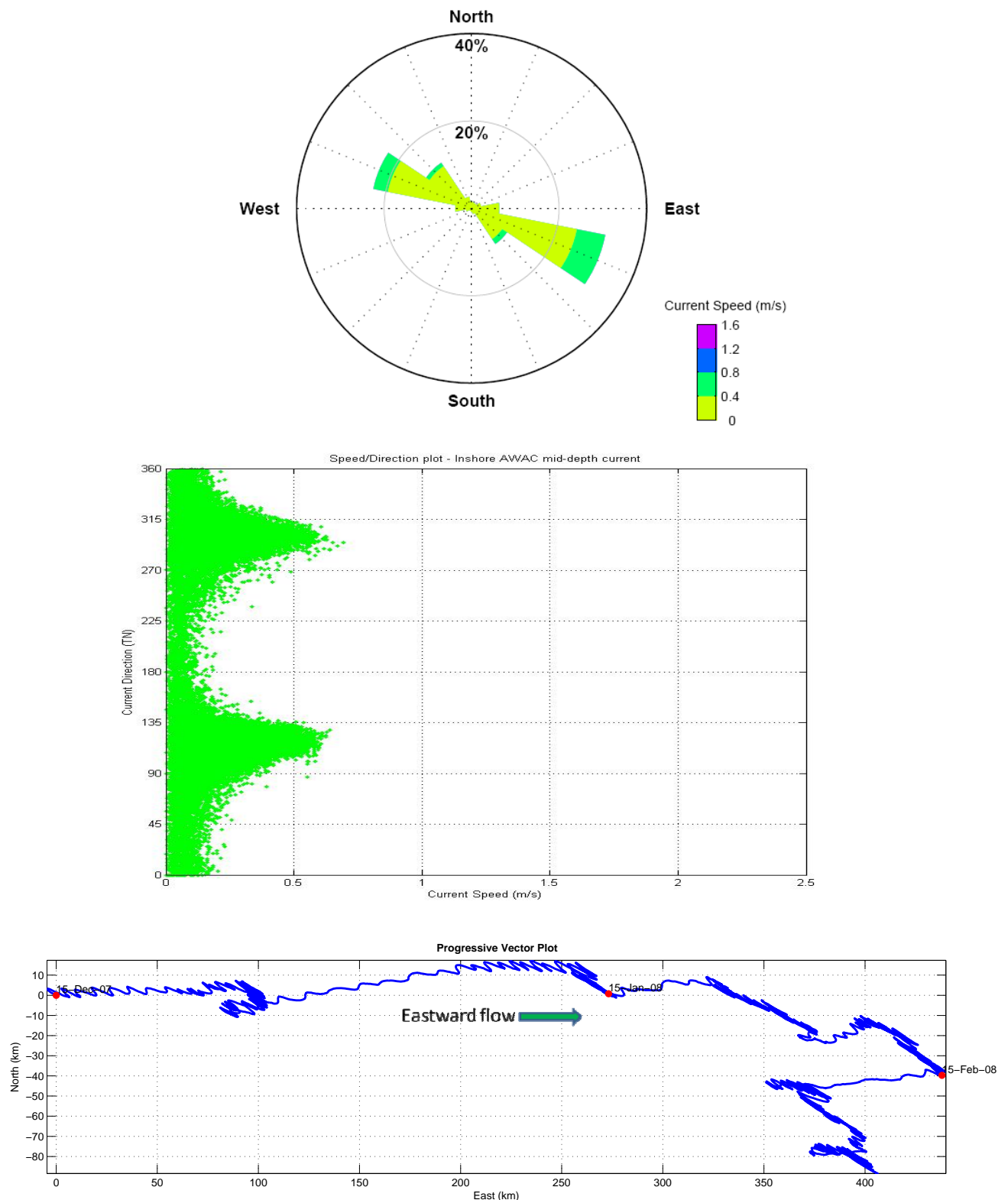
Figure 5-7 Quantum Inshore AWAC current data summary (mid-depth currents): TOP: Current Rose (direction TOWARDS), MIDDLE: Current Direction versus Speed scatter, BOTTOM: Progressive Vector Plot which shows integrated advection (km) over time from the start of the current record. Red dots are shown at monthly intervals.
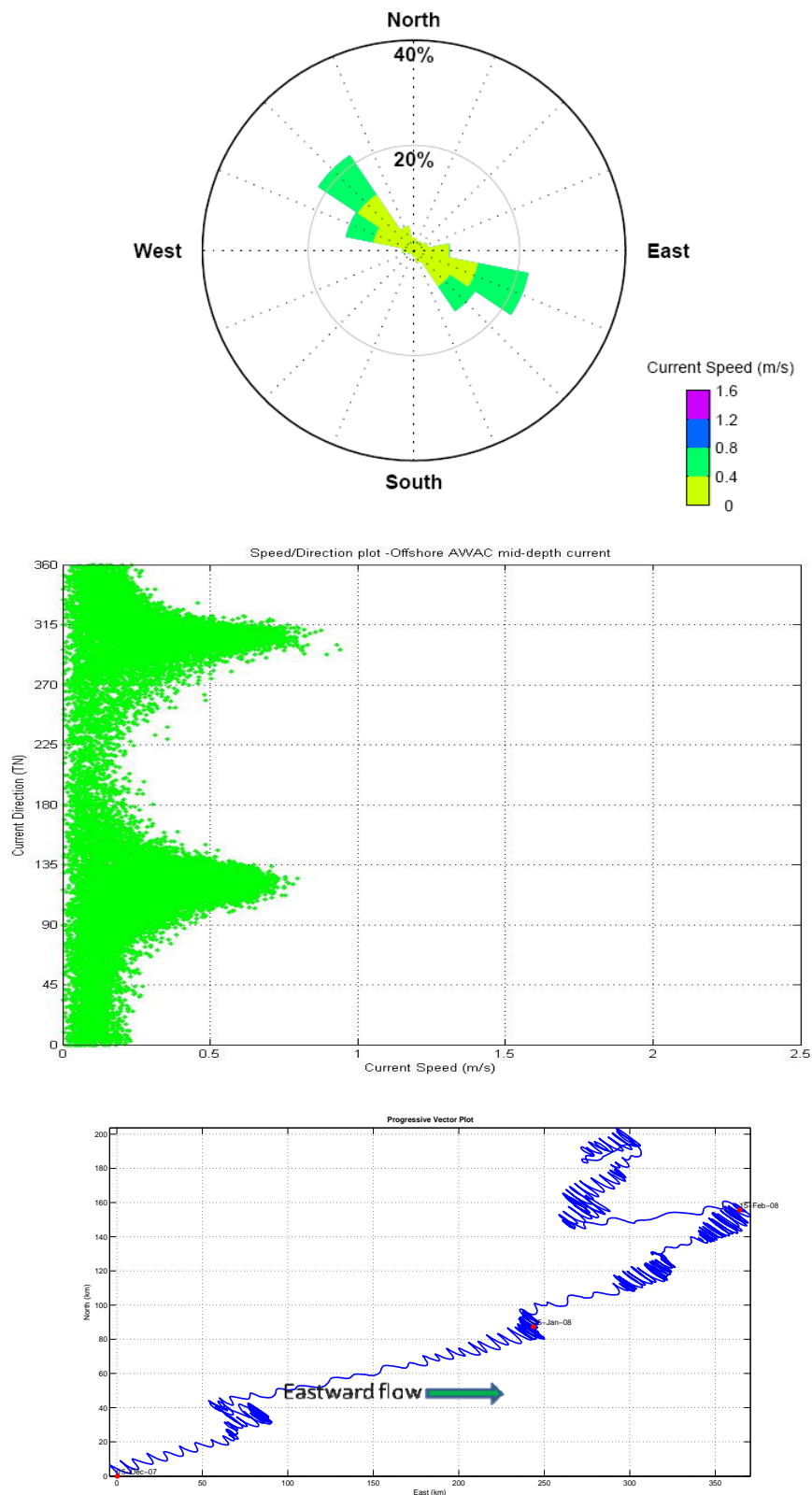
Figure 5-8 Quantum Offshore AWAC current data summary (mid-depth currents): TOP: Current Rose (direction TOWARDS), MIDDLE: Current Direction versus Speed scatter, BOTTOM: Progressive Vector Plot which shows integrated advection (km) over time from the start of the current record. Red dots are shown at monthly intervals.

Figure 5-9 Beacon 15 AWAC current data summary (depth averaged currents): TOP: Current Rose (direction TOWARDS), MIDDLE: Current Direction versus Speed scatter, BOTTOM: Progressive Vector Plots which show integrated advection (km) over time from the start of the current record – top panel is whole record, bottom panel is shorter duration for clarity. Red dots are shown at quarterly intervals.

The data shows the interesting phenomenon that the main tidal axis also closely approximates the dominant wind directions. This results from the orientation of the coastline which will steer the bulk advection in a general east-west alignment offshore from Port Hedland. This steering is clearly evident in the progressive vector plots shown for each site. These plots show the long term net drift in the current record, with the shorter term tidal variations overlain in each tidal cycle.

The most instructive of these data sets is the long term Beacon 15 record. Starting from the origin (0, 0) at 1 July 2007, hence in winter, the vector initially moved towards the NW, but then underwent a prolonged period of eastward drift. After around 10 months, commencing in early winter, the vector underwent a persistent northwest movement, reverting back to eastward drift approximately 3 months later. This behaviour was found to be consistent for each year of the record. Hence, there is a longer-term disparity indicated with the eastward drift lasting 3-4 times longer than periods of north-west drift.

The typical eastward movement of water along the coastline results from the dominance of the westerly component winds, that drive downwind currents in an along shore direction. Current directions are expected to be approximately parallel to the coastline in the near shore region, and as a result should rotate towards the north further to the east.

The net drift is therefore of great importance to the dispersion of sediment plumes that persist over a time-scale greater than the tidal cycle. Although the tide accounts for most of the variance in the record, longer term predictions of sediment fate will reflect the magnitude and persistence of the mean flows. Tidal excursion lengths (the distance a water particle might move under the sole action of the tidal flow) varied up to around 15 km during springs at Beacon 15, while the net drift over periods of 7 days reached over 100 km from a residual, or mean current of around 0.15 m/s. The net drift was typically weaker and less persistent in the westward directions, and usually occurred during the winter months.

Based on the data available for this study, sediment plumes generated in the region are expected to show the following advective characteristics:

- Oscillate with the tide over distances of up to 15 km, with reciprocating motion in a general SE-NW alignment over a 12 hour period;

- Generally drift eastward over periods of days to weeks during the summer, spring and early autumn periods;

- Generally drift westward to north westward over periods of several days during the winter months.

Periodic storms or tropical cyclone events will create short term, highly dispersive, conditions where currents may reach 2.6 m/s in some areas. Currents of this magnitude can advect a plume a distance of 9 km within an hour and over 100 km within half a day.

5.5   Waves

Waves are an important consideration in the simulation of long term sediment fate as wave action acts to increase the resuspension potential at the seabed. The wave climate off the coast of Port Hedland has been measured using a ground-based wave radar system (AWAC marine navigation radar) mounted on the Beacon 16 navigation beacon (118.5066° E; 20.1745° S). The AWAC measures the directional spectrum of the surface water velocity which is related to the wave height using linear wave theory. The instrument provides accurate measurements of the wave spectrum under most conditions and has been used to analyse the regional wave conditions. The dataset available for this study spans 3 years from 1 July 2004 to 30 June 2007.

The joint frequency table of significant wave height (H_s) against direction (θ) is given in Table 5-3. Significant wave heights at Beacon 16 are below 2 m for 99.2% of the record. Wave heights in the range 2-4 m are rare and typically associated with cyclones. Waves are from the northwest quadrant for ~92% of the record. Less frequent waves from the east would be generated from easterly winds that prevail in winter at times when the oceanic swell is very low.

Table 5-3 Joint Frequency Table, Wave Height (Hs) and Direction, Beacon 16 July 04 – June 07.

N=26279	N	NE	E	SE	S	SW	W	NW	Total	Cumul.
0–0.5	2.17	0.45	0.05	0.06	0.04	0.12	4.72	15.63	23.24	23.24
0.5–1	7.85	2.98	0.16	0.10	0.09	0.28	21.59	27.02	60.06	83.30
1–1.5	1.55	1.57	0.13	0.03	*	0.02	8.02	2.92	14.24	97.54
1.5–2	0.32	0.07	0.02	0.01	–	–	0.77	0.46	1.66	99.20
2–2.5	0.18	0.04	*	*	–	–	0.04	0.20	0.47	99.67
2.5–3	0.08	–	0.01	–	–	*	0.02	0.10	0.21	99.88
3–3.5	0.06	*	–	–	–	–	*	0.03	0.10	99.98
3.5–4	*	*	–	–	–	–	–	–	0.02	100.00
4–4.5	–	–	–	–	–	–	–	–	–	100.00
4.5–5	–	–	–	–	–	–	–	–	–	100.00
Total	12.21	5.13	0.38	0.20	0.13	0.42	35.16	46.37		
Cumul.	12.21	17.34	17.72	17.92	18.05	18.47	53.63	100.00		

* denotes values less than 0.01%   – denotes no records in bin

The joint frequency table of peak wave period (T_p) against direction (θ) is given in Table 5-4. In general, the shallow-water shelf around Port Hedland experiences wave conditions that occur in three distinct frequency bands. Long-period swells occur at mean wave periods of about 12 s to 20 s. There is usually little wave energy at mean wave periods of 8 s to 12 s, with the exception being waves produced as the result of summer cyclone activity.   The locally generated wind seas occur with mean wave periods of 4 s to 8 s. Long period swell and wind seas do not always occur together, consistent with the swell arriving from outside the area and with local wave generation. The long period swell often appears as bursts, or periodically stronger episodes occurring at intervals of about 4 to 5 days.

Table 5-4 Joint Frequency Table, Peak Wave Period (s) and Direction, Beacon 16 July 04 – June 07.

N=26279	N	NE	E	SE	S	SW	W	NW	Total	Cumul.
0–2	0.01	–	–	–	–	–	*	*	0.03	0.03
2–4	3.94	1.56	0.12	0.08	0.08	0.19	5.55	5.17	16.69	16.72
4–6	4.02	2.57	0.21	0.06	0.02	0.12	19.58	8.02	34.60	51.32
6–8	3.11	0.89	*	–	–	*	3.12	2.03	9.16	60.49
8–10	0.74	0.09	0.02	0.04	*	*	0.20	1.67	2.76	63.25
10–12	0.15	*	–	–	–	–	0.15	0.80	1.11	64.36
12–14	0.11	*	0.02	–	0.01	0.02	1.56	6.12	7.85	72.21
14–16	0.12	0.02	*	0.01	*	0.06	3.42	14.68	18.33	90.54
16–18	0.03	–	–	0.01	–	0.02	1.37	6.76	8.19	98.72
18–20	*	*	–	–	–	*	0.24	1.02	1.28	100.00
Total	12.24	5.14	0.38	0.20	0.13	0.42	35.21	46.27		
Cumul.	12.24	17.38	17.76	17.96	18.10	18.51	53.73	100.00		

* denotes values less than 0.01%   – denotes no records in bin

Wave conditions over the outer shelf region are typically bimodal as the result of the presence of perennial Southern Ocean swell and locally generated sea, with the sea/swell separation occurring at about 9 s. The wave conditions at Beacon 16 are dominated by wind seas with peak periods < 8 s comprising ~60% of the record. Westerly and north-westerly swell account for the remaining component.

Wave refraction and reflection strongly influence the wave directions in the shallow region near the coast around Port Hedland, confusing the trends in wave direction and magnitude. However, some general observations are possible. Long period swell in mid-year generally comes from the south-west. The southerly and south-westerly swells reach the shallow waters by refraction, with the incident direction eventually being from west to north-west. When the sea breeze is dominant, wind sea waves come from the north-west. Dominant swell directions for the ocean areas west and north-west of Australia are considered to be consistently seasonal.

The seasonal pattern of wave and swell for Port Hedland is strongly correlated with the typical seasonal wind and weather conditions for the north-western Australian coast and the variability of the oceanic swells. As can be seen in Figure 5-10 and Figure 5-11, wave conditions do vary seasonally, with a typical monsoonal pattern, i.e. summer/spring conditions are consistent with each other, as are winter/autumn.
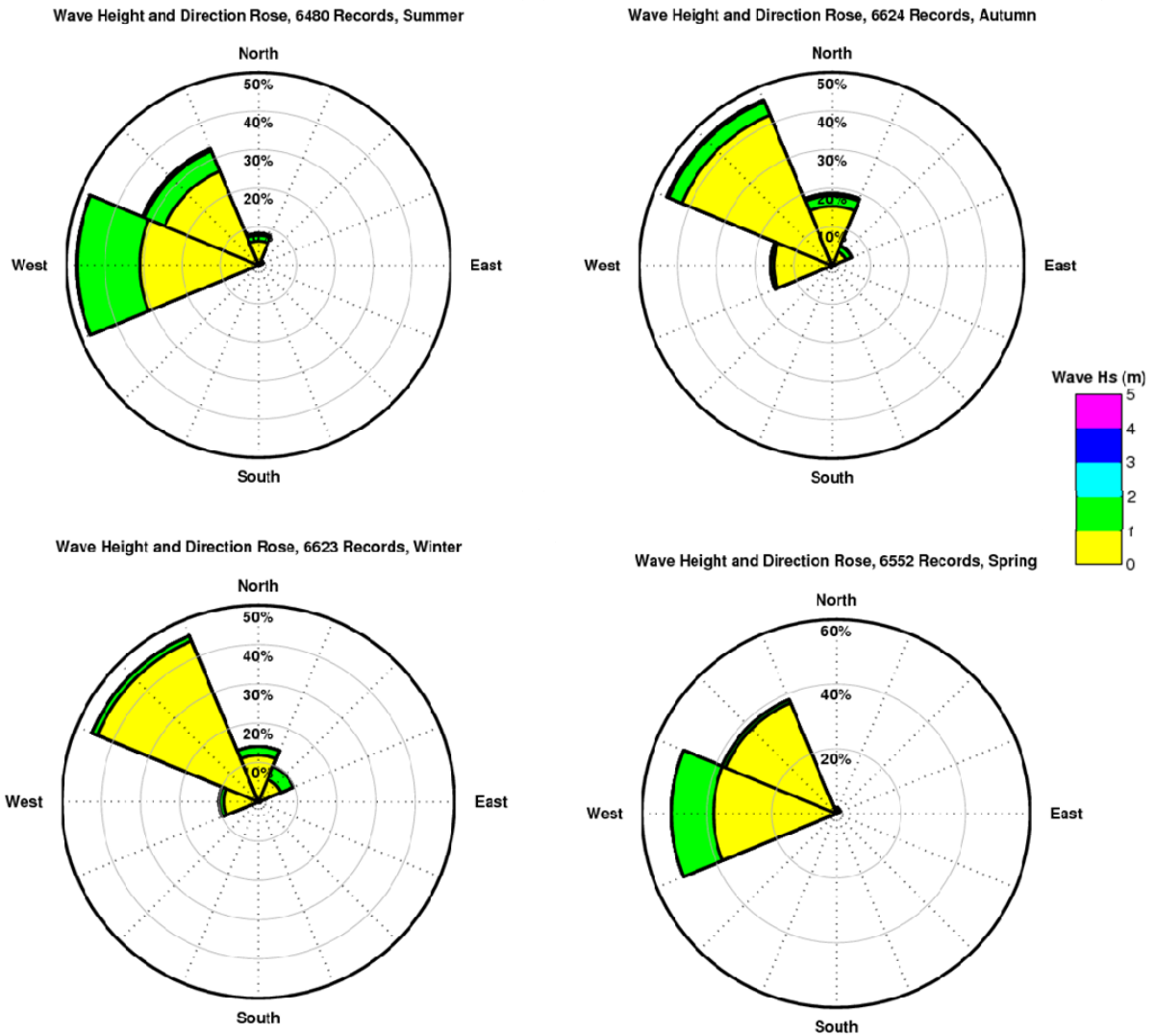
Figure 5-10 Seasonal wave roses, Beacon 16, Port Hedland - Wave Height and Direction. Roses show frequency of occurrence around the compass, with wave height represented by the colour scale. Direction convention is Direction From.
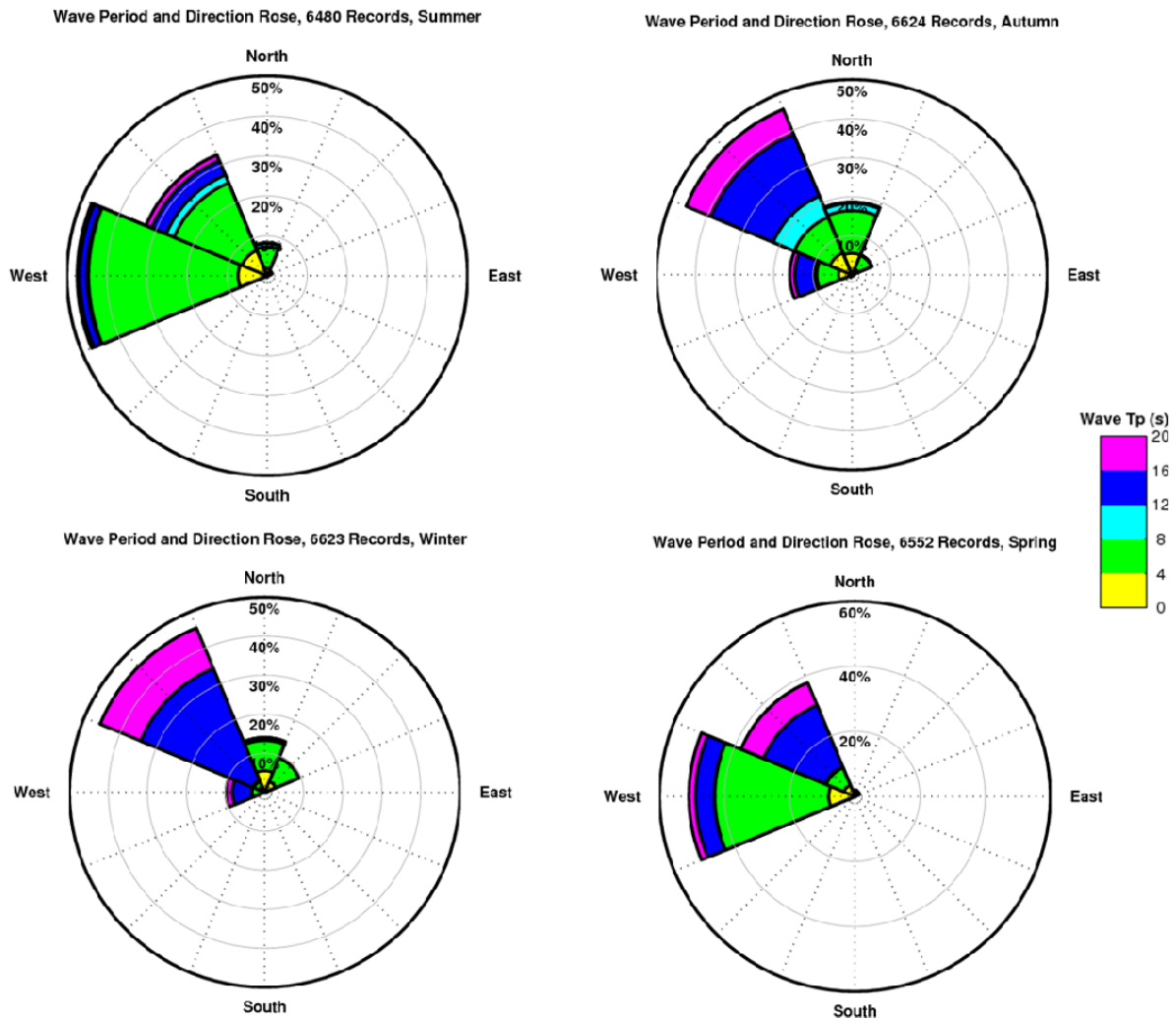
Figure 5-11 Seasonal wave roses, Beacon 16, Port Hedland – Wave Period and Direction. Roses show frequency of occurrence around the compass, with wave period (T_p) represented by the colour scale. Direction convention is Direction From.

5.6 Interannual Variability and ENSO

The variability of the oceanographic conditions over annual time-scales was assessed by analysing the wind conditions with reference to the SOI which can be used as an indicator of the regional interannual variability. The SOI broadly defines neutral, El Niño (strongly negative SOI) and La Niña (strongly positive SOI) conditions based on differences in the surface air-pressure between Tahiti on the eastern side of the Pacific Ocean and Darwin, on the western side.

El Niño episodes are usually accompanied by sustained warming of the central and eastern tropical Pacific Ocean and a decrease in the strength of the Pacific trade winds. La Niña episodes are usually associated with converse trends. These fluctuations could potentially affect the outcomes of the modelling by affecting the distributions (frequency and intensity from given directions) of wind and wave data used to represent conditions over the study area. Thus, it was important to identify any significant interannual trends.

The monthly value of the SOI from 1992 to 2006 is shown in Figure 5-12. For example, 1997 is shown to be a strong El Niño, and 2005 is a weak El Niño year.
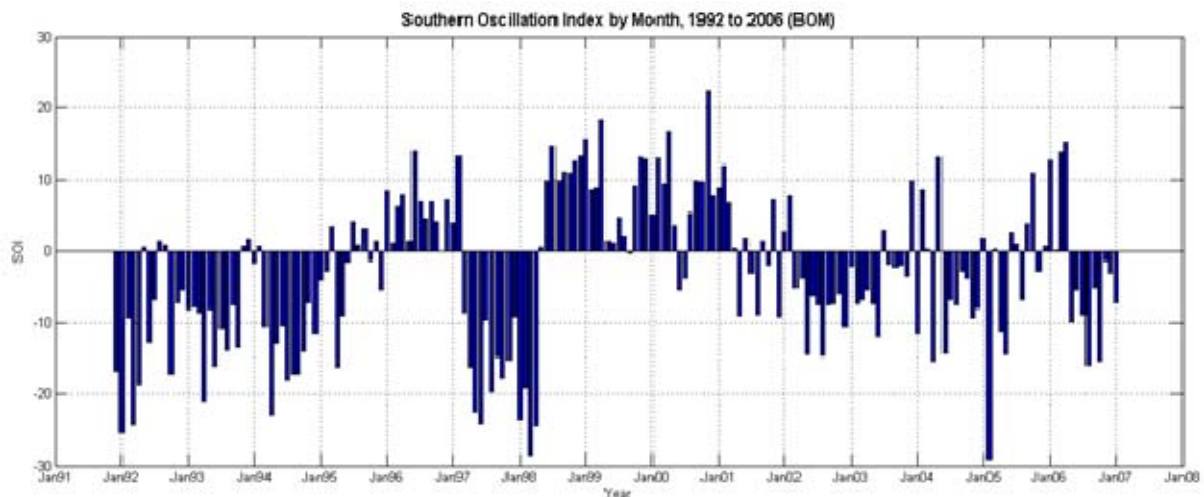
Figure 5-12 Monthly value of the Southern Oscillation Index (SOI). Positive values indicate La Nina conditions while negative values indicate El Niño conditions. Data sourced from Australian Bureau of Meteorology.

Table 5-5 shows a summary of the annual wind statistics together with the SOI categorisation for the year (with reference to Figure 5-12). The data shows no definite trend in wind variability, with the annual statistics being fairly uniform over the 12 year set. The strongest winds occurred during TC Rachael in early January 1997 while the SOI was positive, prior to the onset of the very strong ENSO event in 1997/1998. Slightly weaker than average winds were recorded during 1997/1998, however the variability against the long term averages is very low.   Directional characteristics were also found to be consistent between all the assessed years (see Figure 5-13 for example).

Efforts were also made to compare the monthly SOI values with monthly wind statistics. No clear correlations were found that would suggest the need to consider this long term variability in the overall modelling scope. The variations are small compared to the more consistent net currents and tidal fluctuations. Moreover, the long duration of the model simulation would ensure that current, wind and wave data incorporated the interannual variability in the sample data. In conclusion, it is expected that modelling using a data span of up to 5 years will capture suitable variability and present a good prediction of the sediment fates.

Table 5-5 Annual wind statistics and ENSO condition summary for 1995 to 2006

Year	SOI Description	Wind Speed Statistics (m/s)				
		Mean	Median	Max	P95	S.Dev
1995	Mixed/weak	5.12	4.84	17.94	9.97	2.61
1996	La Nina	4.79	4.27	19.08	9.40	2.53
1997	Strong El Niño	4.60	4.27	34.46	9.11	2.48
1998	Early El Niño to La Niña	4.91	4.27	18.51	9.40	2.49
1999	La Niña	4.65	4.27	26.77	8.83	2.57
2000	La Niña	4.76	4.27	21.64	9.40	2.57
2001	Mixed/weak	4.86	4.27	17.94	9.40	2.48
2002	El Niño	5.28	4.84	16.23	9.40	2.45
2003	El Niño to mixed	5.45	4.84	21.07	9.97	2.46
2004	El Niño to mixed	5.45	4.84	17.94	9.97	2.45
2005	Mixed	5.33	4.84	18.51	9.40	2.42
2006	Mixed to El Niño	5.28	4.84	24.21	9.40	2.53
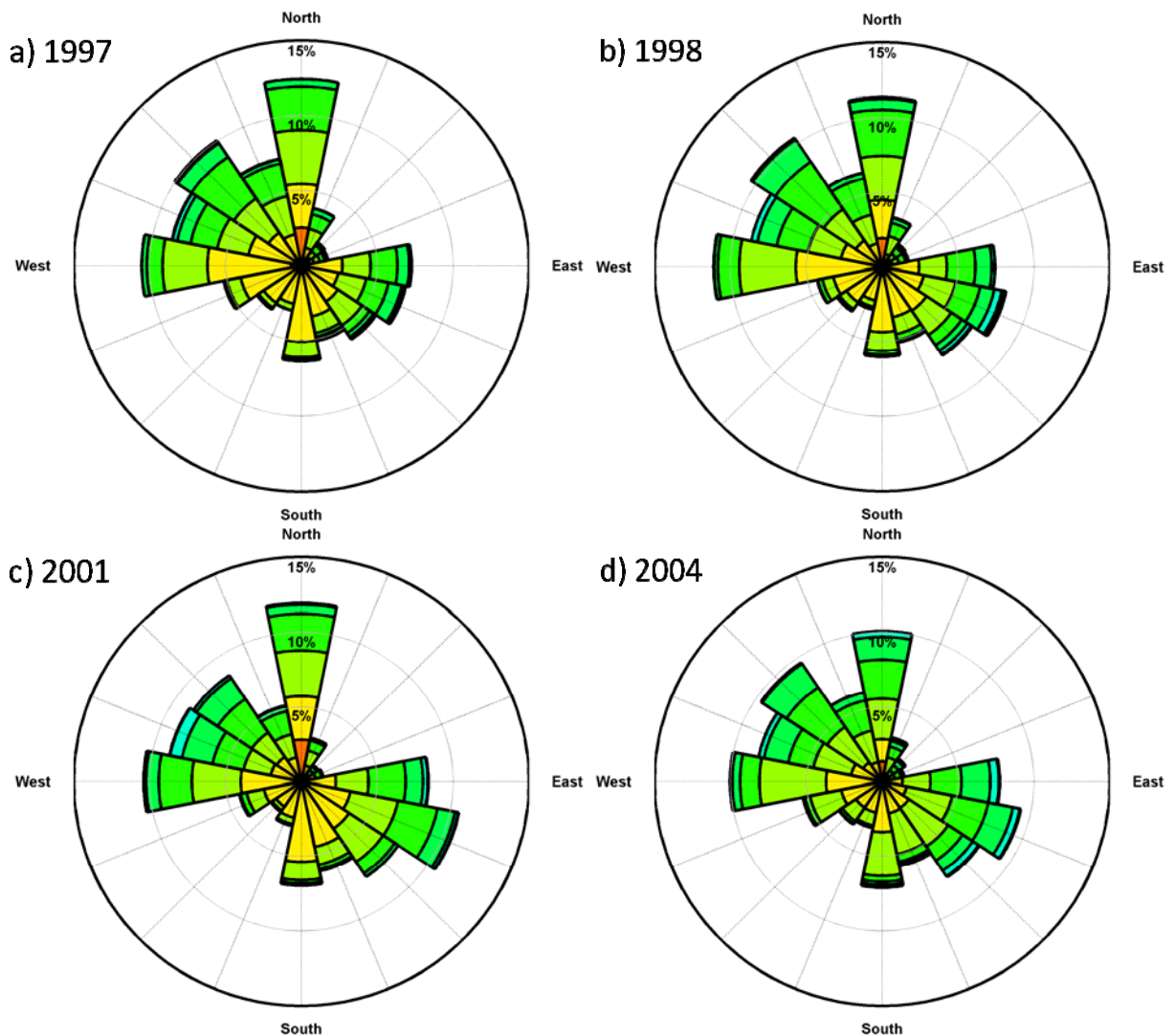
Figure 5-13 Comparative wind roses for 1997, 1998, 2001 and 2004, Port Hedland Airport.

6   HYDRODYNAMIC MODELLING

6.1   Model Description

Three-dimensional current fields were generated for sample periods by hindcasting, using a three-dimensional ocean/coastal circulation model, HYDROMAP. This is a peer-reviewed and published model (Spaulding & Isaji 1984, Isaji *et al,* 2001, Zigic et al, 2003) that has been successfully applied in many regions around the world including many applications by APASA over the North West Shelf and Timor Sea.

HYDROMAP is formulated to describe the flow-field locally induced when tides and winds are the most important sources of forcing. The HYDROMAP model solves the three-dimensional Navier–Stokes equations under an incompressible flow assumption for Newtonian fluids, with the inclusion of terms for Coriolis effects. The equations are solved using a Cartesian coordinate system. The momentum equations retain the non-linear acceleration terms which may optionally be turned off in the model setup. The Coriolis acceleration term may also be turned off, if required. The dominant frictional forces are assumed to be the vertical diffusion of momentum due to wind shear at the water surface, as well as friction at the sea bed. The horizontal diffusion of momentum is neglected. Also, vertical accelerations are neglected and the pressure distribution is hydrostatic. These assumptions are valid for modelling the wind and tidal driven circulation over the area of interest.

The hydrodynamic equations of motion are solved using a finite-difference grid in the horizontal (x,y) coordinates and the Galerkin method in the vertical (z) coordinate. Rather than calculating currents for discrete depth bands, the Galerkin approach uses depth-varying functions to provide continuously variable estimates with depth. The numerical solution methodology follows that of Davies (1977 a, b) with further developments for model efficiency by Owen (1980) and Gordon (1982). The finite difference scheme is fully explicit and uses a space staggered grid scheme with vertical velocities specified at the centre of each grid cell, and the horizontal velocities given at the grid cell faces. Space-staggering refers to an internal nesting scheme that subdivides grid cells equally into 4 cells at each level of subgridding. The model formulation allows for 6 levels of subgridding (i.e. a range in resolution to 1024 times the coarsest grid scale) over one or more freely placed areas of particular interest, or high complexity, within a larger domain, while maintaining model efficiency and stability. Nesting situations usually require smaller time steps over areas of finer sub-gridding. However, to allow for stable estimation of currents at a common and larger time step that would otherwise exceed the Courant-Friedrichs-Lewy (CFL) condition, the free-surface elevation is treated separately from the internal, three-dimensional flow variables. The output from the model is a three-dimensional current field at a uniform time step across all levels of subgridding. The scheme has been extensively tested through comparison with analytic solutions as well as for real word situations over a wide range of ocean settings.

A detailed presentation of the model and applications can be found in Isaji and Spaulding (1984) and Isaji *et al.,* (2001) and more detail on the extensive comparison with analytical solutions is found in Owen (1980).

6.2 Domain and Bathymetry

The model domain established for this study needed to be large enough to capture the full effects of wind and tidal-induced forcing on the circulation within the coastal region near Port Hedland. As such, a large model domain was created (Figure 6-1), spanning 131 km in an east west direction (Longitude 117.95 to 119.2E) and 83 km in a north south direction (Latitude 19.72 to 20.47S).
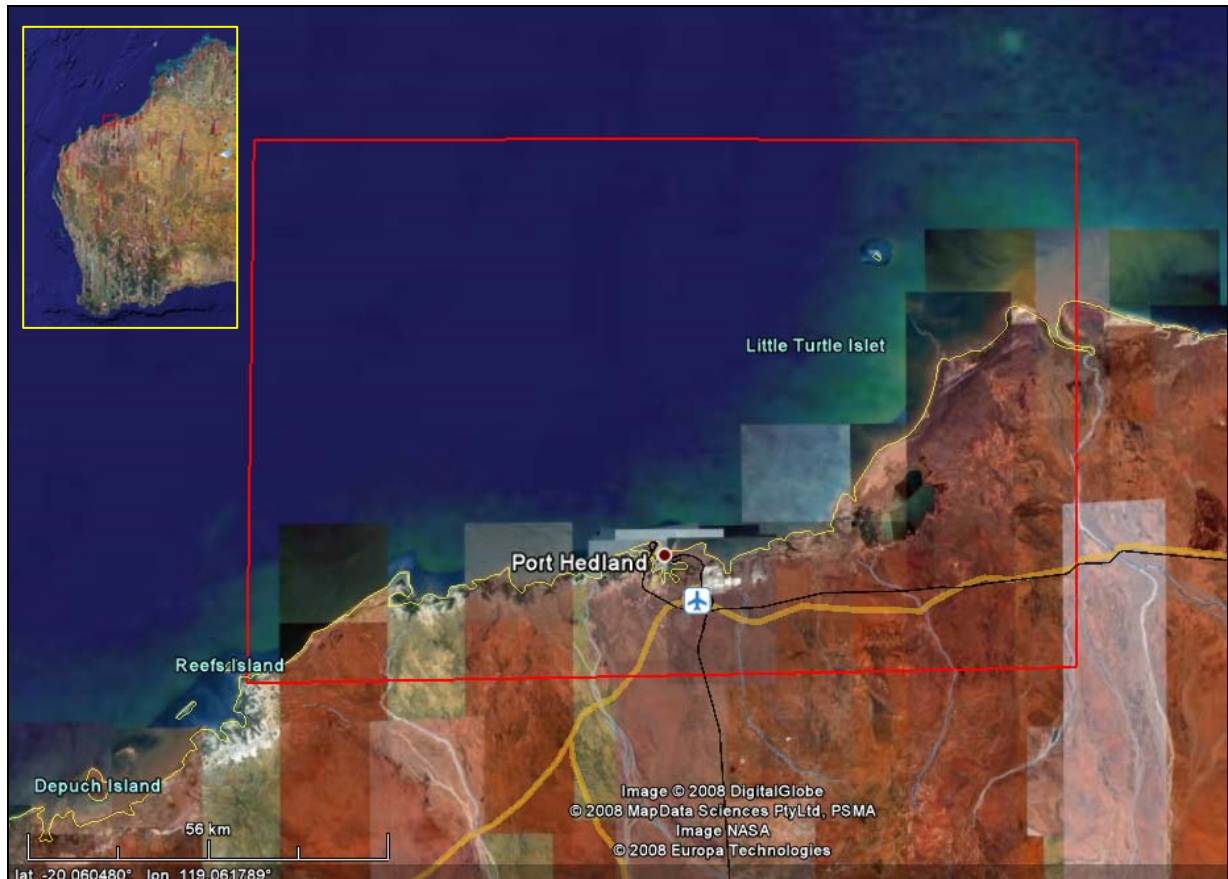
Figure 6-1 Locality map and HYDROMAP domain shown by the red box.

The hydrodynamic grid used a stepped-gridding approach which allowed for higher resolution around areas of specific interest where higher resolution is required. Computational cell sizes, which are square, were specified as 1600 m x 1600 m at the coarsest scale over the outer part of the model. Grid sizes were then decreased in steps towards the main areas of influence, by subdividing larger cells into 4 equal cells. This approach allows the use of a single-grid in the computation of currents that yields computationally stable estimates of current speed across changes in resolution, The grid established around Port Hedland had 5 levels of resolution. Hence the grid cells sizes were:

- 1600 m
- 800 m
- 400 m
- 200 m

- 100 m.

Figure 6-2 shows details of the variable grid resolution employed in the model. The final, validated, grid consisted of more than 55,000 active computational water cells.
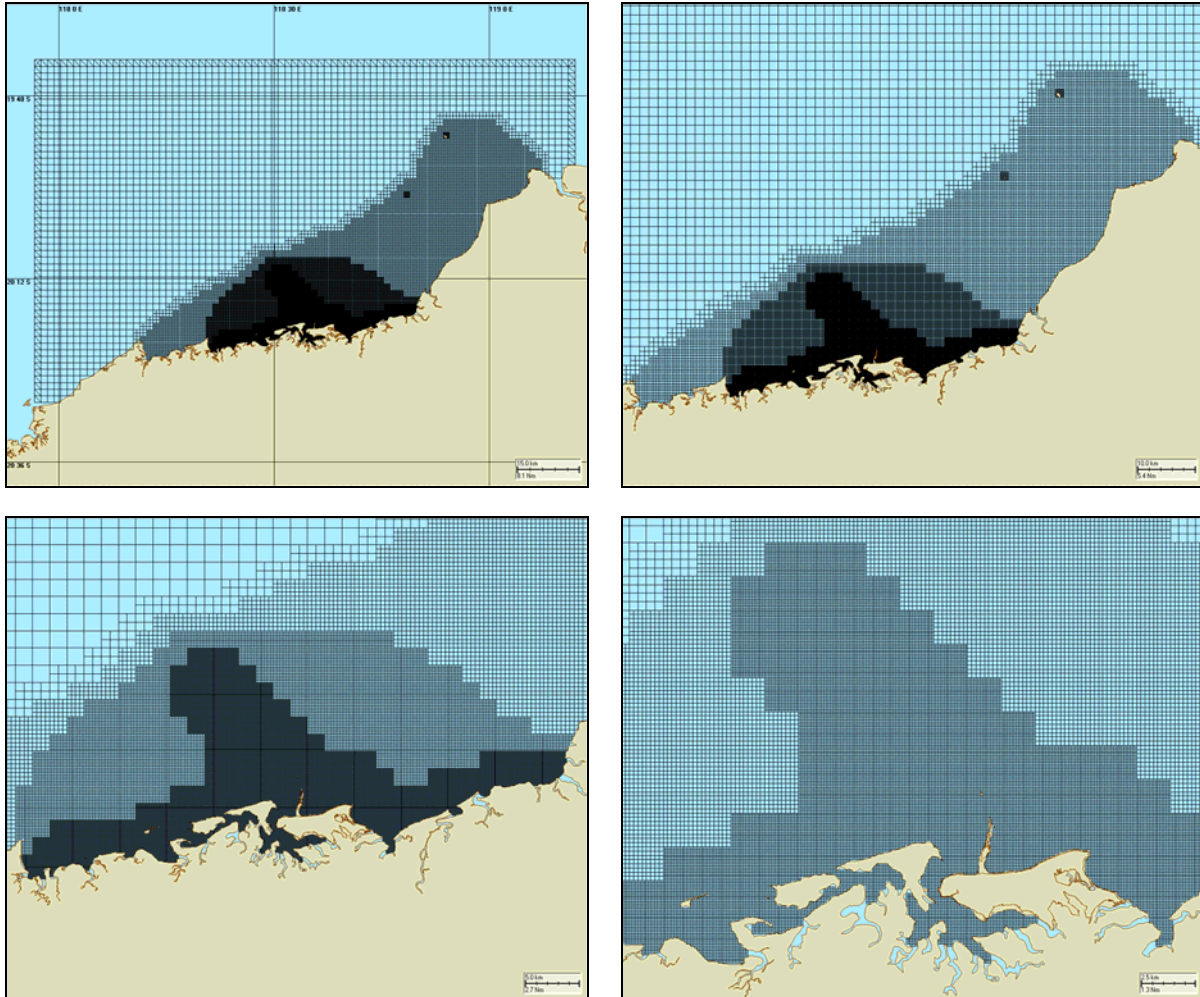
Figure 6-2 Hydrodynamic grid used in HYDROMAP at 4 different magnification levels to highlight the transition from coarse resolution to fine resolution within the domain.

Bathymetric data used to define the three-dimensional shape of the seabed within the model was obtained from multiple sources to optimise coverage and resolution. For the near-shore areas around the proposed development site, bathymetric data was acquired by BHP Billiton Iron Ore from an air-borne LIDAR (**Li**ght **D**etection **a**nd **R**anging) survey. LIDAR is an optical remote sensing technology that measures properties of scattered light and can be applied in shallow water to obtain depth estimates. The data was supplied at a horizontal resolution of 5 m and with a vertical resolution that ranged with the depth, due to increasing interference of turbidity and light scattering with increasing depth (10's cm in the shallows and degrading to a few metres at the deeper offshore extent). The LIDAR data did not cover the full domain and was augmented by a bathymetric interpolation produced for the area produced by GeoScience Australia. This latter data had a spatial resolution of 250 m and a stated vertical

resolution of 0.1 m. However, because of the incomplete coverage used to generate the data, the accuracy of the data was low over the inshore sand banks and mudflats, hence interpretation from aerial imagery was required in some areas beyond the extent of the LIDAR data. The bathymetric data were applied in a sequential manner after standardising data sets for height datum. The highest resolution (LIDAR) data was applied first to define the depth of cells that were within the bounds of this dataset. The coarser data was then applied to set the bathymetry over the further extents of the model grid. Finally, manual corrections were applied to ensure that significant shoals were represented. Figure 6-3 shows the detail and of the bathymetric data generated from the various sources. The extent of the high resolution LIDAR data is also marked. Note that the gridding results in some smoothing of the bathymetry, and this smoothing is enhanced where the coarser data is relied upon. However, the key bathymetric features over the inshore and mid-depths are relatively high. In particular, the grid represents the depth striations running approximately NW-SE over parts of the coastal shelf as well as the limestone ridges running roughly parallel with the coast. The reef platforms surrounding the coastal islands and the shoals extending from the coast are also clearly defined.
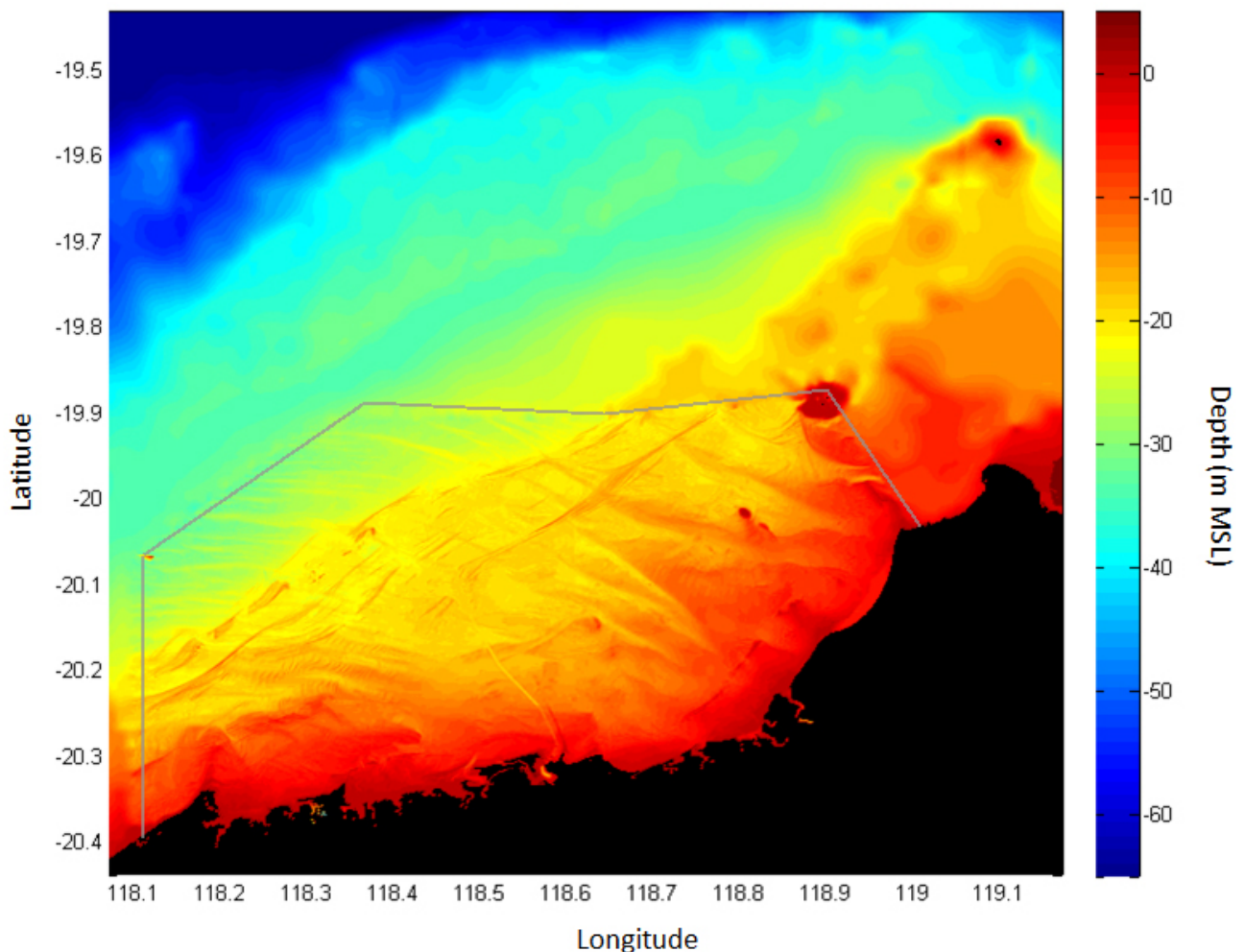
Figure 6-3: Bathymetric grid created for the study domain for HYDROMAP by blending bathymetric data from LIDAR surveys with Geoscience Australia data and manual digitizing from aerial imagery. The grey polygon surrounds the extent of LIDAR data that was available.

6.3   Seabed drag, eddy viscosity and wind drag coefficients

The study area is gently sloping with a seabed that is mostly sand or sand on rock veneer. These units are interrupted by a series of low linear limestone ridges that are orientated parallel with the coast. The influence of the drag induced by this seabed, at the grid scales applied in the hydrodynamic model, was represented using Manning's formula with a coefficient (n) of 0.025, representative of a coarse sand seabed. A parabolic vertical profile was applied to the vertical viscosity scheme using a 3rd order polynomial profile. Based on initial calibration simulations varying the viscosity profile only, the peak viscosity was set at 250 cm^2 s^{-1}, peaking at a depth of 2 m below surface. The profile varied with local depth. Wind drag was applied dynamically within the model using shear-stress coefficients that varied exponentially with the wind speed based on empirically derived values for open coastal waters (e.g. 0.001 Nm^2 at 1 m^2 s^{-1}; 0.475 Nm^2 at 15 m^2 s^{-1}; Isaji and Spaulding 1984).

6.4   Tidal Forcing

The astronomical tides were included on all the open boundaries, by spatial interpolation of the tidal constituent data (amplitude and phase) provided by the latest Topex Poseidon global tidal set (TPX0 version 7.0; source: NOAA). The eight largest tidal constituents were used in the simulations: K2, S2, M2, N2, K1, P1, O1 and Q1. These eight constituents were selected as they account for the majority of the tidal amplitude. The values of these constituents vary over the latitude and longitude of the model boundary.

6.5   Wind Forcing Data

Two wind records were available for use in this study:

1. Long term record at Port Hedland Airport provided by BOM for 1993 to 2008.

2. Data at Beacon 15 from May 2000 to August 2007.

Both these data sets were inspected and found to contain numerous gaps and compromised data in the records. The Beacon 15 data was measured approximately 14 km offshore, and would therefore be expected to represent conditions over the project area, including sea-breeze effects. However, the duration of quality record available from this location was not sufficient for the generation of the base 10 year hydrodynamic and wave data set, where it was important to capture wider temporal variation. The BOM data was of a high consistent quality from 1995 to 2007 inclusive, giving 13 years of reliable data for the representation of temporal variation. This data is measured from a single location approximately 7 km inland from the coast. Thus, there were potentially two limitations presented by this data:

1. The site on land may not have been representative of wind acting offshore;

2. Spatial variation in the wind distributions could not be allowed for.

While the land in front of the BOM instrumentation site is very flat, and hence there is no or little sheltering, it was first important to determine the effect of the inland location,. Data for all overlapping periods were compared and used to derive an adjustment to match the measured conditions at the Beacon 15 offshore site.

Wind directions were found to be comparable for the two data sets, indicating that the BOM measurements recorded the effects of both synoptic winds and seabreeze effects that occurred over the offshore waters as far offshore as Beacon 15. Discrepancies were observed in the wind speed distributions, indicating that the BOM location registered speeds approximately 10% slower than measured at Beacon 15, for wind speeds > 2 m s^{-1}.

Figure 6-4 shows the result of adjustments to wind speed records for the cumulative occurrence of wind speed. A factor of 1.1 (i.e. a 10% increase) was applied to the measured BOM wind speed (red line) to shift the distribution to best match that of the Beacon 15 location (blue line). The final result is shown by the green line which confirms an excellent match of the wind speed over most of the distribution, and particularly for the median and above. Because stronger winds will have more potential to exert significant advection on the currents, and therefore would have more influence on the extent of the potential impact zone, as predicted by sediment advection modelling, best matching for wind speeds at median speeds and greater was considered more important than matching for very low wind speeds.

Figure 6-5 presents comparative wind roses for the Beacon 15 data and the corrected BOM data, showing that the directionality at the locations is generally consistent for the stronger winds. The main variations observed between the two data sets is the steering of an increased proportion of the winds arriving from the west towards the southwest and a decrease frequency of calm winds in the BOM data. These differences are attributed to the sea breeze component affecting the BOM location to a greater degree than at Beacon 15, due to the further distance offshore.

Beacon 15 is at the outer margins of the project area, hence the dredging and disposal operations being investigated tend to be closer to shore and in shallower water where there is increased potential for the wind to affect currents in the lower water column where sediment plumes are more likely to occur. Thus, it was judged essential for the sea breeze component to be included in the forcing data.

It was recognised that specification of a spatially constant wind (as represented by the corrected BOM data) would apply a uniform effect of the seabreeze with distance offshore to the full outer extent of the model domain. Hence, it is likely that the effect of the seabreeze would be overstated over the offshore margins of the model. Modelled wind data, such as data available from the NCEP reanalysis (source: US National Oceanographic and Atmospheric Administration) and the Local Area Prediction System (Source: Australian Bureau of Meteorology) were available for locations further offshore for part of the period of interest and were assessed for suitability over the site. From technical specifications available for the model and a comparison to the BOM data it was identified that these data did not represent the seabreeze and provided synoptic wind estimates only, hence were not suitable for use alone in the simulation of the coastal circulation.

The alternative of applying spatial interpolation between the offshore (modelled) data and the inshore (measured) data was assessed but it was recognised that this was also likely to introduce an undesirable bias, requiring untestable assumptions for the offshore extent of the seabreeze and how it becomes modified with distance offshore.

Because sediment derived from dredging and disposal discharges was expected to occur very low in the water column if they drifted into the offshore margin, where wind forcing

effects would be reduced, any bias generated by the overstatement of the seabreeze effect at this outer margin was considered less critical than the more accurate representation of currents closer inshore. Consequently, it was concluded that the adjusted BOM wind data set for Port Hedland, applied constantly over the domain, provided the most suitable long term representation of winds over the area for sediment fate modelling. The validation studies provided further opportunity to test this decision.
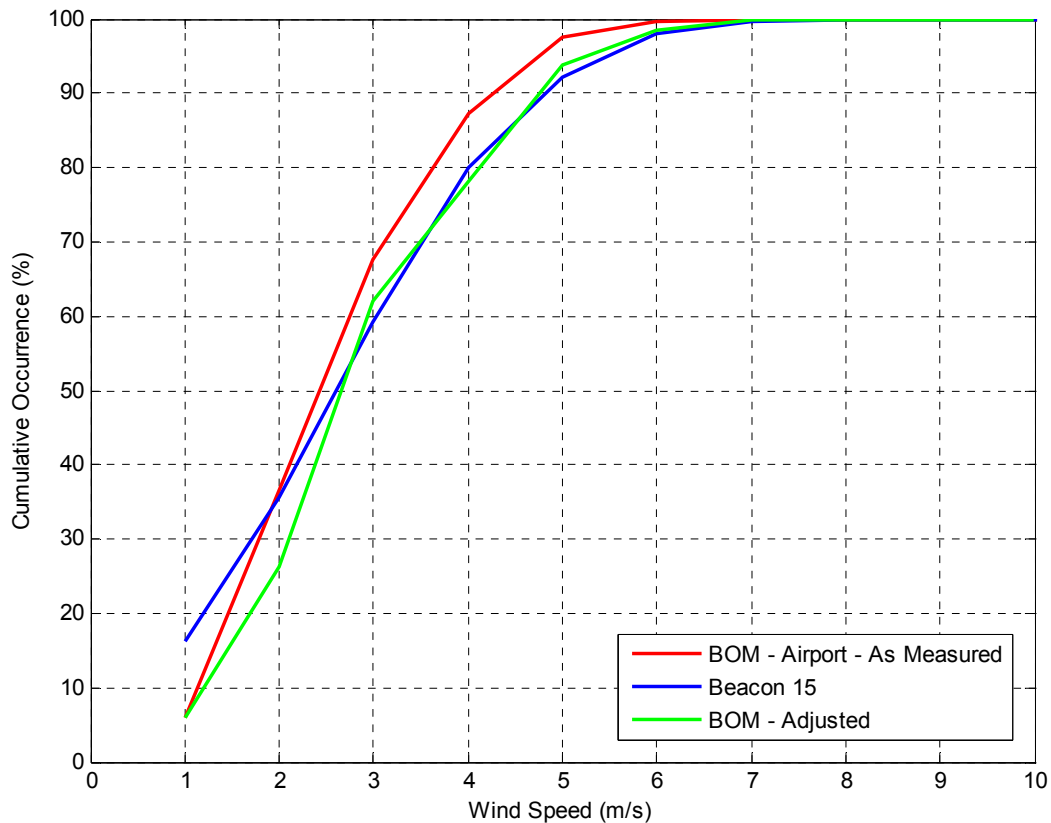
Figure 6-4 Comparison of cumulative occurrence distributions for wind speed at Beacon 15 and BOM Port Hedland Airport. Blue line is the Beacon 15 comparison data, red line is the original BOM data and the green line is the final adjusted BOM data.
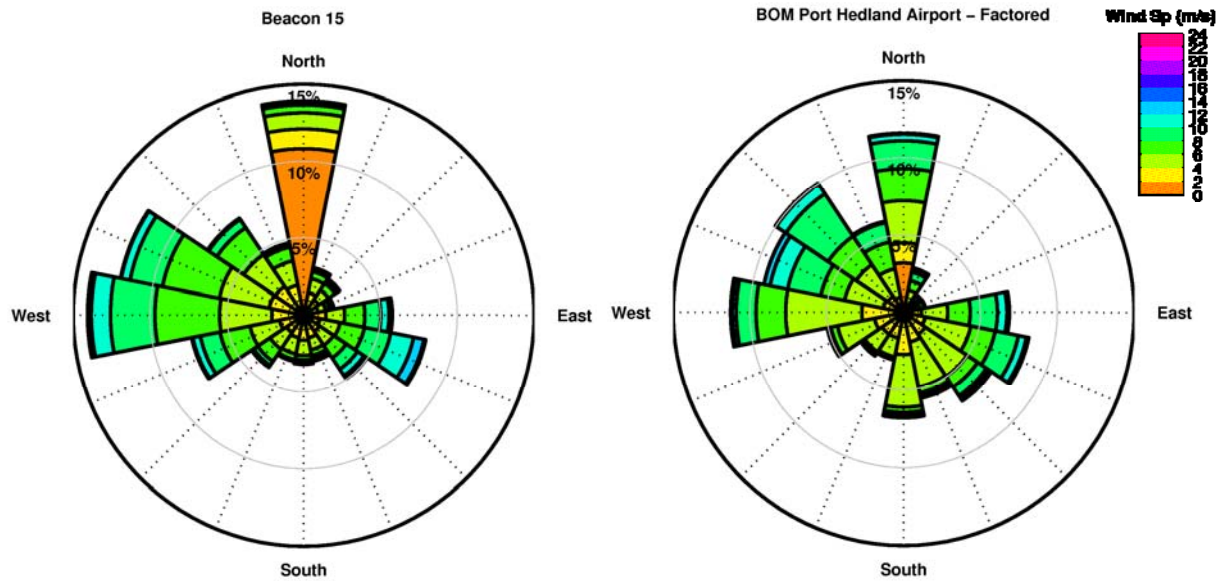
Figure 6-5 Comparative wind roses for wind data from Beacon 15 (left) and BOM Port Hedland Airport after 10% increase applied to wind speed only (right) showing consistent directionality.(Bars indicate direction wind was from and their intensity in this and all wind roses)

6.6   Validation studies

Current data available from three AWAC sites (Figure 5-6) were used for validating the predictions of the hydrodynamic model. The model was run for a number of periods to allow validation at each of the Quantum AWAC sites for summer, winter and transitional seasons:

Beacon 15

- February 2006 (summer)

- April 2006 (autumn transitional)

- June 2006 (winter)

- October 2006 (spring transitional)

Quantum Inshore and Offshore AWAC

- February 2008 (summer)

- April 2008 (autumn transitional)

- June 2008 (winter)

- October 2008 (spring transitional)

The current simulations were conducted only once for each period, hence the data from the Inshore and Offshore AWAC were extracted from the same model run for a test of the models stability over space. No adjustments were made to any model coefficients between the

periods. Thus, the comparisons also tested the temporal stability and accuracy of the model for that one configuration.

Model results were assessed in a number of ways. Firstly; surface elevations were compared at the three AWAC sites (Figure 6-6). A linear regression analysis was carried out on all data for the periods, yielding a correlation (R^2) value of 0.98, at both AWAC sites, indicating that astronomical tidal variations predicted by the model explained 98% of the elevations observed at both AWAC sites. This indicates that the model was very accurately propagating the tidal waves over the study area using the tidal boundary data for the eight largest tidal constituents extrapolated from the Topex-Poseidon global tidal set. The result also indicates that other factors, such as atmospheric pressure variations, explain only a very small proportion of the variations in water elevation at the sites and could be justifiably ignored.

To further validate the model performance, measured and predicted current speeds at the surface, mid-depth and bottom were compared over each period for the two Qantum AWAC sites and the Port Hedland Port Authority AWAC site (Beacon 15). These comparisons are provided in full in Appendix A (Quantum Inshore AWAC), Appendix B (Quantum Offshore AWAC) and Appendix C (Beacon 15 site). Figure 6-7 to Figure 6-12 show summary comparisons for the seabed currents over objectively selected summer and winter month samples. Seabed currents are used for summary purposes because sediments, which are negatively buoyant, will tend to concentrate within and be transported by currents near the seabed.

Results have been illustrated as rose plots, time-series comparisons of the velocity components and scatter plots of current speed and direction. Multiple methods were employed because of the inherent biases associated with any one type of analysis or plot. The rose plots, for instance, have been generated with 11.25 degree directional bins which can create possible discrepancies relating to bin allocation near the defined bin edges. To investigate whether there is any significant discrepancy between the measured and predicted results that may be apparent in the rose plots, the scatter and time series comparison plots may be consulted. Also note that positive values in the time-series plots represent currents flowing towards the north and east for the respective current velocity components. The major use of the north-south velocity plots is to confirm that the model is correctly representing the magnitude and timing in the onshore-offshore tidal flow and that there is no loss of match over time. Matches in the east – west current component, which will be primarily due to wind-induced longshore drift can be observed by comparison of the rose and scatter plots.

The comparisons indicated that the current amplitudes and vertical current profile were predicted to a good level of accuracy by the model for all three locations, indicating that the model has suitable spatial stability. The scatter and rose plots indicate that the magnitude and range in current speeds was well represented. Similarly, the direction of the currents was simulated suitably well by the model for each layer, but with an offset in the tidal current direction between the model and measured data of +5 to +10 degrees. Tidal currents were observed to flow towards the northwest during the ebb and to the southeast during the flood at all three sites, consistent with the observations. The measured data indicated a marginally larger east-west component than that predicted in the model. If this outcome is general for all parts of the model, the comparisons indicate that the model may marginally underestimate migration to the east or west, at least in the deeper parts of the model. The east-west

component in the modelled current was a response to the wind data specified over the domain. It was recognised that the wind directions had a small onshore-offshore bias due to the application of a spatially constant wind, using wind directions observed at Port Hedland (with magnitudes alone scaled up to match the offshore measurements). Currents will tend to steer shoreward on approach to the land. Hence, the small shoreward discrepancy observable in the current direction at the offshore sites was considered to be a small and acceptable bias. The effect of this small bias on the sediment modelling would be a small overstatement of migration onshore for the deeper sections of the model and, hence would be conservative in terms of the concentrations predicted over time over shallower sections of the model domain.

Comparisons for the Beacon 15 data show a higher correlation between measured and modelled data at the seabed than at the surface (Figure 6-11, Figure 6-12; Appendix C). The surface measurements at Beacon 15 show a number of erratic amplifications in current speed which are likely to be measurement faults. The slight deviation of the model-predicted current direction from the measurements is again apparent at this site, again relating to a moderately lower east-west current velocity being generated in the model.

Further statistical analysis of the model skill at replicating the hydrodynamics was conducted through the use of the Index of Agreement (IOA), presented in Wilmott (1981). This index, commonly used to assess model skill, is calculated as:

$$\mathrm{IOA} \;=\; 1 - \frac{\sum |X_{\mathrm{model}} - X_{\mathrm{obs}}|^2}{\sum \left(|X_{\mathrm{model}} - \overline{X_{\mathrm{obs}}}| + |X_{\mathrm{obs}} - \overline{X_{\mathrm{obs}}}| \right)^2}$$

In this equation, *X* represents the variable being compared. *X* under a bar indicated the mean over time for that variable. A perfect agreement can be said to exist between the model and field observations if the index gives a measure of one, and complete disagreement will produce an index measure of zero (Wilmott 1981). This IOA was applied to each of the current velocity components. Consistently, the IOA was above 0.9, indicative of a strong correlation between the measured and modelled datasets. For the Quantum Inshore and Offshore AWAC sites, the model produced the highest IOA during February and October, with IOA's consistently above 0.92. The Beacon 15 site indicated strong correlations during February and April, with IOA's above 0.94, reducing during June and October to 0.91.

The results of the combined analysis indicated that the predicted current data was fit for the purpose of calculating the transport and resuspension of sediments.
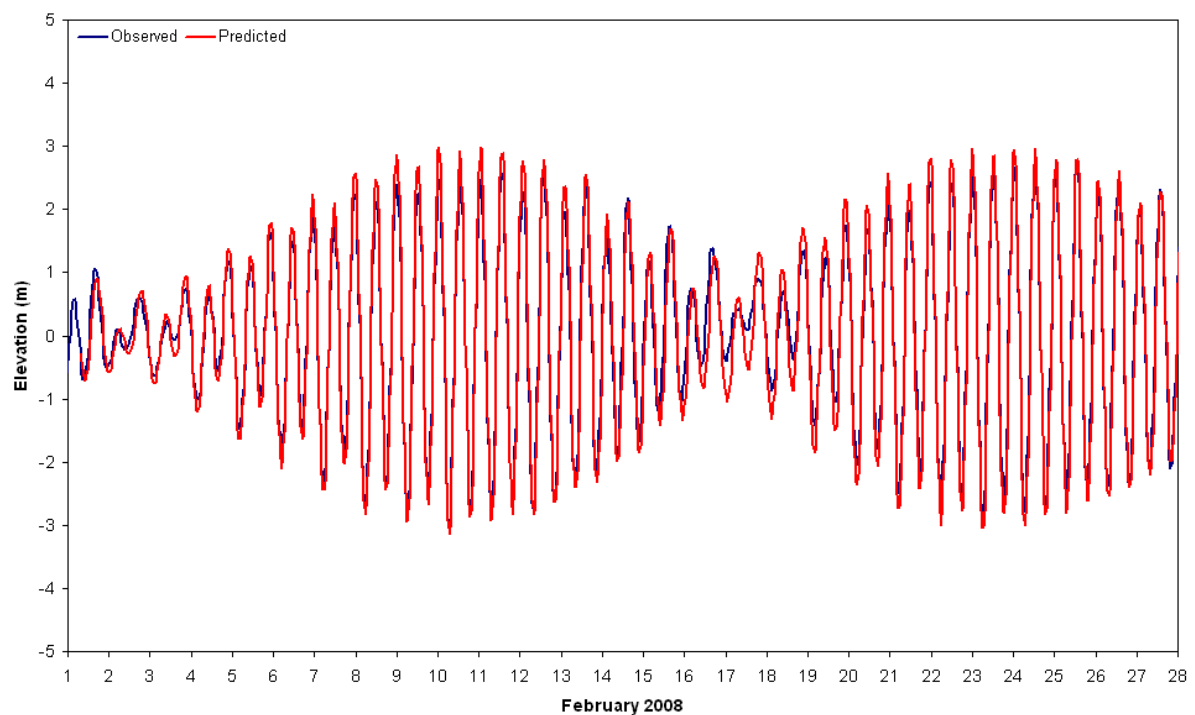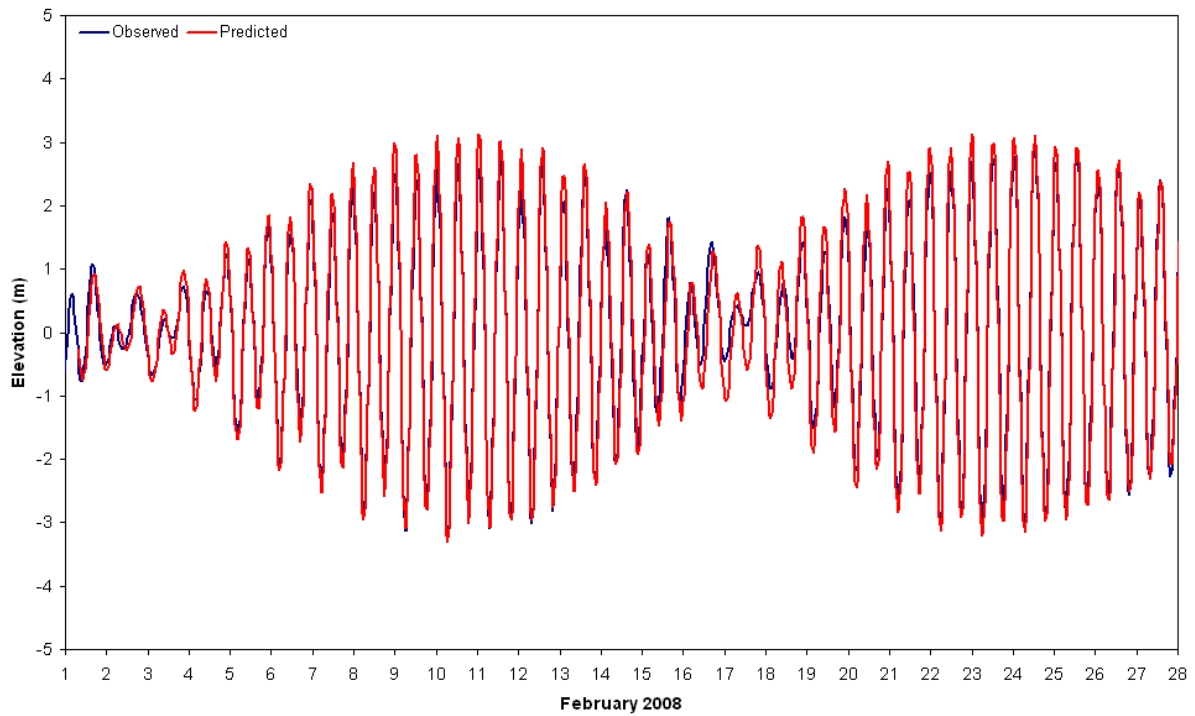
Figure 6-6 Comparative surface elevation during February 2008 for Quantum Inshore AWAC site (top) and Quantum Offshore AWAC site (bottom). Blue lines show observed data and red lines show the model results.

Measured   **Predicted**
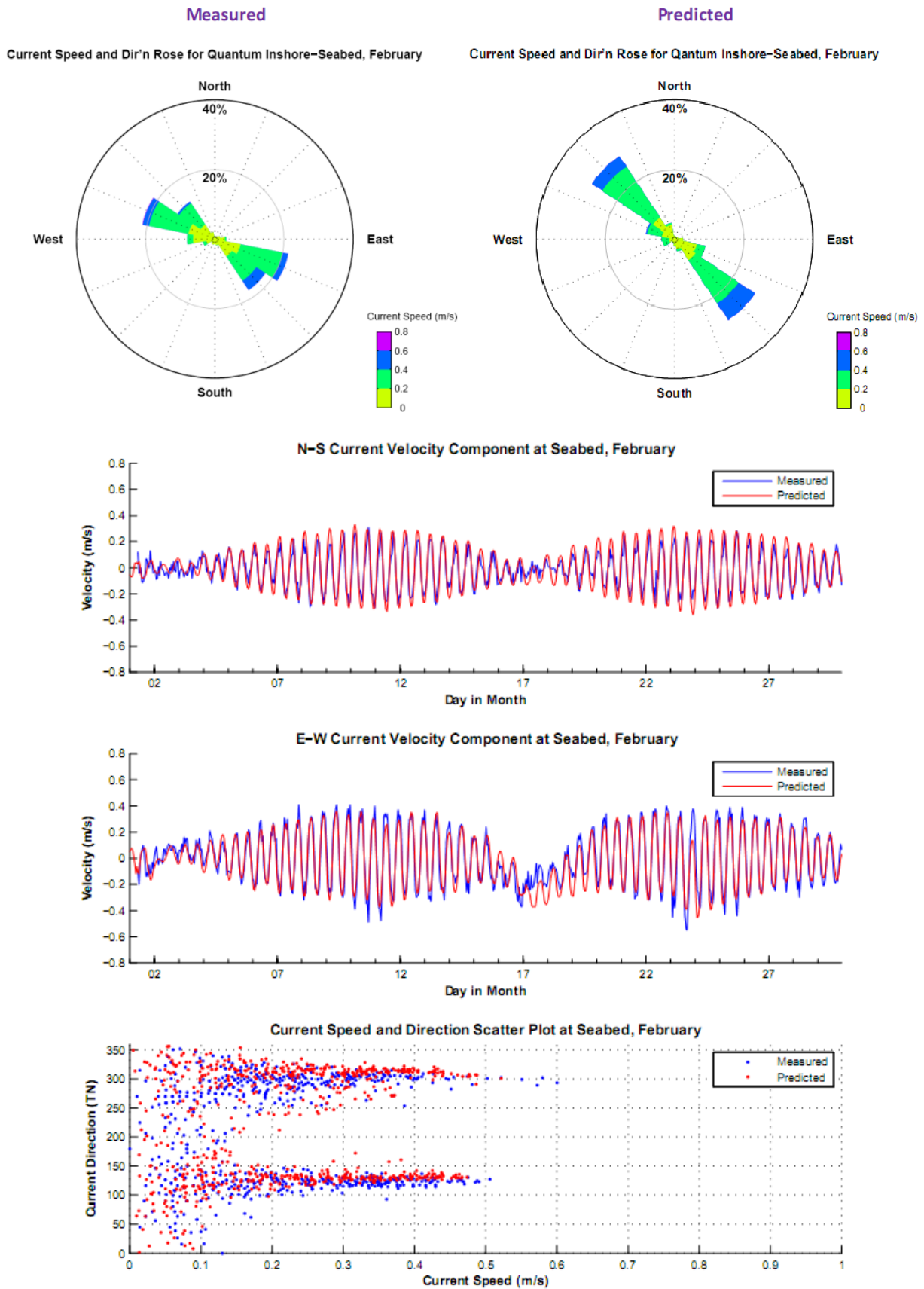
Figure 6-7 Comparison between current magnitude normalized for the north direction during a representative summer month (February 2008) for the Quantum Inshore AWAC site at the Seabed. Note: positive values in this graph represent currents flowing to the north.
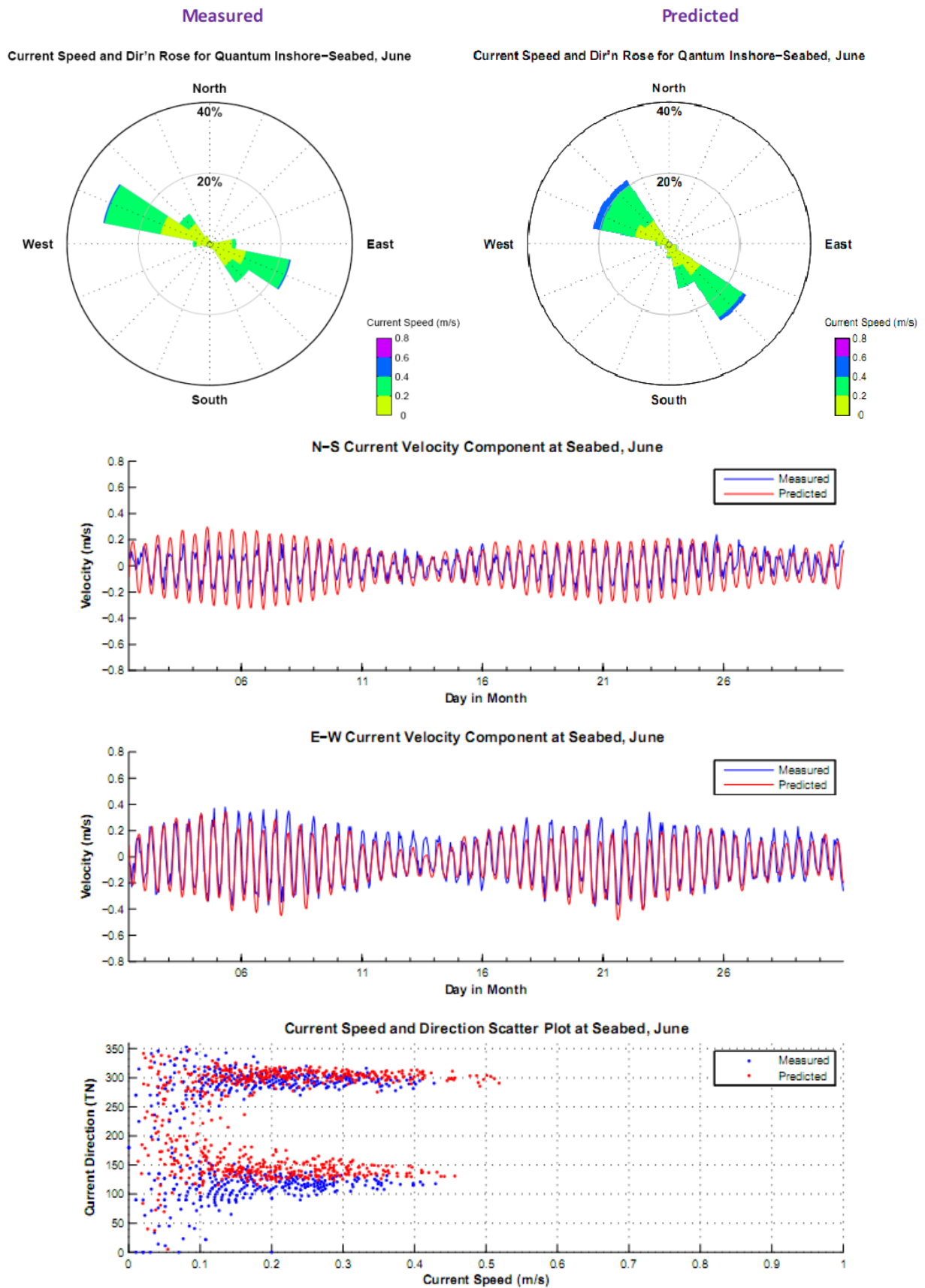
Figure 6-8 Comparison between current magnitude normalized for the north direction during a representative winter month (June 2008) for the Quantum Inshore AWAC site at the Seabed. Note: positive values in this graph represent currents flowing to the north.
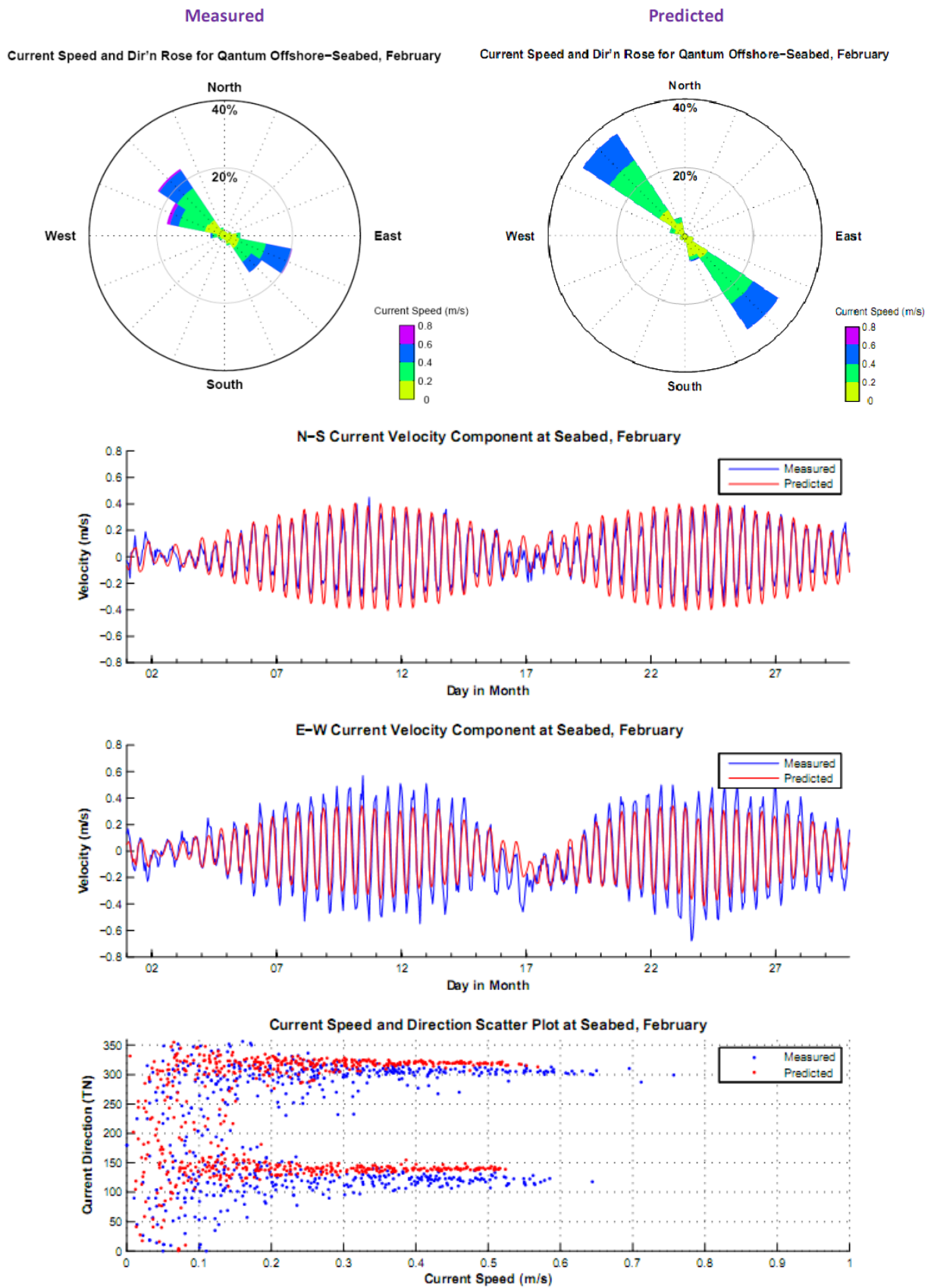
Figure 6-9　Comparison between current magnitude normalized for the north direction during a representative summer month (February 2008) for the Quantum Offshore AWAC site at the Seabed. Note: positive values in this graph represent currents flowing to the north.
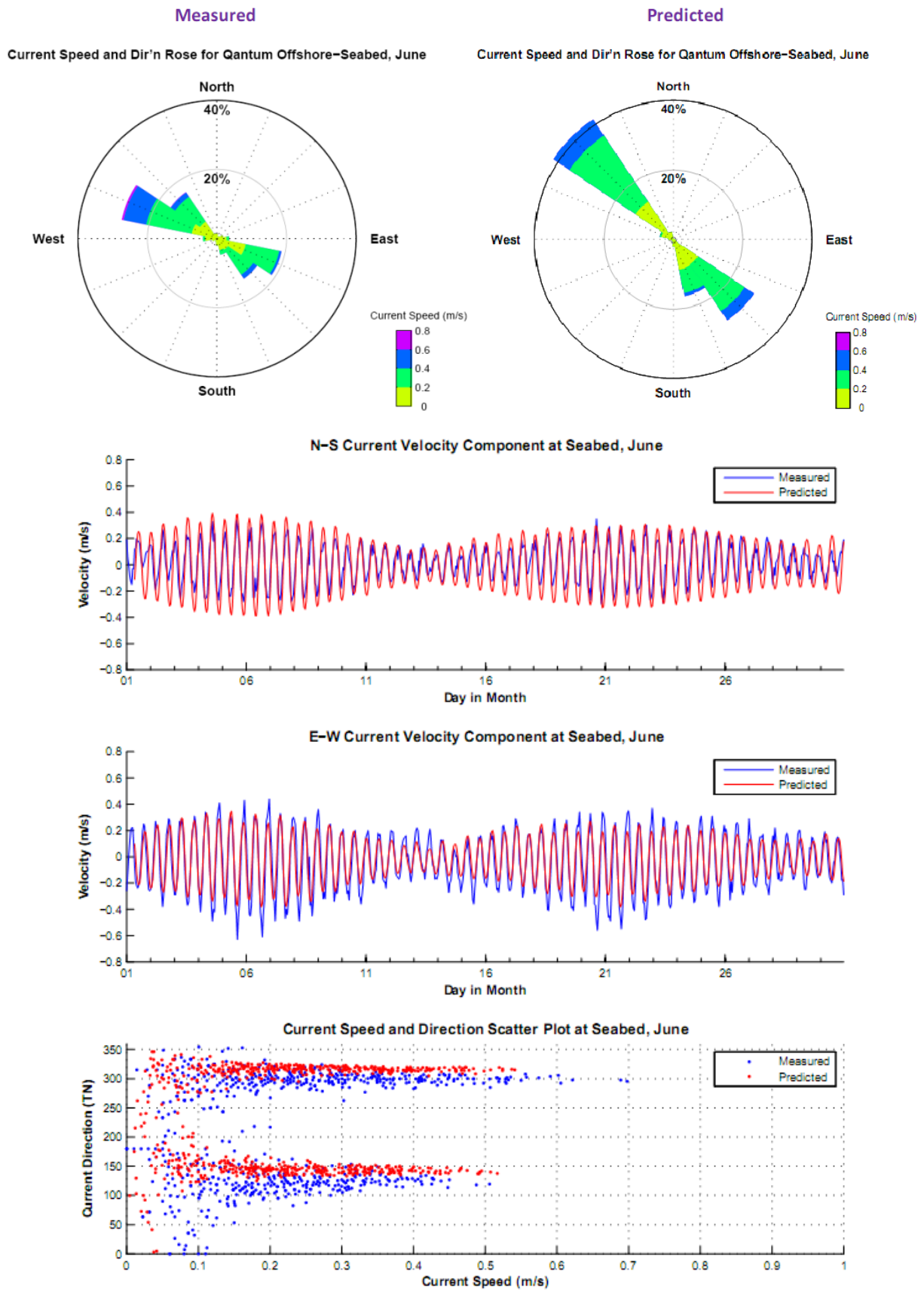
Figure 6-10 Comparison between current magnitude normalized for the north direction during a representative winter month (June 2008) for the Quantum Offshore AWAC site at the Seabed. Note: positive values in this graph represent currents flowing to the north.
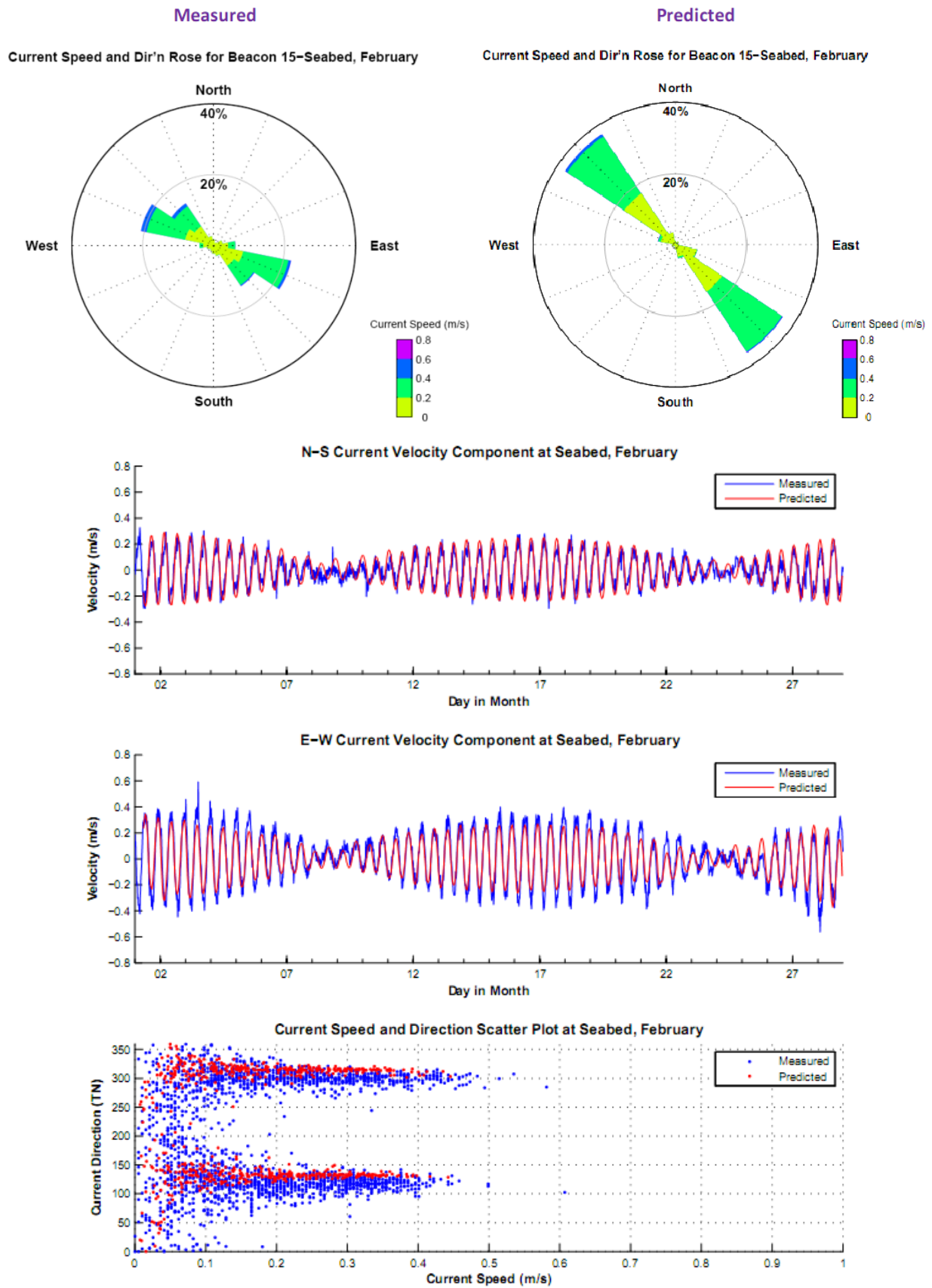
Figure 6-11 Comparison between current magnitude normalized for the north direction during a representative summer month (February 2006) for the Beacon 15 site at the Seabed. Note: positive values in this graph represent currents flowing to the north.
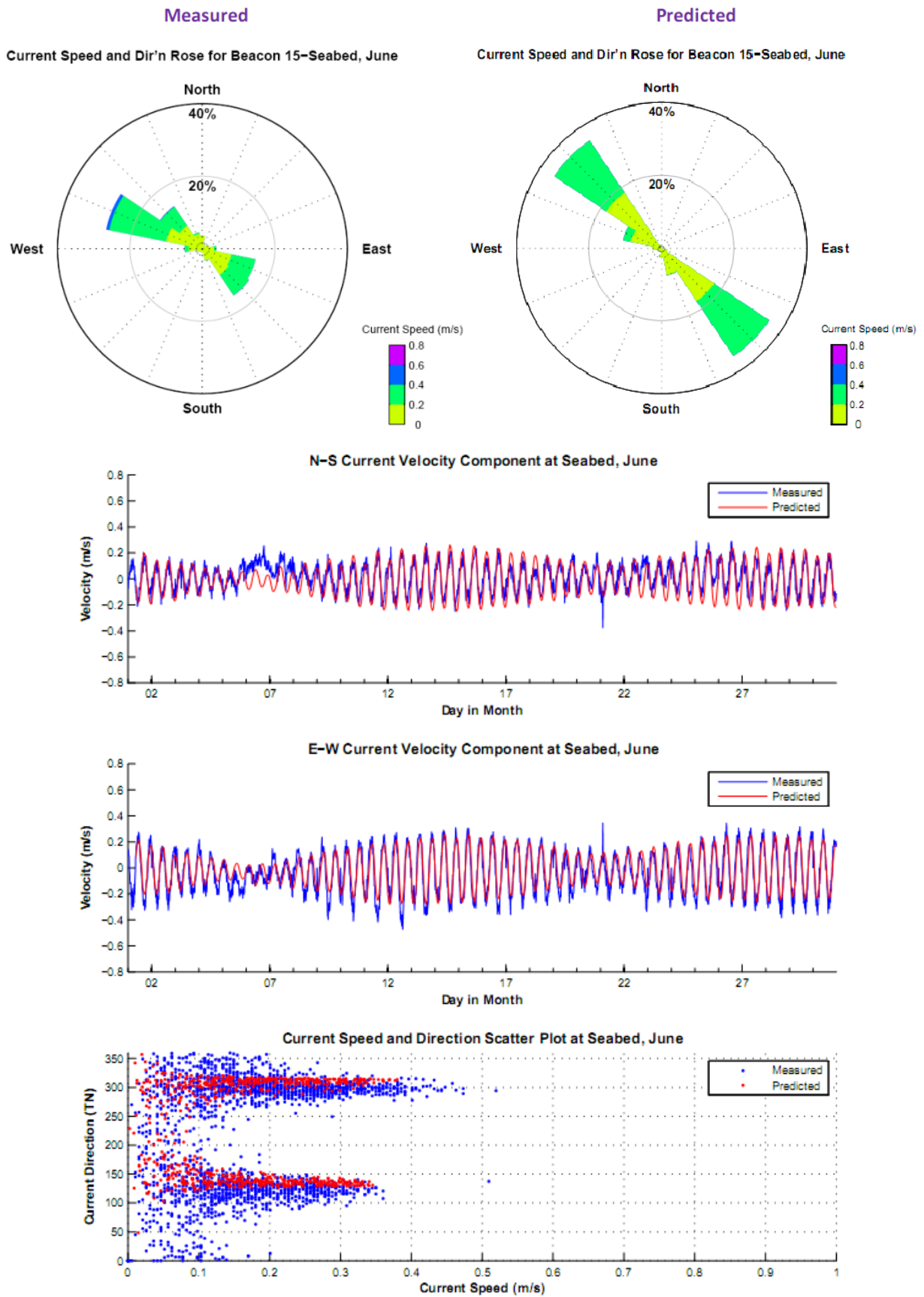
Figure 6-12 Comparison between current magnitude normalized for the north direction during a representative winter month (June 2006) for the Beacon 15 site at the Seabed. Note: positive values in this graph represent currents flowing to the north.

6.7   Typical Circulation

Typical flood and ebb tidal circulation patterns in the nearshore region are shown in Figure 6-13 and Figure 6-14 respectively. The current vectors (yellow arrows) show the typical SE (flood) – NW (ebb) setting of the tide in the area, together with the strong modification in the vicinity of the harbour entrance. Note that the arrow density varies in this display with the model resolution.

6.8   Hydrodynamic sample data

Modelling was completed to create a 10 year hydrodynamic data set spanning 1998 to 2007 inclusive. The data was archived as three-dimensional current vectors, varying horizontally and vertically, for each hour of each year of simulation.
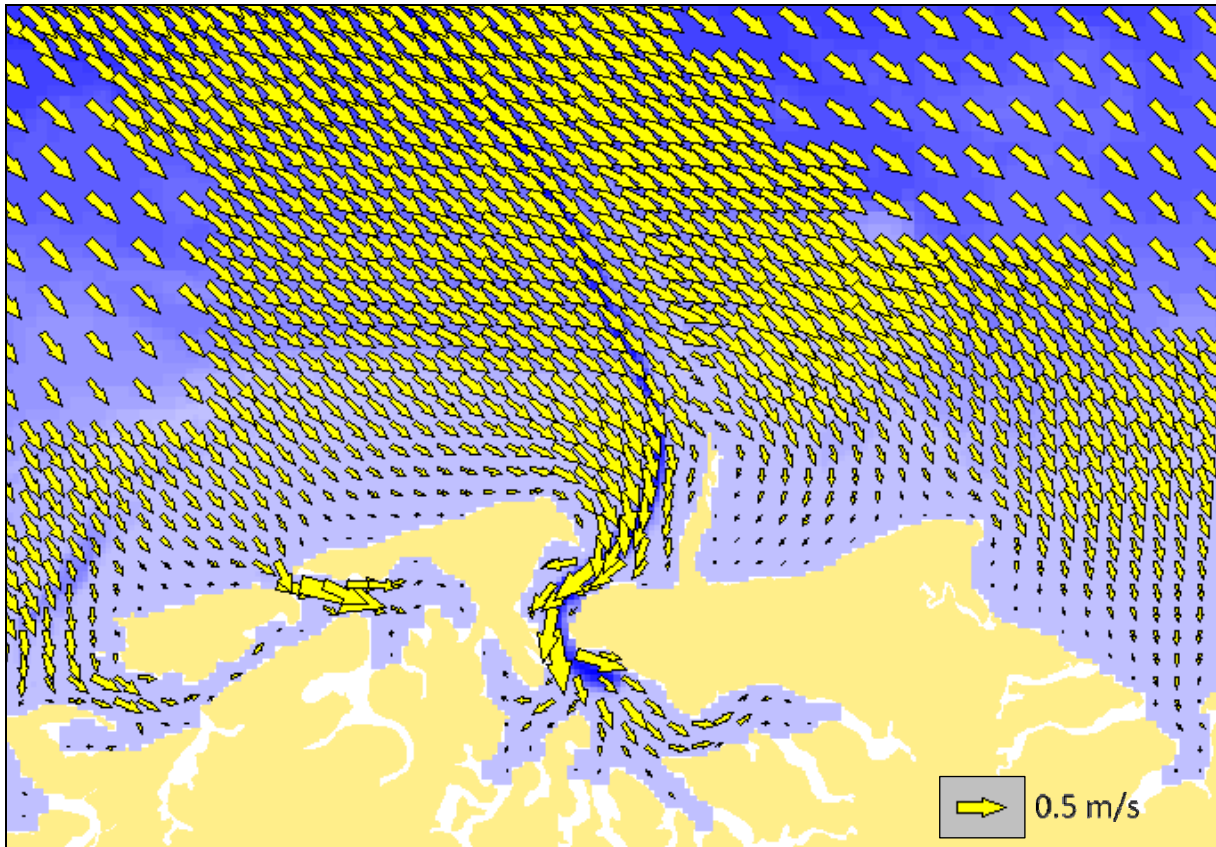
Figure 6-13 Typical flood tide circulation patterns for the mid-water column over the nearshore area.
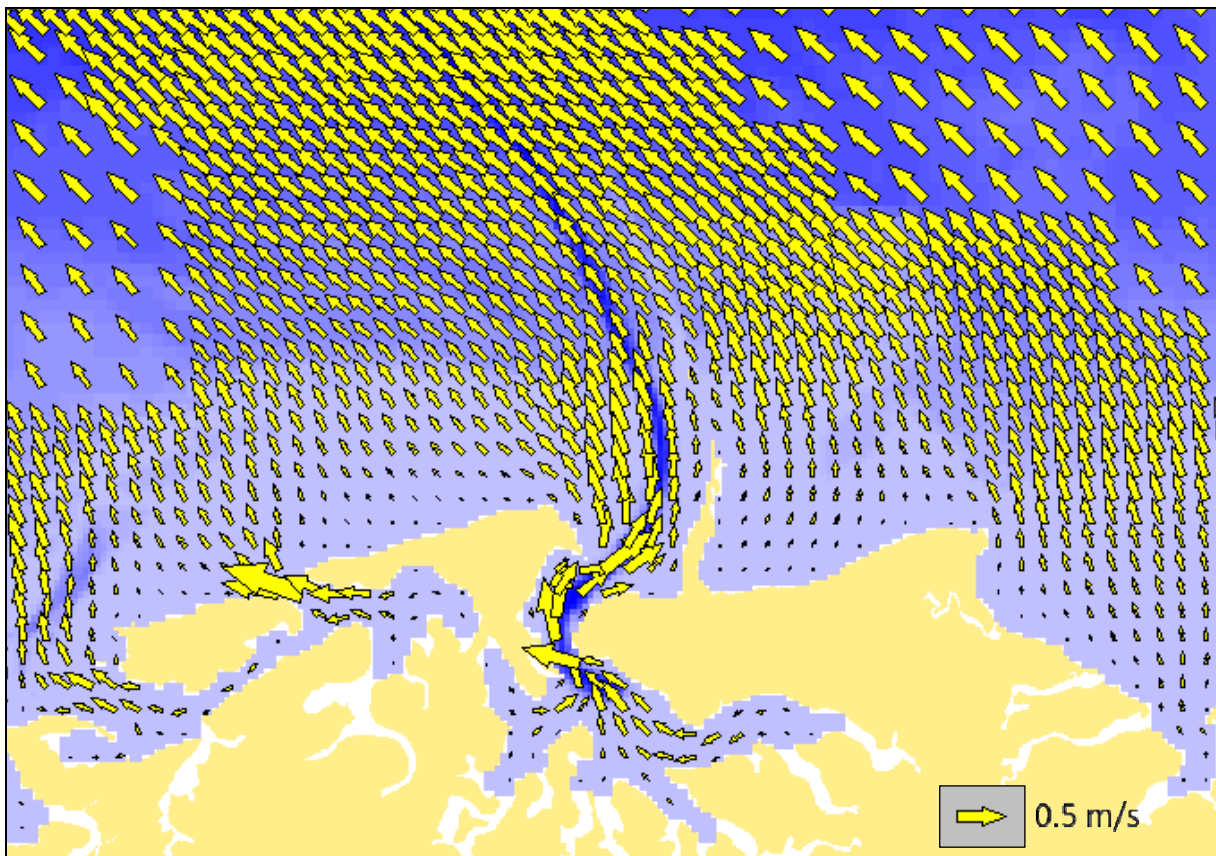
Figure 6-14 Typical ebb tide circulation patterns for the mid-water column over the nearshore area.

7   WAVE MODELLING

7.1   Introduction

To represent the wave-induced component of resuspension, a regional wave model has been established using the Simulating Waves Nearshore (SWAN) model. The SWAN model was developed to simulate spatially-varying wave conditions over a wide domain – spanning at least 75 km either side of the Port Hedland port shipping channel. The large size of the wave model domain was required to enable sediments to be tracked over the long time span of the proposed dredging operation.

The model requirements included both a high spatial resolution, particularly close to the proposed dredge operation, to appropriately represent local variations and long run-times to cover the duration of the proposed dredge operation. The complex coastline around Port Hedland, and the need to cover large areas at different resolutions, combined with the long simulation periods was met by developing and applying an unstructured mesh. The regional wave model was developed using the unstructured mesh version of SWAN.

The SWAN model was run by hindcasting spatial wave parameters over the model domain for the same 10 year span that was modelled for current vectors. This database provided a robust sample from which inter-annual variability could be analysed. The model results have been validated against the available measured wave data, as described below.

7.2   Model Description

The SWAN model is a spectral phase-averaging wave model developed by the Delft University of Technology (Holthuijsen et al, 2001). SWAN is a numerical model for simulating realistic estimates of wave parameters in coastal areas for given wind, bottom and current conditions. The model is a third generation model based on the energy balance equation (for this study).   In general, SWAN includes algorithms for the following wave propagation processes: propagation through geographic space, refraction due to bottom and current variations, shoaling due to bottom and current variations, blocking and reflections by opposing currents, transmission through or blockage by obstacles. The model also accounts for the dissipation effects due to whitecapping, bottom friction and wave breaking as well as non-linear wave-wave interactions. SWAN is fully spectral (in all directions and frequencies) and computes the evolution of wind waves in coastal regions with shallow water and ambient current.

7.3   Computational Grid and Bathymetry

The computational grid for the SWAN model was set up using the unstructured mesh option. Unstructured meshes, which have varying cell resolutions, provide a much better representation of complex boundaries such as coastlines and areas around islands than do conventional regular grids. The biggest advantage of unstructured meshes is that they provide the opportunity to concentrate mesh resolution in areas of interest and regions of strong bathymetry variations, to a degree not possible using a regular or curvilinear grid. There is no need for nesting and an unstructured mesh will in general resolve the model area with superior accuracy and with significantly fewer grid points than with regular or curvilinear

grids. Although the computer processing unit cost per iteration is relatively higher than cases with structured grids, this effect is more than offset by the reduction in the number of grid points. Thus, because of the large model domain and long simulation times required, the unstructured mesh version of SWAN was selected as superior for this study. The final computational mesh is shown in Figure 7-1. The high resolution area is shown off the coast of Port Hedland.
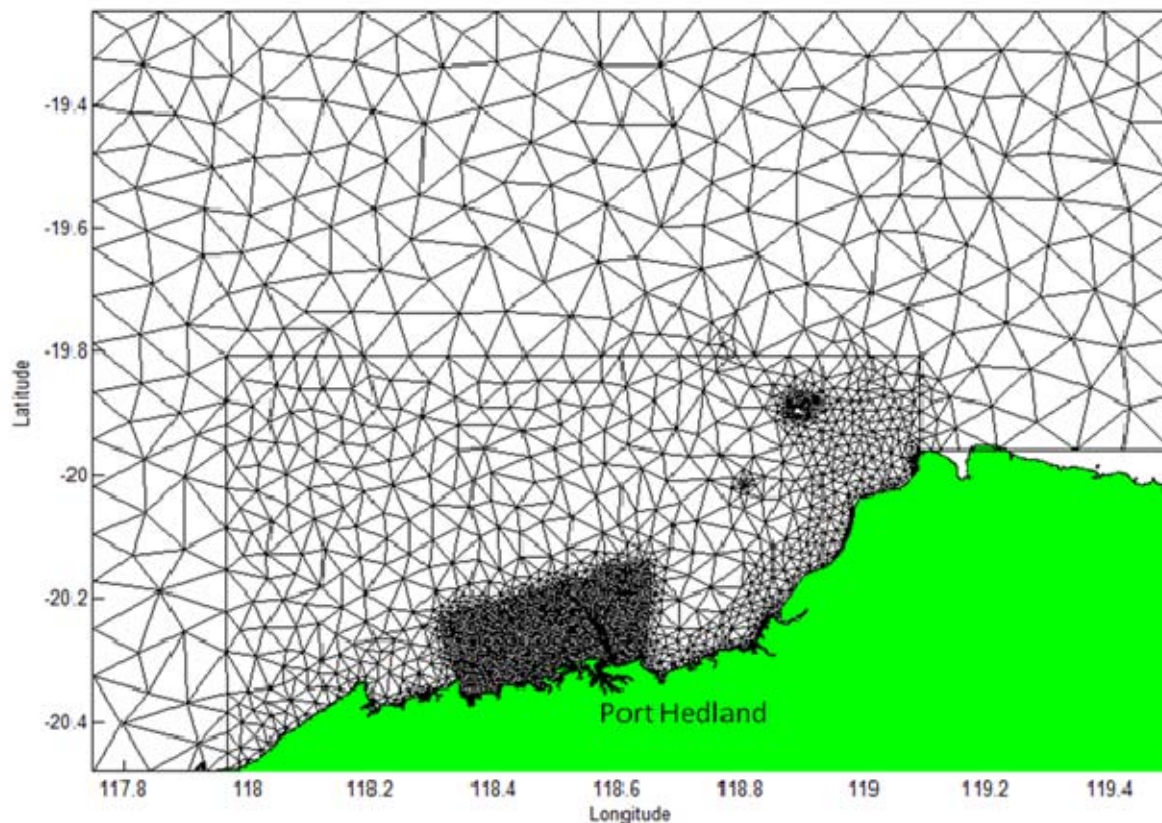
Figure 7-1 Computational mesh covering the domain for the SWAN model.

The mesh resolution has been adjusted to maximise computational efficiency. Generally, the mesh has higher resolution in areas where the bathymetry or evolution of the waves change rapidly and lower resolution in areas where the physics or depth changes less. The final unstructured mesh contained 5,173 triangles with 2,801 vertices. The minimum triangle edge length in the mesh was 124.6 m and the maximum triangle edge length 9,615 m.

The representation of the bathymetry over the mesh is shown in Figure 7-2. The same bathymetric dataset used in the HYDROMAP modelling was applied to set the bathymetry within the SWAN model mesh. Representation of the bathymetry over the immediate area of the operations is shown in Figure 7-3. The area of interest encompasses a boundary that encloses the environmentally sensitive areas and exclusion zones (for environmental impact), and the potential spoil grounds. The area of interest is bounded along the coast by Cooke Point to the north, to the 118.2° longitude to the south and offshore to the 20 m contour. The

mesh resolution ranged from triangles with an edge length of 124 m to 144 m. The mesh provided sufficient resolution for the shipping channel to be represented by no less than two triangles across the width.
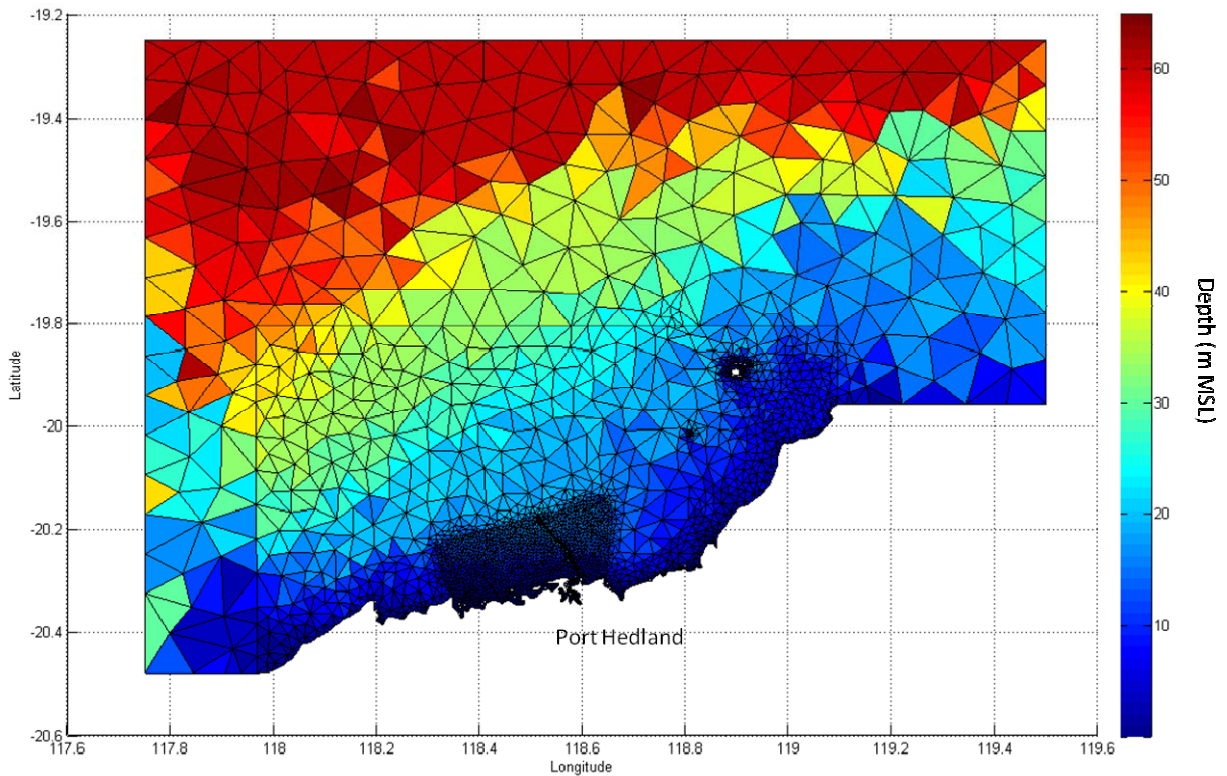
Figure 7-2 SWAN model Bathymetry over the computational mesh. The mesh spans the coast from Cape Cossigny on the west to Larrey Pt. on the east and offshore to a depth of 60 m. Depths are shown with reference to MSL.
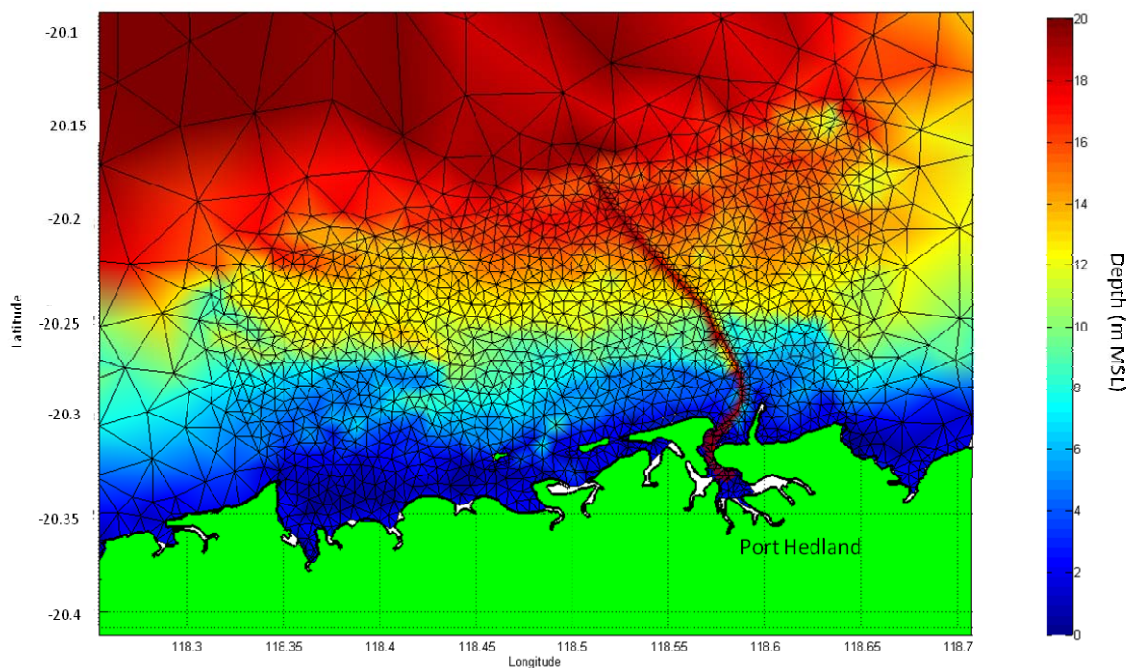
Figure 7-3 Magnified view of the unstructured mesh resolution over the area of interest. Depths are shown with reference to MSL.

7.4   Model Forcing and Boundary Conditions

7.4.1   Water Levels and Currents

Water levels and currents were interpolated from the HYDROMAP output onto the SWAN unstructured mesh. The ambient current can affect the growth and decay of waves and in the case of a strong opposite current the wave steepness and wave height can increase significantly. In the case of Port Hedland, the local wind-generated currents are not generally strong enough to have a significant effect. However, during storms and periods of strong local winds, current-induced white-capping and wave reflections may have an effect. Thus, currents were included in the SWAN modelling.

The water levels were included to capture the effect where elevated water levels allow larger waves to propagate to the coast. Hence, higher energy waves can be predicted along the coast than that would be predicted by the model if water level variations were not included.

7.4.2   Waves

SWAN requires the input of wave spectra along the three open boundaries of the model domain. For use as boundary input into the SWAN model, hourly spectral wave data was supplied by MetOcean Engineers Ltd from their WW3 global wave model. In total, spectral wave data was provided at 5 locations around the perimeter of the model grid. The locations of the supplied boundary data are presented in Table 7-1.
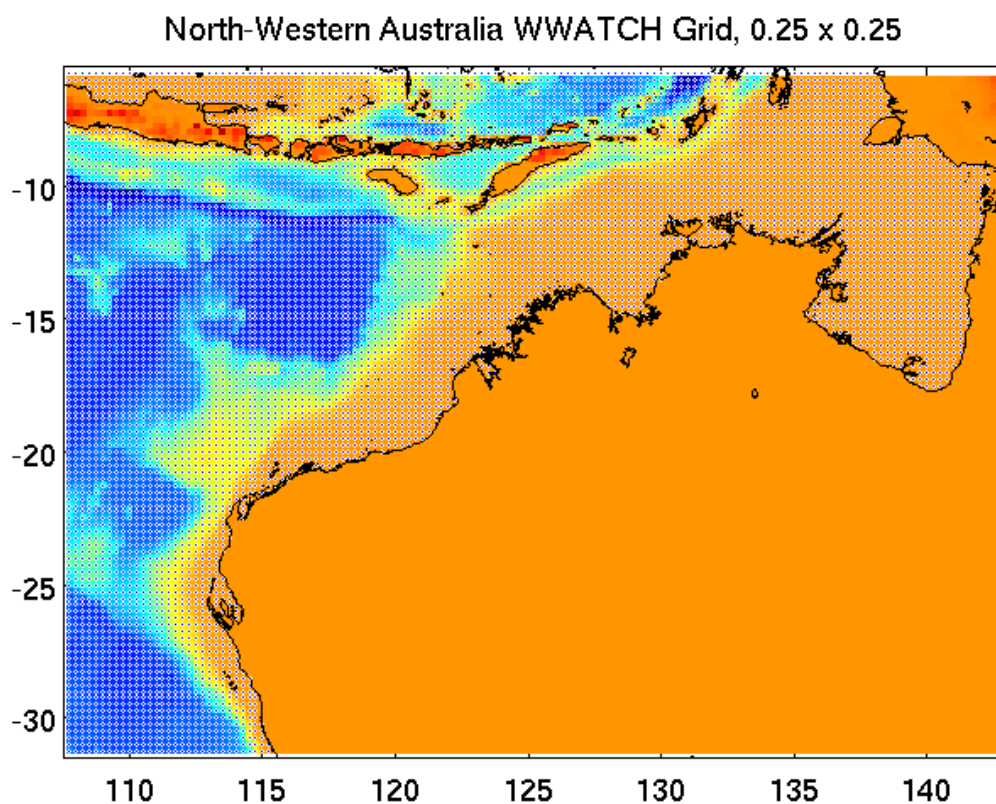
Figure 7-4 North-west shelf WW3 wave model grid (supplied by MetOcean Engineers Pty Ltd)

The spectra are imposed over segments along the boundary of the computational mesh. The supplied wave spectra had 25 logarithmically spaced frequency bins with a frequency range of 0.0418 to 0.4114 Hz and 24 equally spaced directional bins. The provided spectral boundary data was reformatted for the SWAN model. Only the incoming wave components of these spectra are used by SWAN. The incident wave field is prescribed at a point for each segment, these points are characterized by their distance from the begin point of the segment. The wave spectra for each grid point on the boundary of the computational grid are calculated by SWAN by the spectral interpolation technique internal to the model.

The distribution of the supplied input wave data along model grid boundary is shown in Figure 7-6.
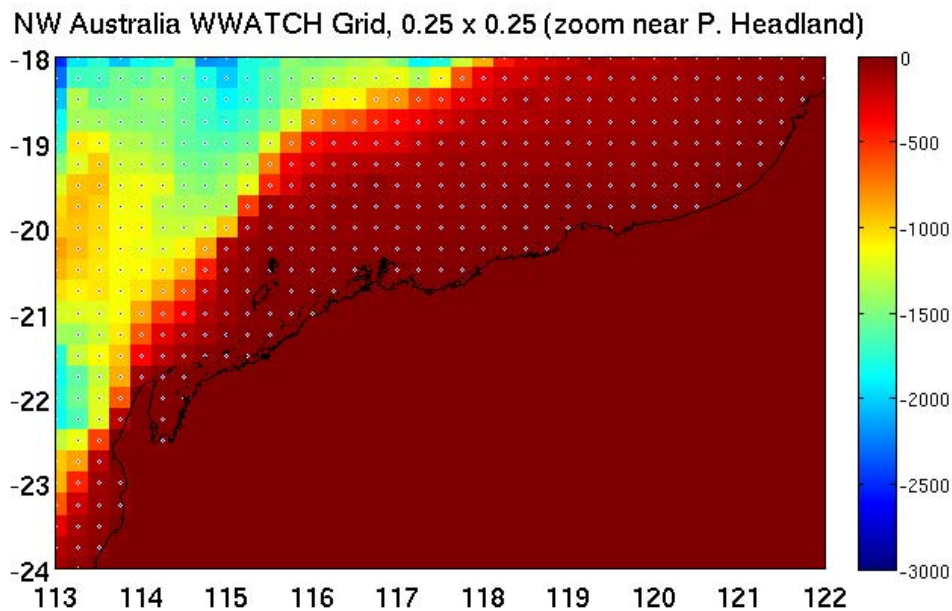
Figure 7-5 Magnified region of the WW3 grid around Port Hedland (courtesy MetOcean Engineers Pty Ltd).
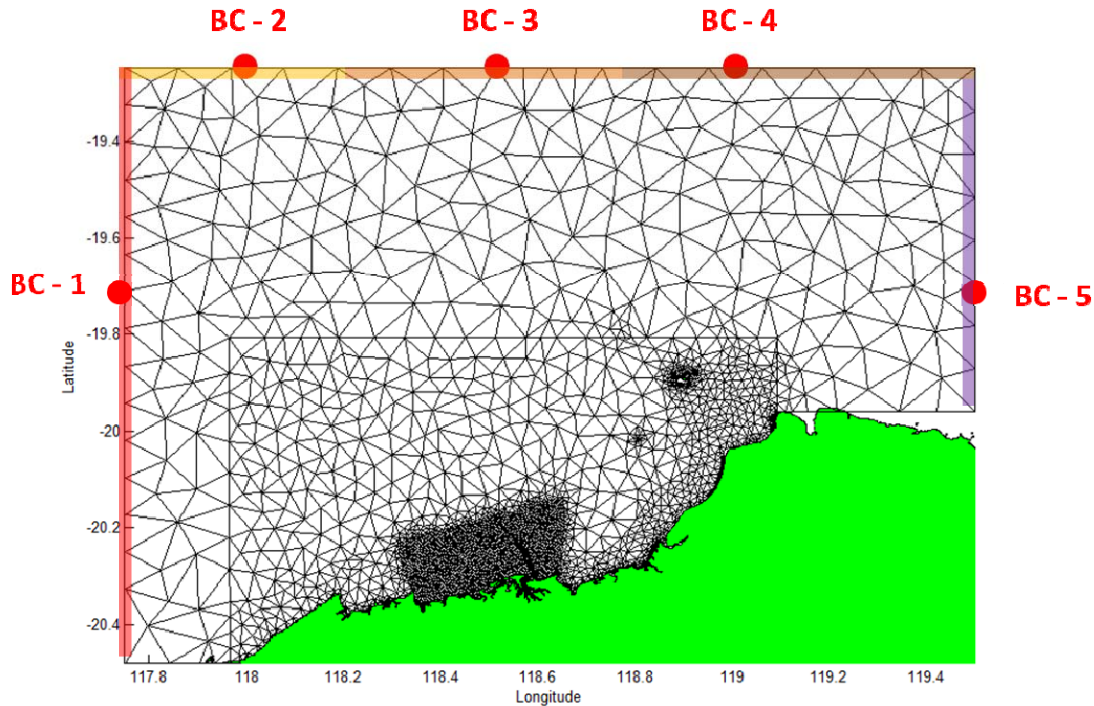
Figure 7-6 Distribution of boundary conditions along the boundary of the computational grid.

The southern boundary is specified completely as land. The land boundary does not generate waves and in SWAN it absorbs all incoming wave energy.

Table 7-1 Location of supplied spectral wave input data.

MetOcean Point No.	Longitude	Latitude
1	117.75°E	19.75°S
2	118.00°E	19.25°S
3	118.50°E	19.25°S
4	119.00°E	19.25°S
5	119.50°E	19.50°S

A plot showing the summary wave parameters of the supplied wave data at the northern (Point 3), western (Point 1) and eastern (Point 5) boundaries of the model domain is presented in Figure 7-7. The parameters were calculated from the supplied wave spectra.
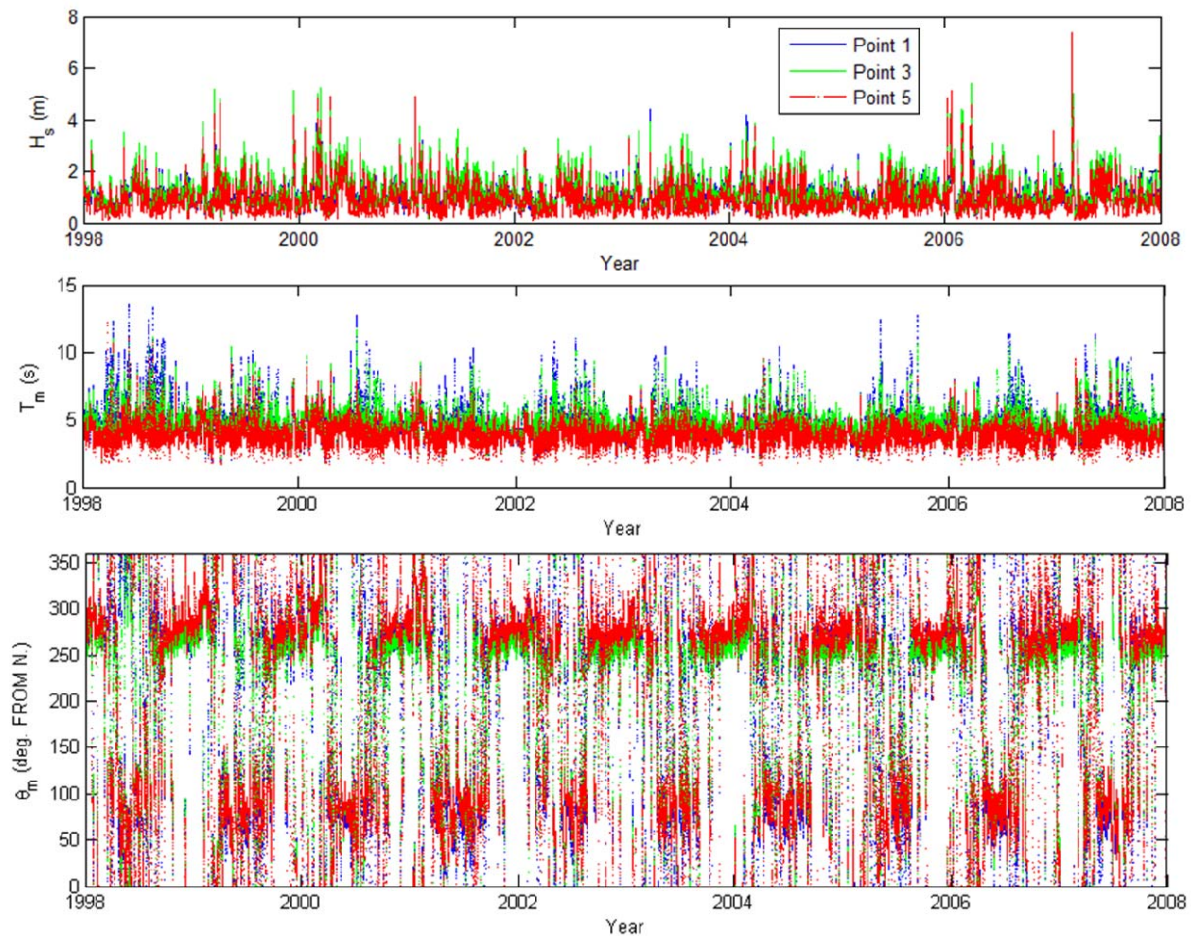
Figure 7-7 Summary wave parameters for the supplied spectral boundary conditions.

7.4.3   Wind

The same wind dataset as used in the hydrodynamic modelling was adopted for the SWAN assessment. Two wind records were available for use in this study:

1. Long term record at Port Hedland Airport provided by BOM for 1993 to 2008.

2. Data at Beacon 15 from May 2000 to August 2007.

The BOM data was selected for use in the wave model and was adjusted to match the measured conditions at the Beacon 15 offshore site as per the hydrodynamic model setup.

7.5   Model Parameters

The physical processes selected for the simulations were: whitecapping, depth induced wave breaking, bottom friction and triad wave-wave interactions. The process of whitecapping in the SWAN model is represented by the pulse-based model of Hasselmann (1974), reformulated in terms of wave number as to be applicable in finite water depth (Komen *et al.*, 1984). The default SWAN parameterisation of depth induced wave breaking was used with a 0.73 constant breaking factor (Eldeberky *et al.*, 1996b).

Bottom friction was activated using the Madsen model (Madsen *et al* 1988). This formulation is similar to that of Hasselmann *et al.* (1968), but in this case the bottom friction factor is a

function of the bottom roughness length scale and the wave conditions. The bottom roughness length scale was set to 0.05 m. For modelling the triad wave-wave interaction SWAN uses the Lumped Triad Approximation (Eldeberky, 1996a) in each spectral direction. Quadruplet wave-wave interaction was set to default.

A non-stationary SWAN simulation was performed with the time step of 1 minute with the convergence requirement set to 98.0% of computational points. After an initial model spin-up, the convergence was generally obtained in the first few iterations, occasionally requiring up to 20 iterations when the sea state became particularly dynamic.

Model output was written on an hourly time-step for the entire computational grid that was later post-processed to obtain wave parameters at the validation sites.

7.6   Model Validation

The wave model was validated against various measured data available for the region. The data is summarised below:

- Port Hedland Port Authority Beacon 15 and Beacon 16 - contiguous wave height and period (Electromagnetic Wave and Tide Monitoring System (EWS) spanning 2000 to 2007).

- Port Hedland Port Authority Beacon 16 - wave height, period and direction (Acoustic Waves And Current profiler (AWAC) spanning 2004 to 2007).

- Port Hedland Port Authority Beacon 15 - wave height, period and direction (Directional Waverider Buoy (DWR) spanning 2006 to 2007).

- MetOcean Engineers – wave height, period and direction at offshore and inshore locations (Acoustic Waves And Current profiler (AWAC) spanning 12/15/2007 to 3/10/2008).

- MetOcean Engineers – wave height, period and direction at offshore and inshore locations (Directional Waverider Buoy (DWR) spanning 12/15/2007 to 3/10/2008).

7.6.1   Beacon 15 EWS

Data for the Port Hedland Port Authority Electromagnetic Wave and Tide Monitoring System (EWS) at navigation Beacon 15 has been used to validate the model predicted significant wave height and mean wave period.
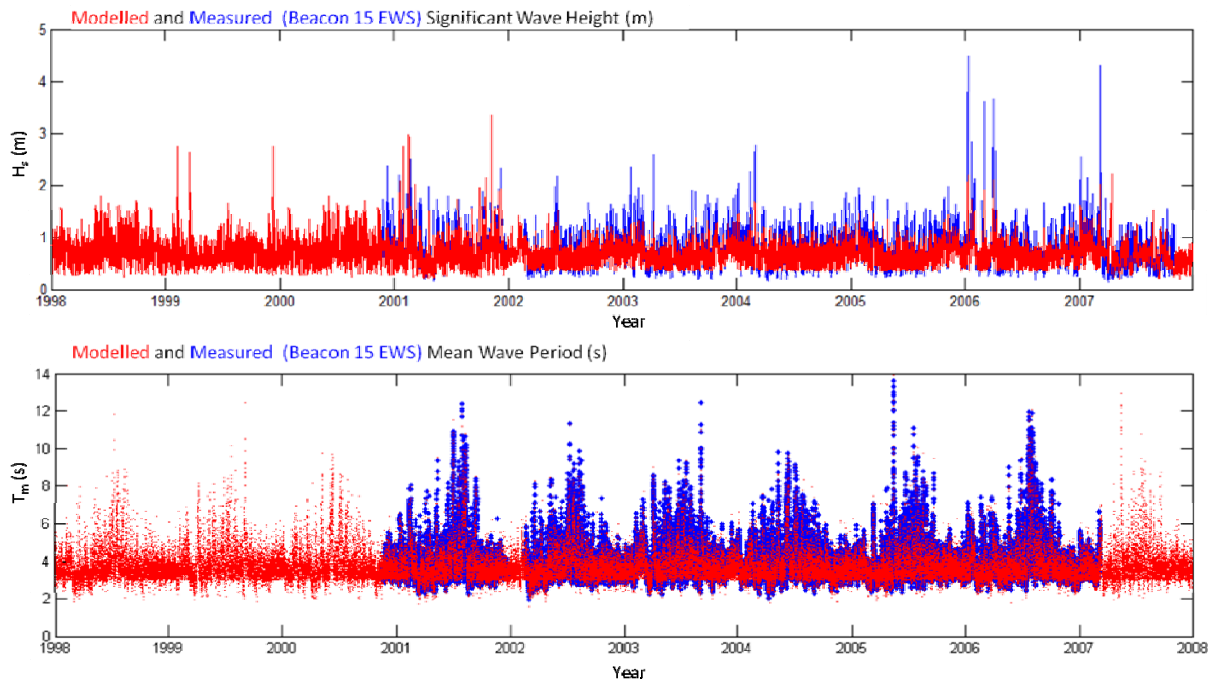
Figure 7-8   Comparison of measured H_s and T_m at the Beacon 15 EWS site (shown in blue) with SWAN model wave parameters (shown in red).

The model results show an excellent agreement with the measurements for the parameters analysed (H_s and T_m). The correlation coefficient between the modelled and measured is 0.85 and the mean error was calculated to be 11 cm (root mean square error = 14 cm). The modelled mean wave period also gave good agreement with the measured mean wave period. The model is able to capture the switching between sea and swell conditions evident in the Beacon 15 data.

Comparison between summary statistics for the SWAN wave model and the Beacon 15 station significant wave heights are shown in Figure 7-9. The model results are able to accurately capture the variations in wave height in the Beacon 15 data. The SWAN model under-predicts wave heights for the >95 percentile waves, which were likely the result of cyclones not resolved in the modelling.

Comparison between summary statistics for the SWAN wave model and the Beacon 15 station mean wave periods are shown in Figure 7-10. The model results are able to accurately capture both the range and variations in wave periods in the Beacon 15 data.
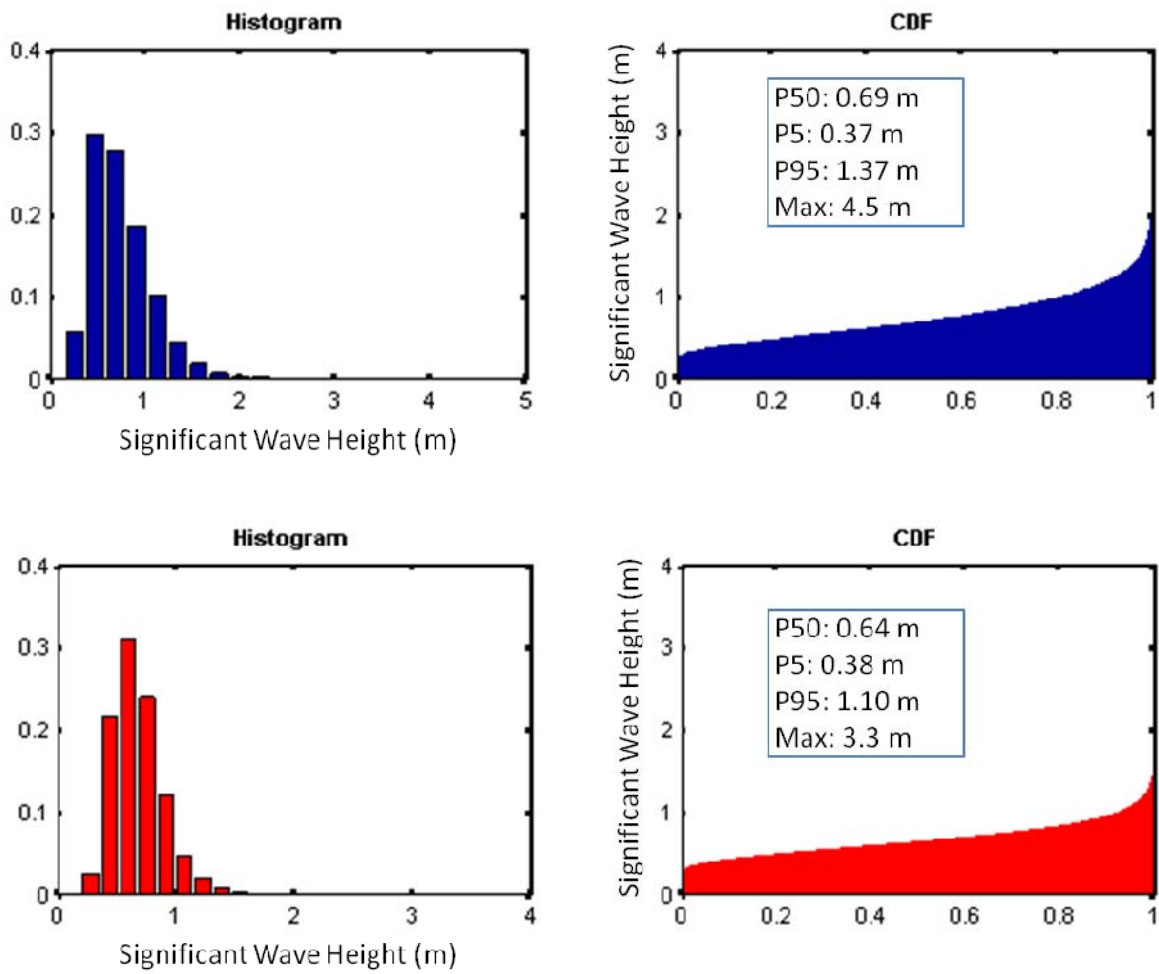
Figure 7-9   Comparison of summary statistics between modelled (Beacon 15) and measured significant wave height.
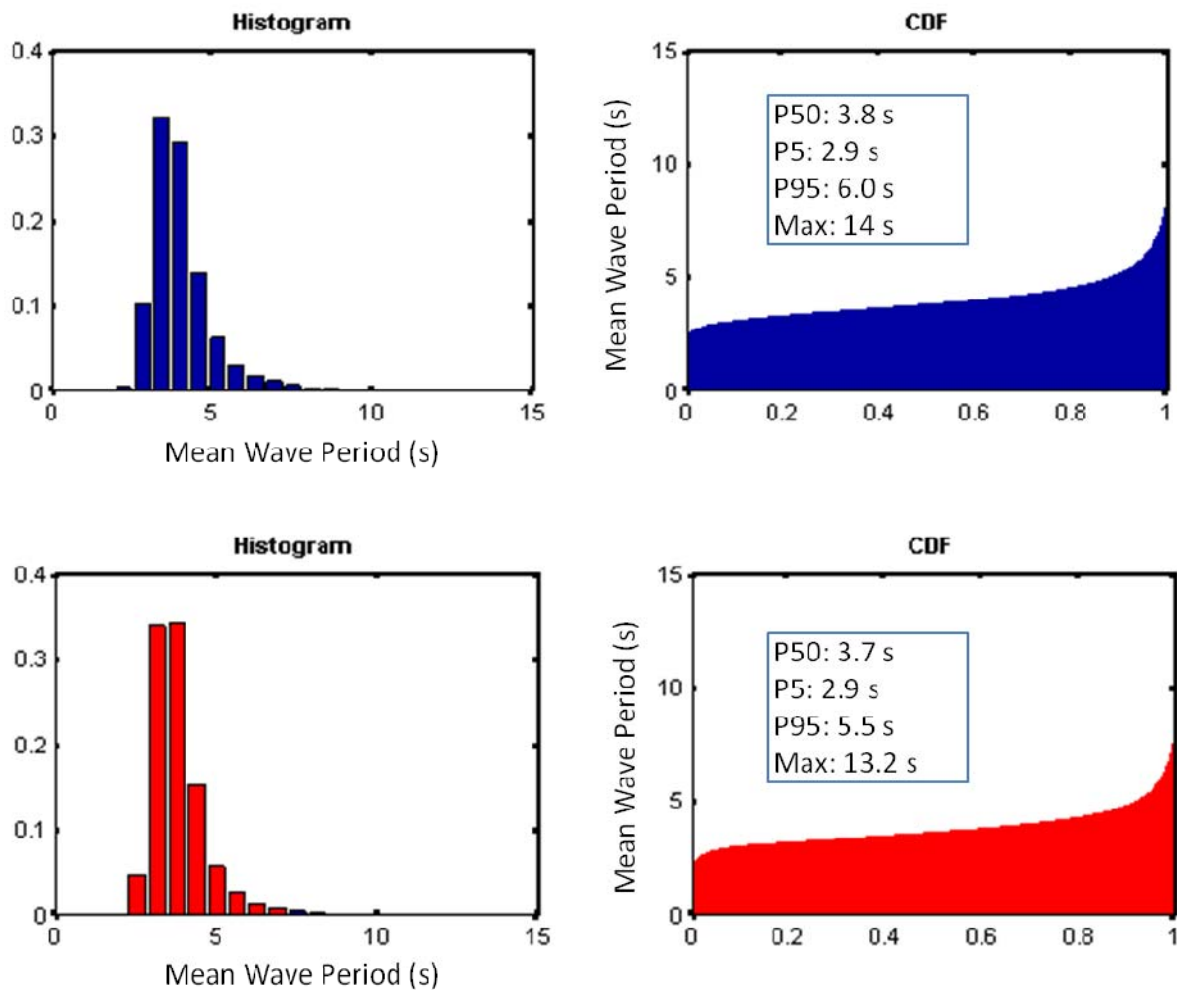
Figure 7-10 Comparison summary statistics of model mean wave period against Beacon 3 data.

7.7   Modelled Ambient Wave Climate

The modelled ambient wave conditions are summarised below as joint frequency (percentage occurrence) tables for the 10 year hindcast dataset (1998-2007) as:

- Significant wave height (H_s) vs. Peak wave period (T_p)   (Table 7-2)

- (T_p) vs. Direction   (Table 7-3)

- (H_s) vs. Direction   (Table 7-4)

Table 7-2: Joint frequency for significant wave height (Hs) against peak wave period (Tp) in the10-year data archive.

Joint Frequency Table (%) Showing Hs Against Tp for the Period 01-Jan-1998 to 31-Dec-2007 23:00:00

N=87648	0-2	2-4	4-6	6-8	8-10	10-12	12-14	Total	Cumul.
0-0.25	-	0.06	0.02	*	-	-	-	0.08	0.08
0.25-0.5	0.02	14.68	5.70	0.81	0.15	0.03	*	21.38	21.46
0.5-0.75	0.01	34.03	11.78	1.27	0.25	0.04	*	47.39	68.85
0.75-1	*	16.10	6.44	0.44	0.07	*	-	23.07	91.92
1-1.25	-	3.79	2.02	0.12	*	*	-	5.94	97.86
1.25-1.5	-	0.86	0.67	0.05	*	*	-	1.59	99.45
1.5-1.75	*	0.18	0.16	0.02	-	-	-	0.35	99.80
1.75-2	-	0.06	0.04	*	-	-	-	0.11	99.91
2-2.25	-	*	0.02	*	-	-	-	0.03	99.94
2.25-2.5	-	0.03	*	-	-	-	-	0.04	99.98
2.5-2.75	-	*	*	-	-	-	-	0.01	99.99
2.75-3	-	-	*	-	-	-	-	*	100.00
3-3.25	-	-	-	-	-	-	-	-	100.00
3.25-3.5	-	*	-	-	-	-	-	*	100.00
3.5-3.75	-	-	-	-	-	-	-	-	100.00
3.75-4	-	-	-	-	-	-	-	-	100.00
Total	0.04	69.79	26.87	2.73	0.49	0.08	0.01		
Cumul.	0.04	69.82	96.69	99.42	99.91	99.99	100.00		

* denotes values less than 0.01%   - denotes no records in bin

Metadata:
Project: BHP QUANTUM
Location: Beacon 15 [118.50660 , -20.17450]
Data period: 01-Jan-1998 to 31-Dec-2007 23:00:00
Data source: SWAN version 40.72
Data summary: All Records
Number of Records: 87648

Table 7-3: Joint frequency for peak wave period (Tp) against direction (from) in the10-year data archive.

Joint Frequency Table (%) Showing Tp Against Direction for the Period 01-Jan-1998 to 31-Dec-2007 23:00:00

N=87648	N	NE	E	SE	S	SW	W	NW	Total	Cumul.
0-2	*	-	*	*	*	*	0.01	*	0.04	0.04
2-4	8.69	2.71	5.84	6.82	5.47	5.06	18.28	16.92	69.79	69.82
4-6	3.68	1.23	2.88	3.11	2.48	1.92	5.63	5.95	26.87	96.69
6-8	0.44	0.15	0.39	0.50	0.32	0.21	0.33	0.39	2.73	99.42
8-10	0.08	0.03	0.07	0.09	0.06	0.04	0.03	0.08	0.49	99.91
10-12	0.02	*	0.01	*	0.01	*	*	*	0.08	99.99
12-14	*	-	*	*	*	-	-	-	0.01	100.00
Total	12.93	4.12	9.19	10.53	8.34	7.24	24.29	23.36		
Cumul.	12.93	17.05	26.24	36.77	45.11	52.36	76.64	100.00		

* denotes values less than 0.01%   - denotes no records in bin

Metadata:
Project: BHP QUANTUM
Location: Beacon 15 [118.50660 , -20.17450]
Data period: 01-Jan-1998 to 31-Dec-2007 23:00:00
Data source: SWAN version 40.72
Data summary: All Records
Number of Records: 87648

Table 7-4: Joint frequency for significant wave height (Hs) against peak wave period (Tp) in the10-year data archive.

Joint Frequency Table (%) Showing Hs Against Direction for the Period 01-Jan-1998 to 31-Dec-2007 23:00:00

N=87648	N	NE	E	SE	S	SW	W	NW	Total	Cumul.
0-0.25	0.03	*	0.01	*	*	*	0.01	0.01	0.08	0.08
0.25-0.5	3.92	1.25	1.98	2.36	2.22	1.58	3.47	4.58	21.38	21.46
0.5-0.75	5.63	1.79	4.84	5.35	3.96	3.37	11.47	10.98	47.39	68.85
0.75-1	2.33	0.74	1.81	2.22	1.59	1.61	6.92	5.85	23.07	91.92
1-1.25	0.75	0.22	0.41	0.48	0.40	0.50	1.73	1.44	5.94	97.86
1.25-1.5	0.17	0.08	0.11	0.08	0.12	0.15	0.50	0.36	1.59	99.45
1.5-1.75	0.05	0.02	0.01	0.01	0.03	0.02	0.13	0.08	0.35	99.80
1.75-2	0.02	*	*	*	0.01	*	0.03	0.02	0.11	99.91
2-2.25	*	*	*	*	-	-	*	0.01	0.03	99.94
2.25-2.5	0.01	*	-	-	-	-	*	0.02	0.04	99.98
2.5-2.75	*	*	*	-	-	-	*	-	0.01	99.99
2.75-3	-	-	*	-	-	-	*	-	*	100.00
3-3.25	-	-	-	-	-	-	-	-	-	100.00
3.25-3.5	-	-	-	-	-	-	*	-	*	100.00
3.5-3.75	-	-	-	-	-	-	-	-	-	100.00
3.75-4	-	-	-	-	-	-	-	-	-	100.00
Total	12.93	4.12	9.19	10.53	8.34	7.24	24.29	23.36		
Cumul.	12.93	17.05	26.24	36.77	45.11	52.36	76.64	100.00		

* denotes values less than 0.01%   - denotes no records in bin

Metadata:
Project: BHP QUANTUM
Location: Beacon 15 [118.50660 , -20.17450]
Data period: 01-Jan-1998 to 31-Dec-2007 23:00:00
Data source: SWAN version 40.72
Data summary: All Records
Number of Records: 87648

The ambient wave conditions can be summarised as follows:

- Significant wave heights are < 1.5 m for 99% of the time with all waves having a significant wave height < 2.75 m over the 10 year simulation dataset.

- The waves are dominated by wind seas, with peak wave periods < 8 s for 99% of the dataset.

- Long period waves (i.e. swells) occur only with low wave heights.

- Waves propagate from all directions but most frequently from the western quadrant (SW to NW).

8   SEDIMENT FATE MODELLING

8.1   Background

Modelling of the dispersion of suspended sediment resulting from dredging and disposal operations has been undertaken using an advanced fate model – SSFATE. This model computes the TSS concentration above background that directly results from dredging operations given the prevailing current and wave conditions.

8.2   Description of SSFATE

SSFATE is a computer model originally developed jointly by the U.S. Army Corps of Engineers Engineer Research and Development Center and Applied Science Associates to estimate the water column suspended sediment concentrations and bottom deposition patterns resulting from dredging operations (Johnson *et al.*, 2000).

SSFATE is formulated to simulate far field (~25 m or larger) effects in which the mean transport and turbulence associated with ambient currents are dominant. A particle-based model predicts the transport and dispersion of the suspended material. Particle advection is based on the simple relationship that a particle moves linearly with a local velocity, obtained from the hydrodynamic model, for a specified model time step. Particle diffusion is assumed to follow a simple random walk process.

The model requires specification of circulation and wave parameters in the area of interest, the type of dredging technology used, and the loss rate and vertical distribution of initial material release.   Using a random walk procedure, the model tracks representative particle classes as they disperse in the water column and settle to the bottom. Particle diffusion is affected by estimates of the local horizontal and vertical diffusion rates. Sinking rates vary with particle size and the concentration of particle size. Sinking rates of clay and fine silt-sized particles are enhanced at increased concentrations, accounting for clumping of these particles to form larger particle sizes. Rates of sedimentation (the process where particles move from the suspended state to accumulate on the seabed) are calculated as a dynamic process, varying with time and space due to estimates of the combined shear-stress due to current and wave forcing, following the formulation of Soulsby (1997). The model also calculates sediment resuspension if the combined shear stress subsequently increases above critical thresholds.

Different thresholds are applied for resuspension depending upon the duration that sediments have been deposited based on empirical studies which demonstrate that newly settled sediments will have higher water content and will be suspendable by lower shear stresses (Swanson *et al* 2007). Resuspension flux (mass per time leaving the seabed) for lighter fractions will be affected by the magnitude of the estimated shear stress at a location, the cohesivity of the sediment and the average particle size distribution of the deposits. The cohesion settings, which are fixed for a situation, account for the electrostatic bonds between deposits that resist resuspension. The calculations for the average particle size, which are calculated dynamically, account for armouring of fine particles within the interstitial spaces of

larger particles. Resuspension flux will decrease to zero at a location once all resuspendable material is removed or the average particle size reaches a threshold. Thus, the model can indicate whether deposits will stabilise or erode over time.

SSFATE formulations and proof of performance have been documented in a series of USACE Dredging Operations and Environmental Research (DOER) Program technical notes (Johnson *et al* 2000 and Swanson *et al* 2000), and published in the peer-reviewed literature (Anderson *et al* 2001, Swanson *et al,* 2004; Swanson *et al,* 2007).

8.2.1   Disposal site selection studies

Initial modelling investigations were undertaken to test and compare the influence of disposal location on the outcome of this component of the operation. The study used two procedures to identify the optimum disposal location, in terms of the stability of deposited sediments and the potential for sediments to impinge upon adjacent sensitive habitats from either the initial release or from remobilisation of deposited sediments.

Firstly, predictions of shear-stress were calculated at seabed level throughout the domain shared by the hydrodynamic and wave models. This analysis provided an indication of the likely stability of spoil that is initially deposited within each area.

Secondly, disposal was simulated into areas that had been identified as potentially suitable for disposal of dredge spoil on the basis of logistic and environmental considerations (Figure 8-1). The results were primarily judged by examining overlap of the expected distributions of TSS and sedimentation with buffer areas that are designated around limestone ridges that were adjacent to the disposal areas.
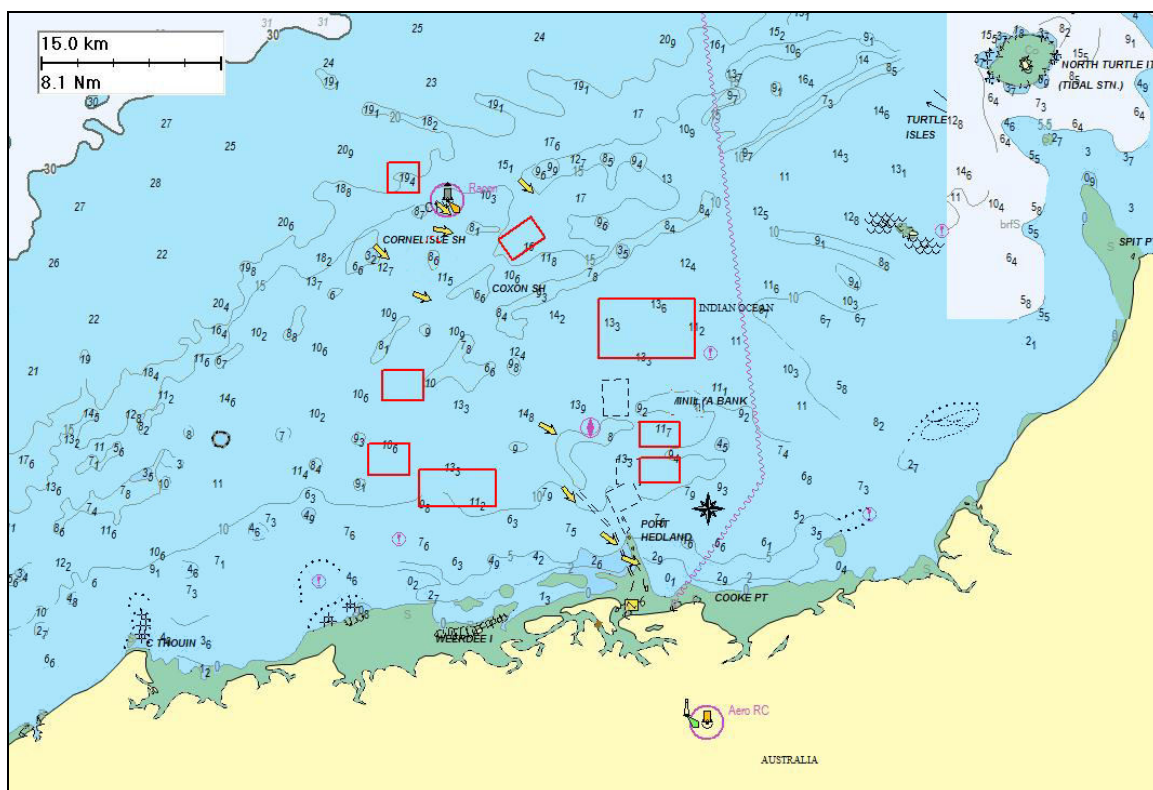
Figure 8-1: Location of the disposal areas investigated in the selection studies, shown by the red boxes. The location of existing spoil grounds is shown as black dashed boxes.

8.2.2 Scenarios and input data

Theoretical estimates of shear stress at the seabed (bottom-stress) were derived for each grid cell within the domain of the hydrodynamic model at hourly time steps from the hindcast of current and wave parameters for the duration of one year. Current and wave data for the year 2001 were used on the basis that the SOI was variable during this year. However, as previously discussed, the influence of the SOI is expected to be small.

Shear stress was calculated for each grid cell in the model domain, at hourly time steps following the method of Soulsby (1997) for combined current and wave components over non-cohesive rough sediments under non-breaking waves. Soulsby's (1997) formulations uses estimates of the current speed, bottom roughness, water depth, significant wave height, wave period, water density, and gravitational acceleration and bottom orbital velocity. Current and wave parameters were derived from the output of the previously described hydrodynamic and wave models.

Derivation of bottom-stress estimates with an hourly time-step allowed testing for variability at relatively short time scales in response to environmental conditions. Shear stress estimates were also summarised over time as the median and 90th percentile values at each grid cell, to represent more typical and extreme levels at each location. These latter estimates were more relevant to judging the longer term stability of spoil if deposited within each area.

Sediment disposal was simulated into each of the test areas using the SSFATE model, with an identical configuration, representative of hopper discharge. The purpose of this section of modelling was to compare sediment fates among sites, rather than determine the exact magnitude of TSS and sedimentation. Hence, arbitrary, yet consistent, sediment discharge specifications were required. To represent the actions of a TSHD, simulations represented 100 separate releases of 12,750 m^3 of sediment, each 2.5 hours, for 30 days. Release locations were randomised throughout the test areas to achieve an even distribution of spoil. The particle size distribution of the sediments was kept constant among the simulations and was based on PSD data derived for the inner turning circle (0-2 km; Table 8-1):

Table 8-1: Assumed particle size distribution of sediments used for the spoil ground selection study

Size range (µm)	General name	% of mass
0-7	Clay	4.1
7-35	Fine silt	6.9
35-75	Coarse Silt	8.2
75-130	Fine sand	9.7
>130	Coarse sand	71.1

To allow seasonal comparisons, simulations were repeated for each disposal area using wind, tide and current data samples from January 2001, representing summer conditions, and May 2001, representing winter conditions. The simulations included calculations for resuspension of deposited sediments and thus accounted for either direct or subsequent transport of dredged sediments.

8.2.3   Results of Shear stress estimation

Estimates of shear stress for the study area were highly variable over time due to interactions of the tide level, current speeds and wave climate. Figure 8-2 shows estimates for shear stress at 4 points in time separated by 2 hours, spanning from ebb to flood tide. The scale shows the minimum theoretical levels of bottom stress, as units of Pascal (Pa), that are required to commence mobilising particles of a given particle size from the seabed, assuming non-cohesive sediments (Soulsby 1997). Note that the scale is logarithmic. Over this example period, bottom stress during the peak flow of the ebbing tide (1600 hrs) is estimated to be sufficient to mobilise sediments with a grain size ranging up to coarse sand over most of the study area. At the bottom of the tide (2000 hrs), bottom stress estimates have declined to levels sufficient to mobilise only fine silts or smaller particles over most of the model domain but remain high enough to mobilise fine sands closer inshore.

Based on the one year sample, the annual median levels of bottom shear were estimated to be in the range required to mobilise fine to medium sands over most of the study area, with relatively uniform levels predicted for each of the study areas (Figure 8-3). The more extreme levels of shear stress, indicated by the 90th percentile values, were well in excess of the levels required to mobilise coarse sand. Note that the wave and current data for the 2001 year sample included estimates from storm periods, inclusive of cyclone events, and the 90th percentile values can be attributed to these events.

Based on the general particle-size distribution of the sediments to be dredged, which will include clay through to coarse sands, these results indicate that there would commonly be sufficient shear stress acting to mobilise the finer components of the dredge spoil that are not buried by heavier components during the initial disposal while storm events can be expected to mobilise these coarse deposits occasionally. This can be expected to result in a spread of the deposit and a release of additional fine sediments in the process. This outcome was consistent across all disposal areas under investigation, indicating that none of the areas offers significant advantages in terms of spoil stability.
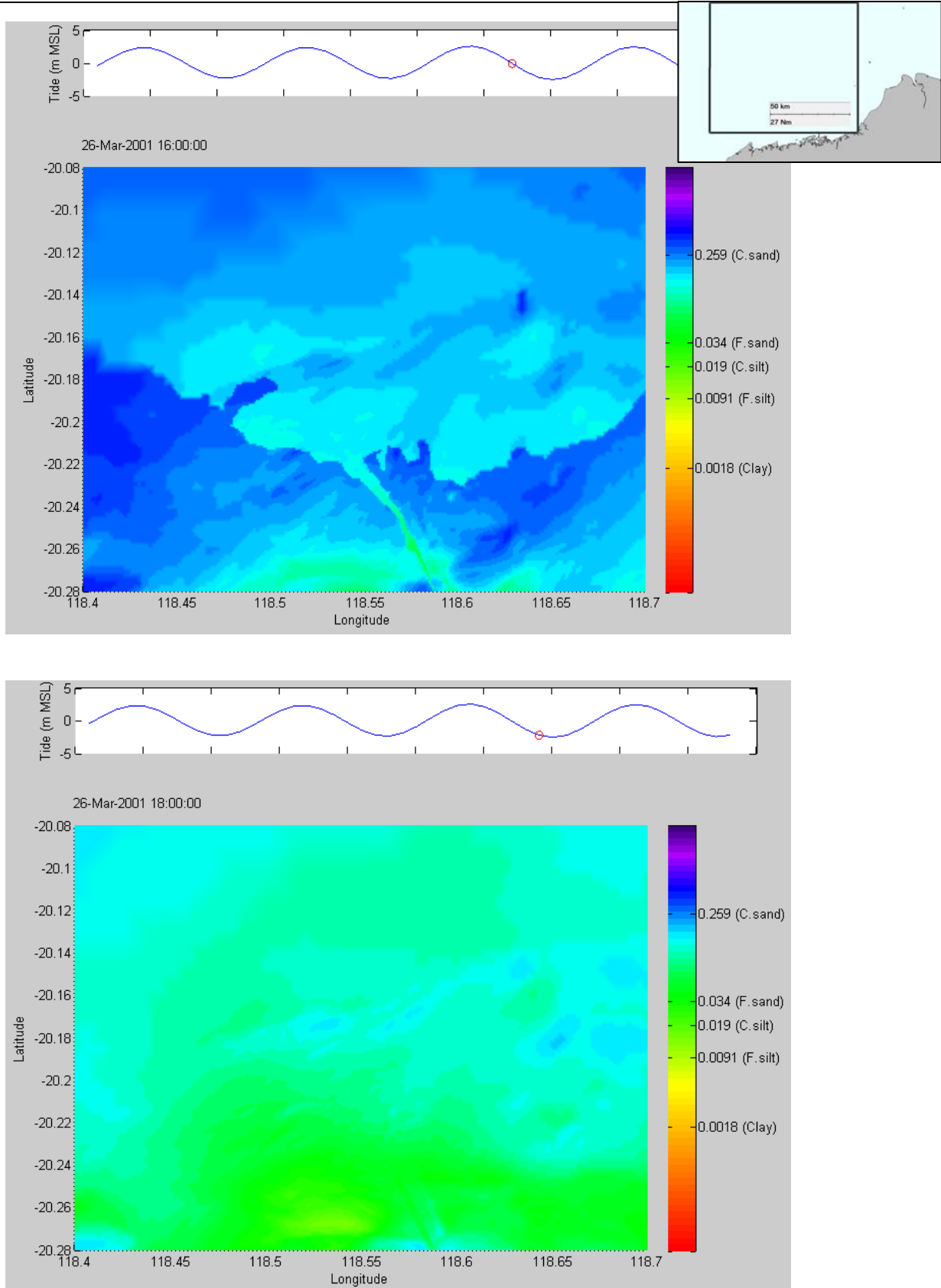
Figure 8-2: Estimates of bottom stress (Pa) for example points in time. The images represent bottom stress at each location for two points in time at 2 hour time steps. The upper panel within each image shows the tide level. The inset image shows the coverage.
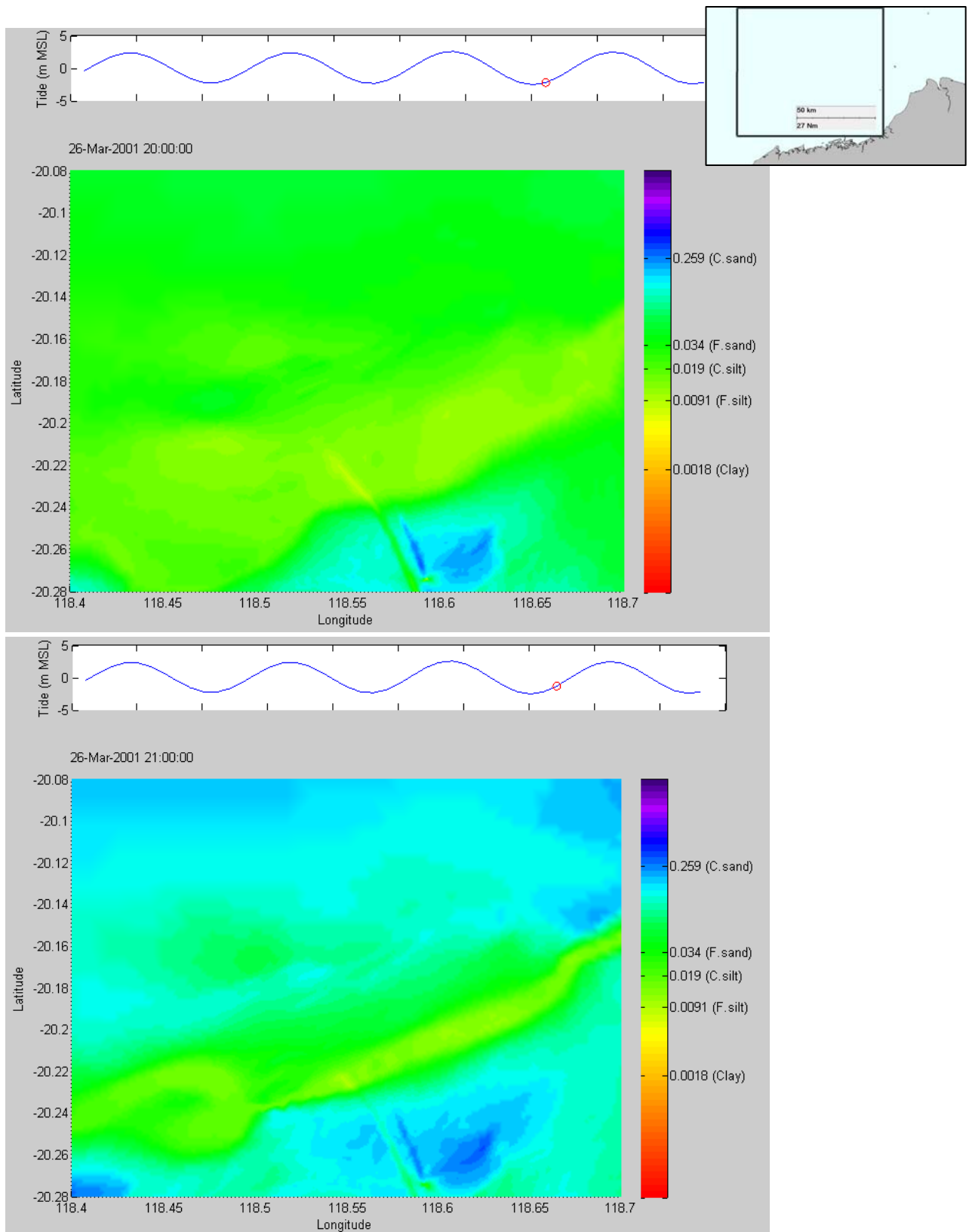
Figure 8-2: (continued)
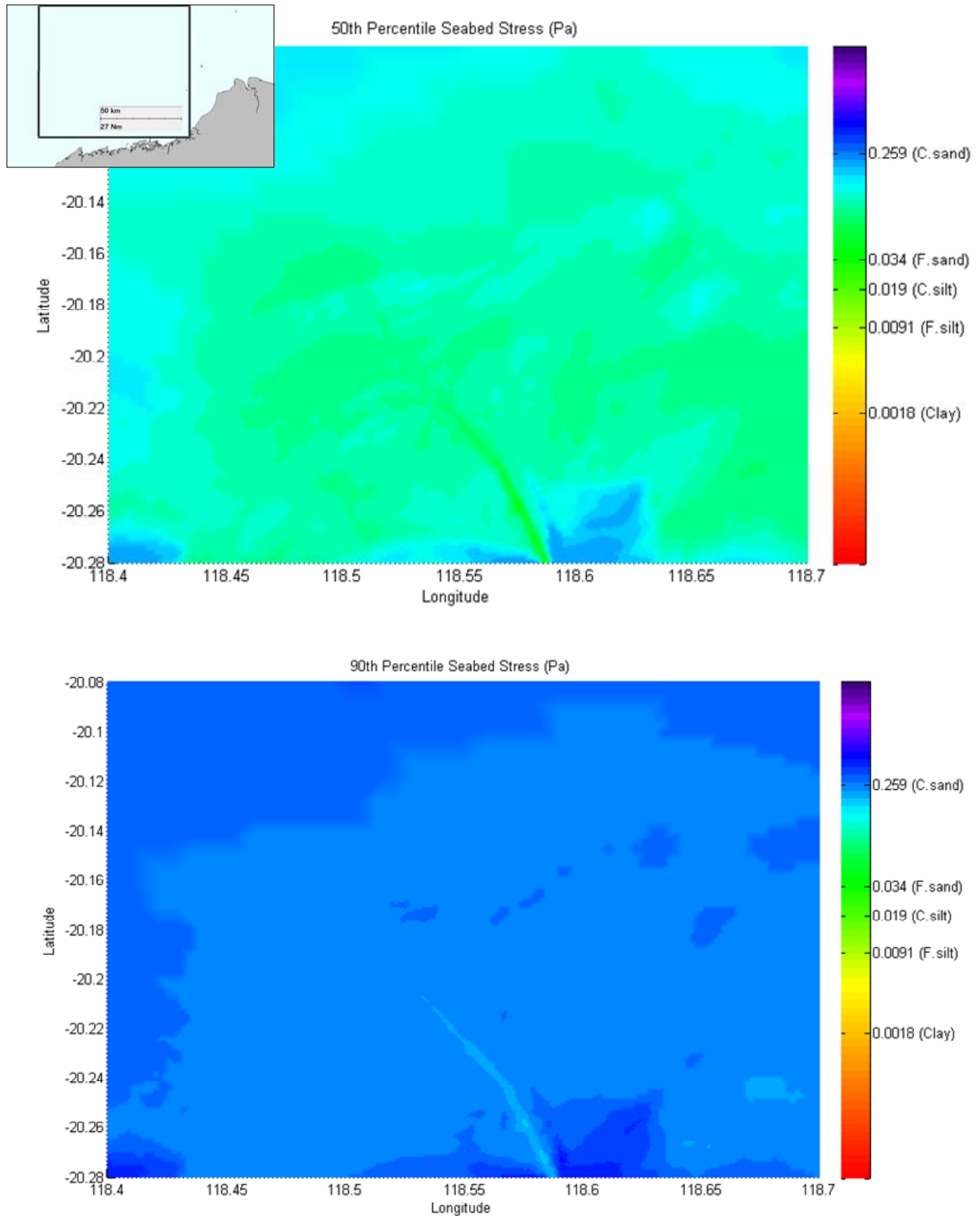
Figure 8-3: Estimates of the median (upper panel) and 90th percentile (lower panel) bottom stress (Pa), over one year (2001). The inset image shows the coverage of the images.

8.2.4   Results of sediment fate modelling for site selection

Simulations of disposal into all test areas indicate that elevated sedimentation and TSS concentrations will occur outside the boundaries of the defined area limits (Figure 8-4 to Figure 8-10). This outcome can be attributed to the strong tidal currents transporting sediments beyond the area boundaries. The predicted distribution of particles around the disposal area was a function of particle size. Particles larger than fine sands are predicted to settle out within the boundaries and to remain relatively stable in the absence of significant swell waves. A proportion of the clay and silt particles are also predicted to initially sink and settle inside the boundaries, due to entrainment and burial by the larger particles. Clay and fine silt components that are not entrained are predicted to drift with the tidal currents while sinking towards the seabed and hence will tend to be transported beyond the disposal area boundaries.

The shear stress generated by the local tidal currents was estimated by the model to be sufficient to keep a high proportion of these finer sediment particles suspended as a turbid layer near the seabed. Hence, they are predicted to drift and disperse along the axis of the flooding and ebbing tide. A high proportion of the fines are expected to settle out at the turn of the tide but then resuspend as the tide speeds increase again. This effect was greatest during the spring tides, with neap tides predicted to generate insufficient shear stress to resuspend fine sands and the coarser silts (Figure 8-11).

The maximum predicted tidal migration was of the order of 10-15 km to the northwest and southeast of each of the disposal areas and this limited the distribution of dredged sediments along that axis. TSS concentrations and net sedimentation are predicted to decrease exponentially over this distance to < 1 mg/L and <10 g/m^2, respectively. At 2 km distance along the tidal axis, maximum TSS concentrations are predicted to reach 30-40 mg/L near the seabed, and short-term sedimentation (at the turn of the tide) is predicted to peak up to 1 kg/m^2.

Net drift of sediments was also observed over longer time scales than a tidal period, involving the migration of fine silt and clay-size sediments over subsequent tidal fluctuations, and after periodic resuspension due to waves. The direction of net drift varied seasonally, with the magnitude of effect varying among disposal areas. The general direction of drift was to the northeast during summer and southwest during winter, and hence perpendicular to the tidal axis and reflecting the net drift observed in the current data. Over the limited duration of the simulations (30 days), the maximum excursions were of the order of 10-20 km towards the northeast, with magnitudes larger for the disposal areas closer to shore (Areas 1, 2 and 7). In general, maximum excursions during the winter cases were limited to 10 km, with the exception of the areas 1 and 2 where the magnitudes were similar to the summer cases. Greater excursions would be expected for a longer disposal programme and with more variable samples of current and wave data.

Disposal area 1

January sample
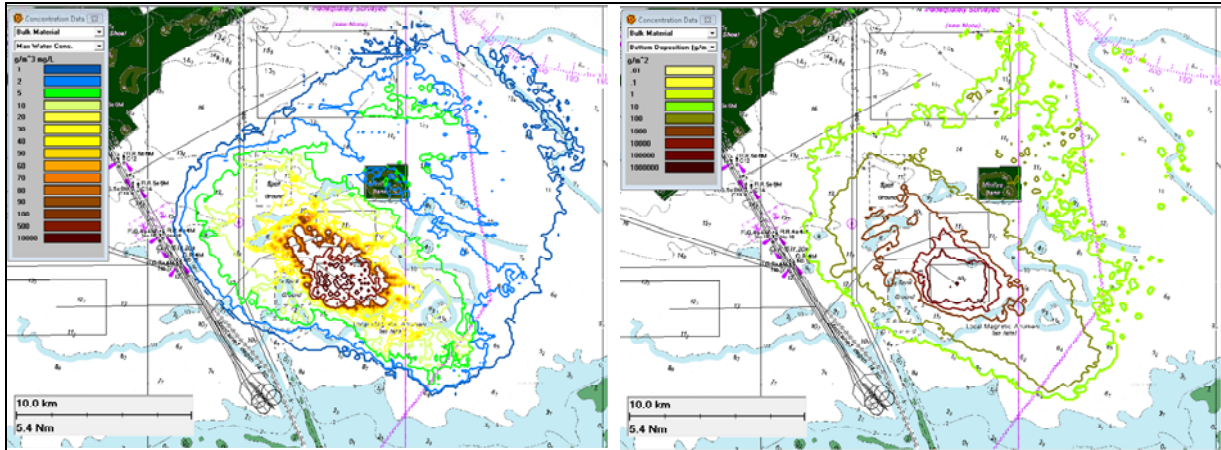
May sample
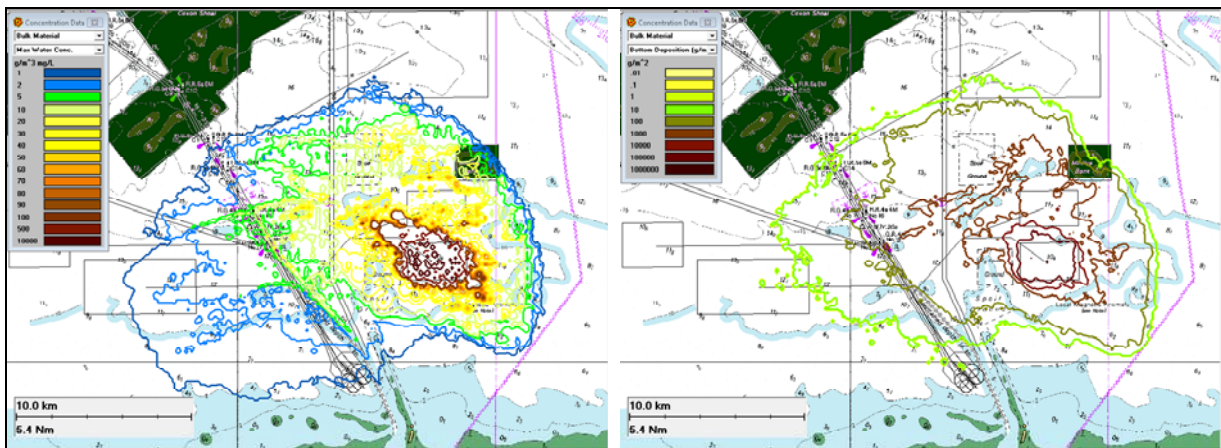
Figure 8-4: Estimates of the highest TSS (mg/L; left), at any depth, and highest sedimentation (g/m^2; right) within each cell at any time during 30 day simulation of discharge into disposal area 1. Results are from simulations using environmental forcing data from January (2001; upper panel) and May (2001; lower panel). The dark green areas surround locations with limestone ridges.

Disposal area 2

January sample
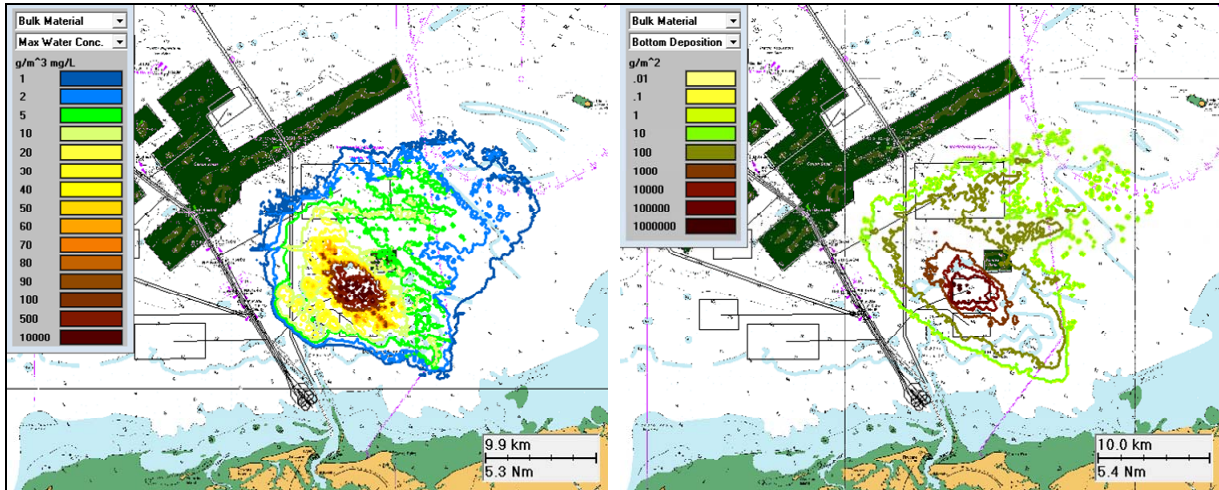
May sample
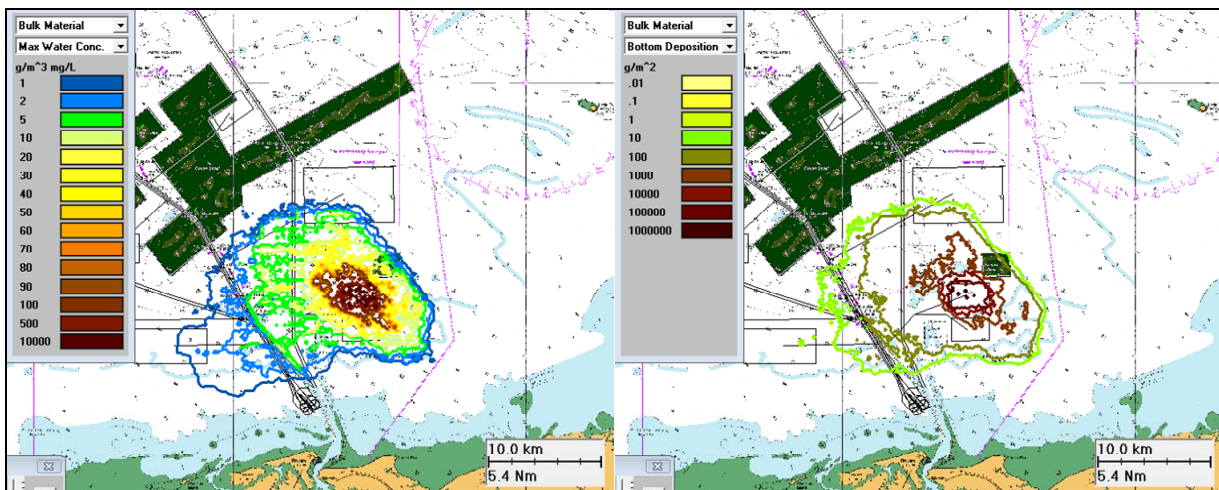
Figure 8-5: Estimates of the highest TSS, at any depth (mg/L; left), and highest sedimentation (g/m^2; right) within each cell at any time during 30 day simulation of discharge into disposal area 2. Results are from simulations using environmental forcing data from January (2001; upper panel) and May (2001; lower panel). The dark green areas surround locations with limestone ridges.

Disposal area 3

January sample
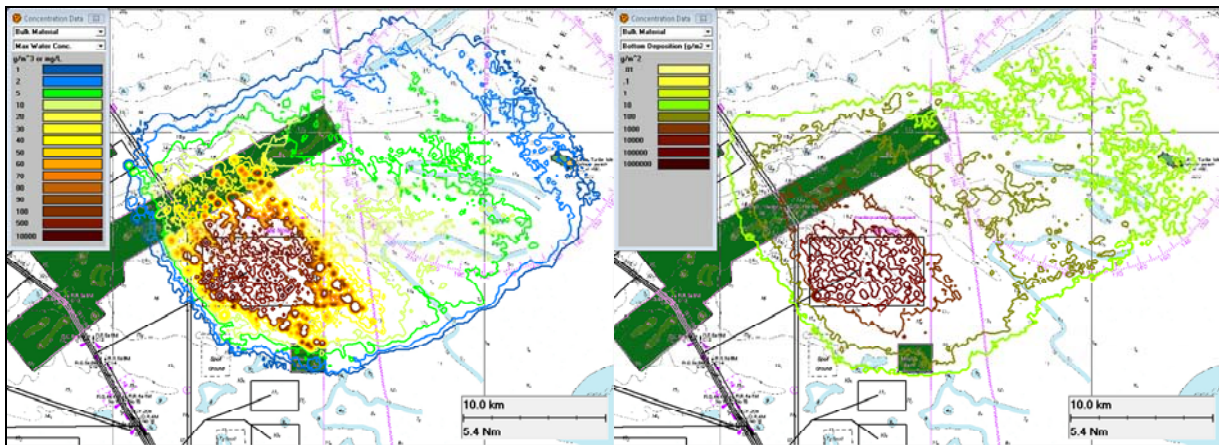
May sample
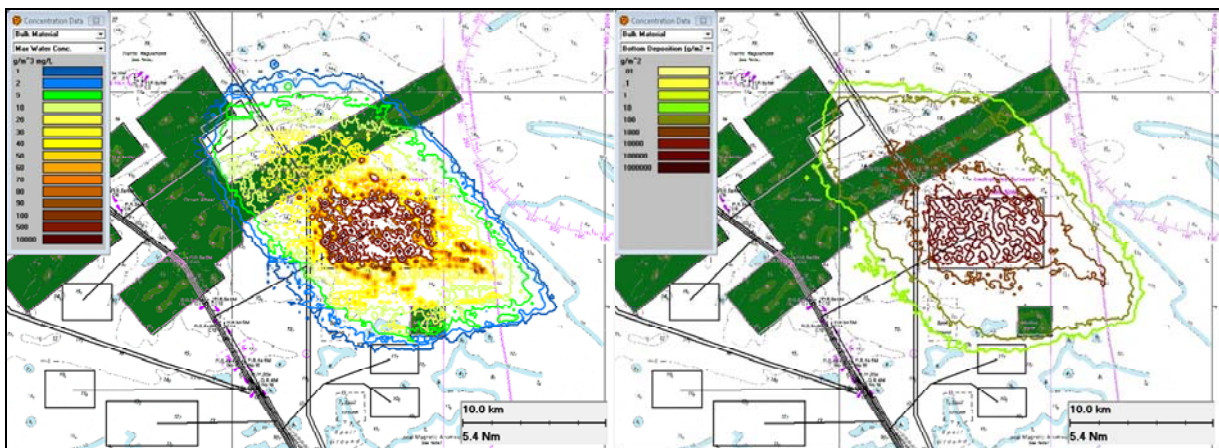
Figure 8-6: Estimates of the highest TSS, at any depth, (mg/L; left), and highest sedimentation (g/m^2; right) within each cell at any time during 30 day simulation of discharge into disposal area 3. Results are from simulations using environmental forcing data from January 2001 (upper panel) and May 2001(lower panel). The dark green areas surround locations with limestone ridges.

Disposal area 4

January sample
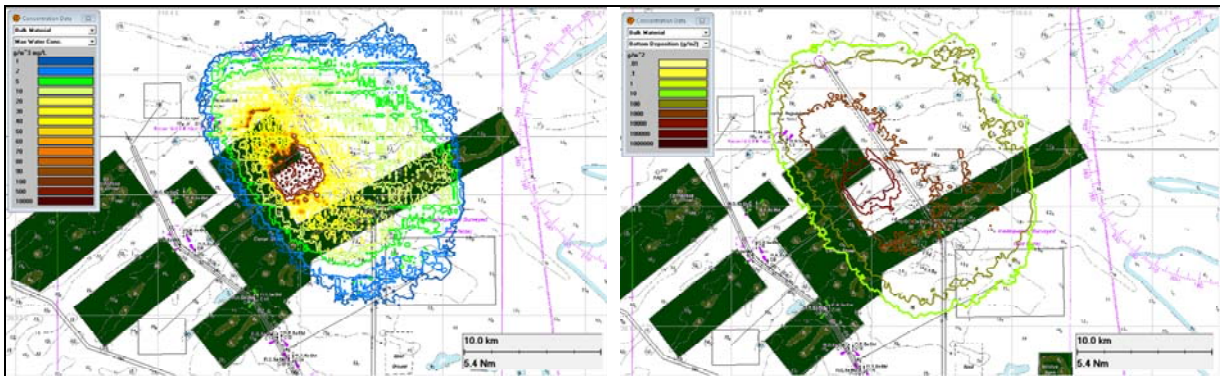
May sample
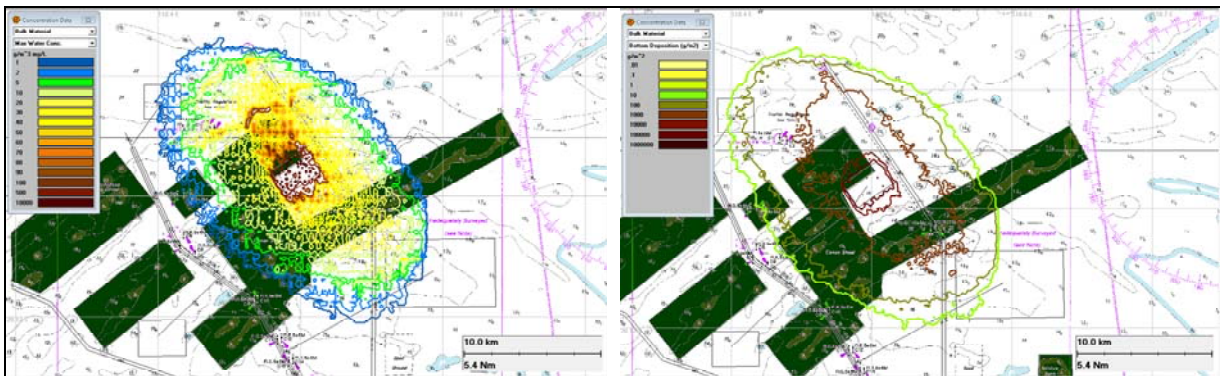
Figure 8-7: Estimates of the highest TSS, at any depth, (mg/L; left), and highest sedimentation (g/m^2; right) within each cell at any time during 30 day simulation of discharge into disposal area 4. Results are from simulations using environmental forcing data from January 2001 (upper panel) and May 2001(lower panel). The dark green areas surround locations with limestone ridges.

Disposal area 6

January sample
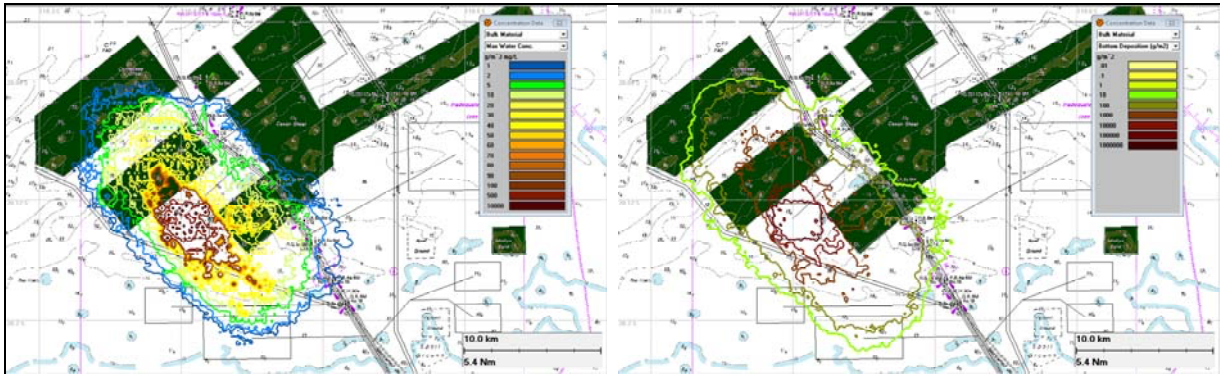
May sample
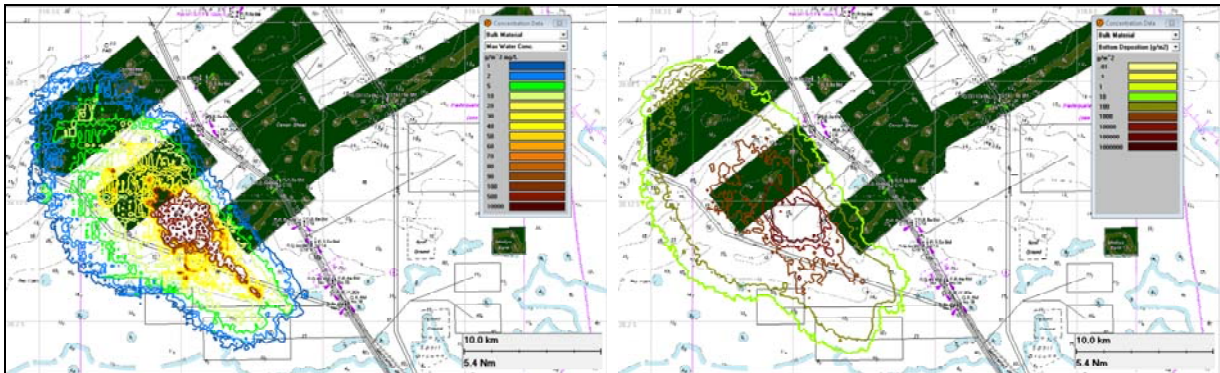
Figure 8-8: Estimates of the highest TSS, at any depth (mg/L; left) and highest sedimentation (g/m^2; right) within each cell at any time during 30 day simulation of discharge into disposal area 5. Results are from simulations using environmental forcing data from January 2001 (upper panel) and May 2001(lower panel). The dark green areas surround locations with limestone ridges.

Disposal area 7

January sample
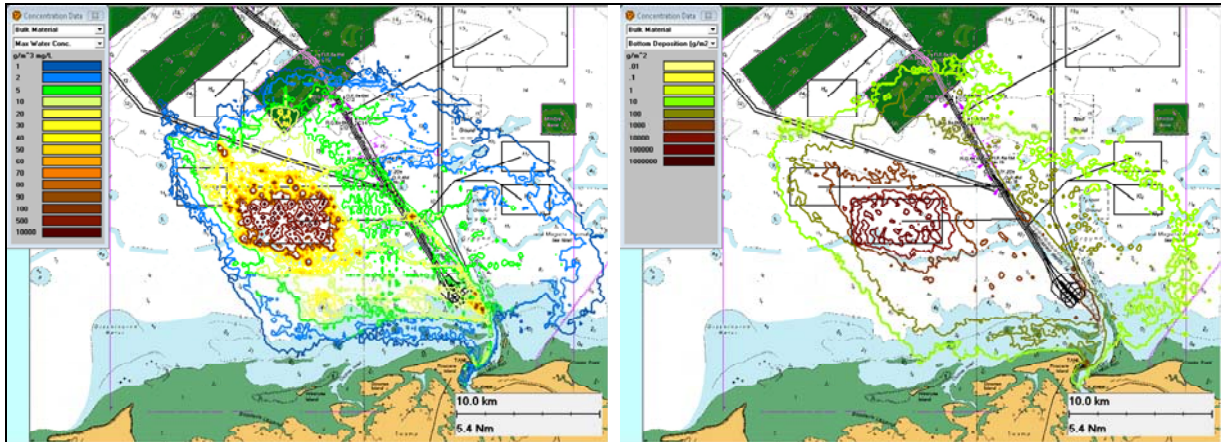
May sample
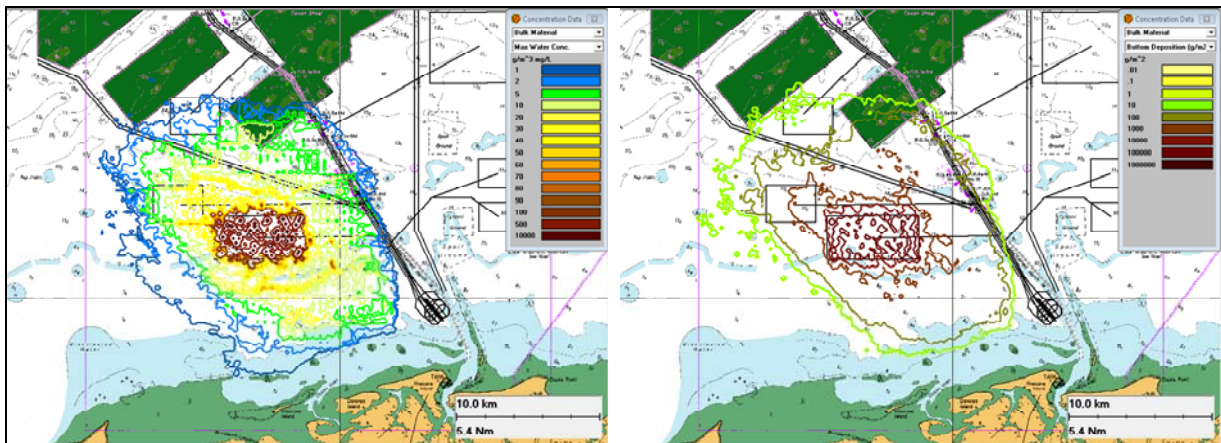
Figure 8-9: Estimates of the highest TSS, at any depth (mg/L; left) and highest sedimentation (g/m^2; right) within each cell at any time during 30 day simulation of discharge into disposal area 7. Results are from simulations using environmental forcing data from January 2001 (upper panel) and May 2001(lower panel). The dark green areas surround locations with limestone ridges.

Disposal area 9

January sample
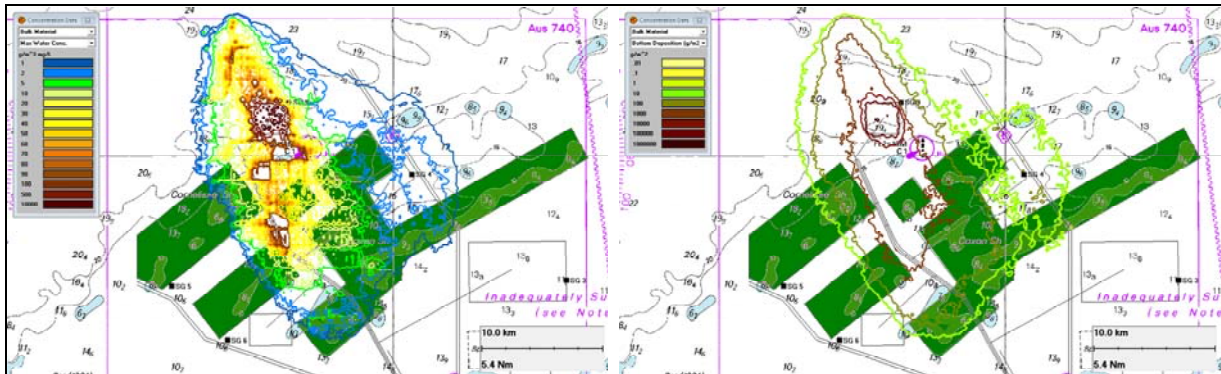
May sample
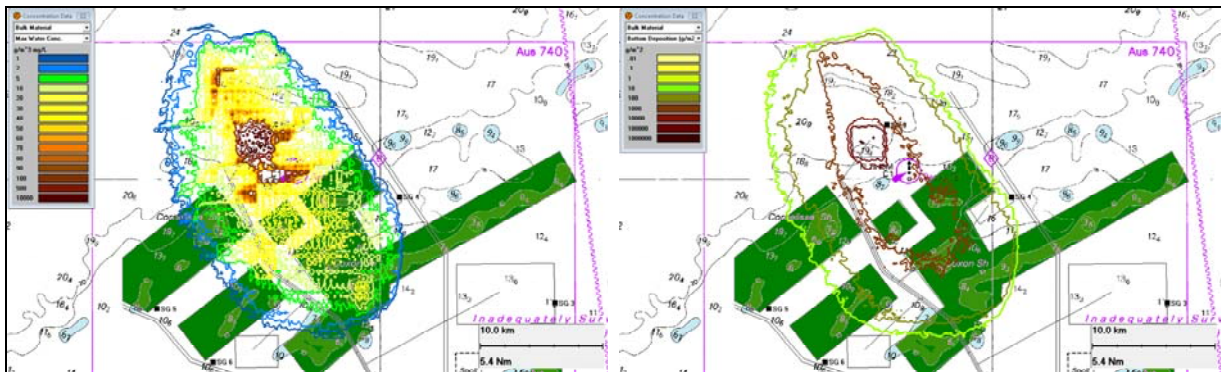
Figure 8-10: Estimates of the highest TSS, at any depth (mg/L; left), and highest sedimentation (g/m^2; right) within each cell at any time during 30 day simulation of discharge into disposal area 9. Results are from simulations using environmental forcing data from January 2001 (upper panel) and May 2001(lower panel). The dark green areas surround locations with limestone ridges.
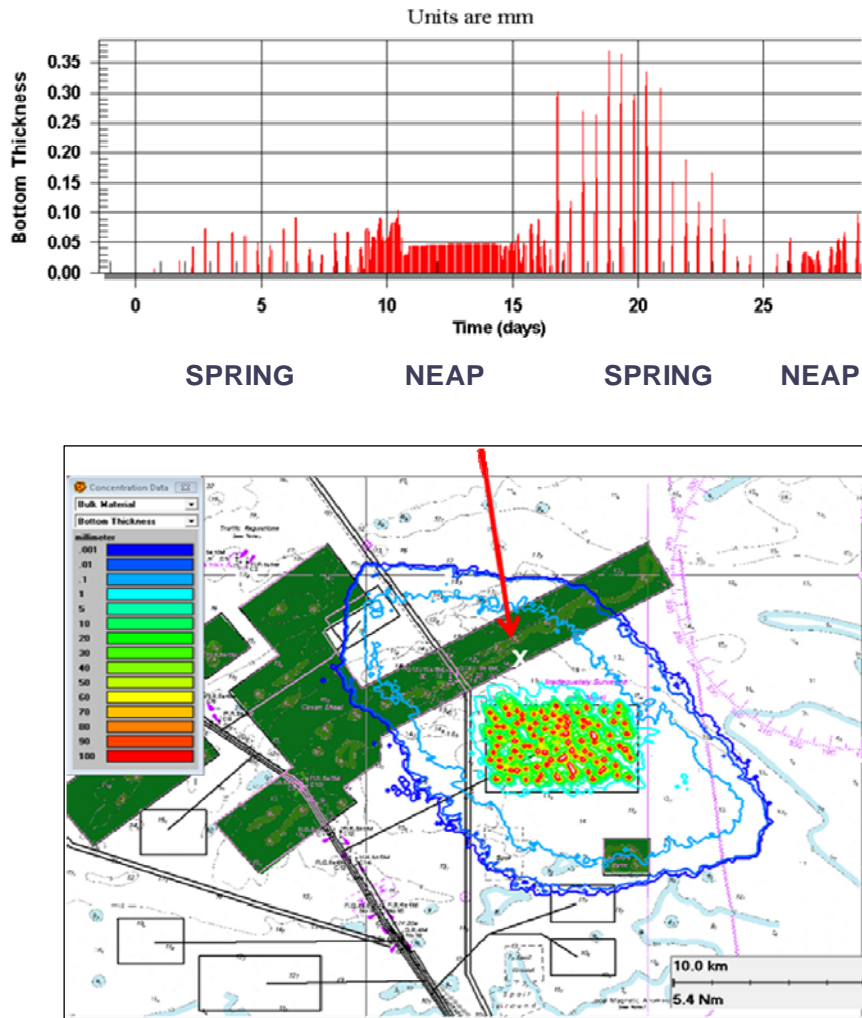
Figure 8-11: Time series of sediment thickness at a limestone ridge site north of disposal area 3. The upper panel shows predicted values at hourly time steps over a 30 day simulation for the position marked with an X, using the January sample data. The lower panel shows the maximum values predicted at all locations resulting from dredging and disposal operations.

8.3   Specifications and assumptions of the main study

8.3.1   Dredging Methodology

Based on specifications provided by FAST Joint Venture (FAST JV), the dredging programme would be carried out in stages: Quantum 1, Quantum 2 and Quantum 3. Quantum 1 and 2 would be dredged sequentially with no delay between the finalisation of Quantum 1 and commencement of Quantum 2. Quantum 3 would occur approximately 15 months after finalisation of Quantum 2.

Geotechnical findings suggest the sediments to be removed will require the use of both a trailer-suction hopper dredge (TSHD) and a cutter-suction dredge (CSD).   The unconsolidated surface sediment would be collected by TSHD before harder underlying material is fractured by the CSD and pumped directly to the seabed. The TSHD would subsequently collect the fractured sediment from the dredging footprint. Table 8-2 displays estimates of the total volume to be dredged in each area during each stage, delineated by handling method.

Table 8-2 Estimates for the volume of material that would be dredged from each section, delineated by handling method. Note that TSHD estimates are for the unconsolidated sediments only. The volumes of CSD material that would be handled by TSHD is indicated by the CSD Crushing & TSHD rehandle volumes. Estimates are rounded to the nearest 250,000 m^3.

Dredge Area	TSHD Volume (m3)	CSD Crushing & TSHD Rehandle (m3)	Total Volume Removed (m3)
Quantum 1			
Wharf and Berth Pockets	1,500,000	3,000,000	4,750,000
Departure Basin	2,500,000	6,500,000	9,000,000
Arrival Basin	2,000,000	1,000,000	3,250,000
Link Channel	4,250,000	1,000,000	5,250,000
Subtotal	10,250,000	11,750,000	22,000,000
Quantum 2			
Departure Basin	2,250,000	6,000,000	8,500,000
Arrival Basin	1,750,000	1,000,000	2,750,000
Link Channel Section 1	2,000,000	500,000	2,500,000
Link Channel Section 2	3,750,000	1,000,000	4,500,000
Link Channel Section 3	1,250,000	0	1,250,000
Link Channel Cross Over	500,000	0	500,000
New Departure Channel 8 - 11.5km	1,750,000	0	1,750,000
New Departure Channel 11.5 -13km	1,500,000	0	1,500,000
New Departure Channel 13- 17km	500,000	0	500,000
New Departure Channel 19.5 - 23km	750,000	0	750,000
New Departure Channel 23 - 26.5km	250,000	0	250,000
New Departure Channel 30 - 32km	250,000	0	250,000
Subtotal	16,500,000	8,500,000	25,000,000
Quantum 3			
Berth and Wharf Pockets Extension	500,000	750,000	1,250,000
Departure Basin Extension	250,000	250,000	500,000
Swing Basin East Extension	1,500,000	750,000	2,250,000
Swing Basin West Extension	1,500,000	750,000	2,000,000
Departure Channel Widening	1,000,000	250,000	1,000,000
Subtotal	4,250,000	2,750,000	7,000,000
Total	31,000,000	23,000,000	54,000,000

Dredge logs representative of the proposed dredging programme were provided by BHP Billiton Iron Ore for each proposed stage. Each log contained schedules with time-series information specifying the activity of each dredge vessel. The time-series consisted of a sequence of tasks, with each task having unique specifications for the dredging equipment, specific operation being carried out (e.g. dredging with or without overflow, manoeuvring, sailing, disposal, maintenance downtime, stoppages for breakdowns etc) rates of operation, locations of operation and the PSD of sediment being discharged. The PSD specifications were calculated from geotechnical sampling with consideration of the selective influence of the dredger type and each unique source of discharge (e.g. overflow, cutter-head etc).

Dredging and disposal operations involve moving and dynamically-varying sources of sediment discharge, which has an influence on the location and concentrations of suspended sediments. For example, more rapid movement and constant relocation of a discharge source will have the influence of dispersing sediments over a wider area than a more static source of the same discharge. The model was configured to move each source in a way that was representative of the operational areas, movement rates and patterns of movement specified in the indicative plan. The time-sequence information provided in the logs was directly used as input into the model, providing for dynamically-variable source terms for the sediment predictions that were based on the indicative dredging plan.

The modelling was carried out to simulate the full dredging plan (Stages 1 through 3) for the cumulative effects of all sediment sources over time. This involved specification of all unique sources, in their expected sequence and at their expected locations, and calculation of cumulative effects on suspended sediment and sedimentation distributions at hourly steps. The indicative plan involved simultaneous discharges from different sources.

The simulations required to cover the full programme spanned the equivalent of approximately five years. To provide estimates with suitable temporal and spatial resolution whilst maintaining acceptable computation times, the minimum time step in the model was set at 30 minutes. This required the durations provided in the logs to be adjusted to multiples of 30 minutes, with the exception of disposal operations, where 10 minute steps were required due to the short duration of discharges. In all cases, the volume dredged and disposed remained consistent with the supplied dredge logs.

8.3.2   Spoil Grounds

The indicative plan specified the location and timing of each disposal, with disposal occurring into two grounds, designated as Spoil Ground 3, on the eastern side of the dredging area and Spoil Ground 7, on the western side. In general, disposal occurred within both disposal grounds within each period of the operations.

The sediment placement followed guidance on general disposal practices provided by a dredging consultant (Baggerman Associates Pty Ltd). Each disposal was represented as a discharge of the hopper contents along a 200 m track over 10 minutes. The placement of the tracks was specified in an ordered manner, to reflect a typical disposal management plan aimed at a level pile. Disposal tracks were placed as parallel lines running parallel with the east-west axis of each disposal ground, the disposal sequences commencing at the closest

boundary in each case. The Tracks were laid out to dispose into Spoil Ground 3 commencing at the western margin and progressing eastward as the operation went on. For Spoil Ground 7, tracks were laid out commencing at the eastern margin and progressing westward. Quantum 1 simulations were specified as parallel tracks with 20m separations. Disposal centrelines for Quantum 2 simulations were then specified as parallel tracks between the Quantum 1 tracks, hence the final spacing of the disposal tracks was 10 m. Quantum 3 disposal tracks were placed over new sections of the disposal ground as parallel tracks 10 m apart.

8.3.3   Particle size distributions

SSFATE employs five material classes based on sediment grain sizes. The classes are biased towards the finer materials (coarse sand and smaller), as these are typically the most dispersive and are responsible for the greatest turbidity increases in the water. Material with a particle size larger than coarse sand is assumed to settle rapidly and directly below the source of suspension.

Based on geotechnical surveys, seven unique particle size distributions (PSDs) were specified in the dredge logs, representing the different types of sediment to be dredged. These were labelled Unit 2a, Unit 2b, Unit 4a, Unit 4b, Unit 4c, Unit 6a and Unit 6b, with details specified in Table 8-4. Unit 6a is hard material to be fractured by the CSD and subsequently collected by TSHD. All other units would be handled by TSHD. The dredge logs indicated the vertical and spatial distribution of the unit types.

Table 8-3: General criteria for defining material types

Soil Unit	Generalised Soil Description
2a	Silica or calcareous sand
2b	Gravelly or Clayey sand & mixed sand, gravel and clay
4a	Siliceous calcarenite & calcareous sandstone
4b	Siliceous calcarenite & calcareous sandstone
4c	Calcareous clayey and or calcareous sand & sandstone
6a	Clayey and/or calcareous sand and sandstone
6b	Sandstone

PSDs estimated for post-handling by the dredging equipment were supplied to APASA to specify the source terms in the model. These PSDs were used to specify discharges for particular equipment types. The PSDs for unconsolidated sediments were used as supplied to represent the disturbance of the bed by the hydraulic draghead and propellers (Table 8-4). However, adjustments were applied to the PSDs to account for the size-selective discharge in overflow water from the TSHD. When sediment is pumped into the TSHD barge, the coarser material will settle in the bottom of the hopper, while a proportion of the finer material will remain suspended in the water column due to slower sinking rates and the high turbulence in the hopper. This finer material is therefore selectively discharged with overflow water. To represent this in the model, the coarser fractions (>75 µm) were removed from the supplied PSDs and the remaining fines applied as an adjusted particle size distribution (i.e. proportions linearly adjusted to sum to 100%). Table 8-5 shows the seven PSDs based on the geotechnical sampling as well as the PSDs adjusted for the TSHD overflow. Overflows were specified as an additional, intermittent, source to the discharges due to propeller wash and the hydraulic draghead.

Cutter suction dredges produce mixed size fractions ranging from fine silts to rock fragments depending on the power of the equipment, shear strength of the rock and the size of imbedded grains, among other factors. No direct measurements were available of the PSD of material that would be liberated from the rock to be fractured with the equipment to be used during this programme. Hence, it was necessary to apply conservative assumptions for this material. While coarse material generated by fracturing the rock with the CSD would settle rapidly, finer material will be selectively suspended by the discharge jet and the rebounded energy of the discharge jet striking the seabed. Given that the rock type to be fractured is hard sandstone with the potential for relatively high clay content, an estimate of the size-composition of the suspendable material was derived with 64% of particles in the clay to silt range (Table 8-6). The suspendable fraction was calculated assuming 80% of the mass of fractured rock would be gravel or larger size, hence the clay and silt represent 64% of the 20% of production that is of suspendable size.

Subsequent dredging of the fractured deposits by TSHD would involve handling of material with a modified PSD, with generally more fines buried during deposition of the heavier fractions. The PSD was specified to suit this material (Table 8-7). This PSD was also used to specify the PSD of material suspended by disturbance due to the propellers and draghead while the TSHD was recovering this material. The PSD for additional sediment discharged as overflows was modified from these specifications by the selective removal of fractions > 75 µm, and linear adjustment of the proportions to 100% (Table 8-8), accounting for the selective discharge of fine sediments.

Table 8-4 Particle size distributions estimated for the sediment released by the TSHD during the non-overflow period for each of the surface sediment types dredged. Particles size estimates are post-handling by the dredger (source: FAST JV)

Material Class	Size Range (μm)	percentage					
		2a	2b	4a	4b	4c	6b
Clay	< 7	3.1	22.3	2.1	1.8	3.7	1.6
Fine Silt	7 to 35	1.4	10.3	1.3	1.4	1.3	1.5
Coarse Silt	35 to 75	1.5	4.4	0.6	0.5	0.8	0.7
Fine Sand	75 to 130	5.3	4.4	0.8	0.7	0.8	0.9
Coarse Sand	> 130	88.7	58.7	95.2	95.6	93.5	95.5

Table 8-5 Particle size distributions estimated for the additional sediment released by the TSHD when overflowing (source: Adjusted from Table 8-4 by removal of fractions > 75 μm)

Material Class	Size Range (μm)	percentage					
		2a	2b	4a	4b	4c	6b
Clay	< 7	27.4	54.0	43.8	40.9	56.9	35.6
Fine Silt	7 to 35	12.4	24.9	27.1	31.8	20.0	33.3
Coarse Silt	35 to 75	13.3	10.7	12.5	11.4	12.3	15.6
Fine Sand	75 to 130	46.9	10.7	16.7	15.9	12.3	20.0
Coarse Sand	> 130	0	0	0	0	0	0

Table 8-6 Particle size distributions estimated for the sediment released by the CSD when dredging unit 6a. Particles size estimates are post-handling by the dredger (source: FAST JV). Note that 80% of the material released is expected to be larger than coarse sand (gravel, rocks).

Material Class	Size Range (μm)	percentage
Clay	< 7	21
Fine Silt	7 to 35	22
Coarse Silt	35 to 75	21
Fine Sand	75 to 130	6
Coarse Sand	> 130	30

Table 8-7 Particle size distributions estimated for the released by the TSHD when dredging unit 6a post-fracturing by CSD, without overflow (source: source: FAST JV)

Material Class	Size Range (μm)	percentage
Clay	< 7	8.8
Fine Silt	7 to 35	3.6
Coarse Silt	35 to 75	2.1
Fine Sand	75 to 130	2.4
Coarse Sand	> 130	83.1

Table 8-8 Particle size distributions estimated for the additional release by overflow from the TSHD when dredging unit 6a post-fracturing by CSD (source: Adjusted from Table 8-4 by removal of fractions > 75 µm)

Material Class	Size Range (µm)	percentage
Clay	< 7	52.1
Fine Silt	7 to 35	21.3
Coarse Silt	35 to 75	12.4
Fine Sand	75 to 130	14.2
Coarse Sand	> 130	0

8.3.4   Initial Distribution of Sediment

The indicative dredge logs specified that the TSHD will dredge for 20 minutes before overflow begins. Accordingly, discharge characteristic for the TSHD were split within each cycle: in the first 20 minutes sediment discharge was configured to represent the action of the dredge arm and propeller wash. Following this, and until the barge was full (hence, for variable periods), additional sediment loads were released to represent the additional input of overflow. The overflow period in each operation was defined by the production rate specified for the individual operation over a given sediment type and the effective barge capacity (10,000 m^3 for a 15,000 m^3 barge). The TSHD then moved out to the dump site and deposited the sediment into either Disposal Ground 3 or 7, in the order dictated by the dredging plan. Consequently, the TSHD was simulated as a moving and intermittent source, with variable outputs when dredging.

The initial vertical distributions of sediments were also following the indicative plan. The hydraulic resuspension from the TSHD dredge arm and propeller wash will be orientated towards the sea bed and decrease in effect towards the surface (Wallingford 2003). Overflow from the TSHD will be to 5-8 m below sea level and the mass of sediment in the release will force the plume to plunge vertically towards the seabed and spread as a density layer. Sediment released from material was assumed to be initially at highest concentration in the lower few metres, with lower concentrations billowing upwards. As overflow will occur near the middle of the water column, the initial vertical distribution of sediment was extended vertically when overflow was included. Material will be generated mainly near the seabed from the cutter head action. Hence a distribution biased towards seabed was specified. Tests of the vertical distributions indicated that only predictions of TSS close to the source will be highly sensitive. Concentrations at increasing distance are more strongly sensitive to the PSD of the sediment and the metocean conditions, by affecting settlement and resuspension.

The proposed areas to be dredged were classified as inshore or offshore. Inshore areas included the berth and wharf pockets, arrival and departure basins, the link channel, and the departure channel widening in Quantum 3. The departure channel was classified as offshore. Different vertical distributions were applied for the offshore and inshore sites to account for the difference in water depth. Table 8-9 summarises the initial vertical distributions applied for the different dredge cases and sites.

Table 8-9 Initial Vertical Distribution of Sediment specified in simulations

Depth Above Seabed (m)	% of Sediment mass		
	TSHD Dredging + Propeller Wash	TSHD Dredging + Overflow	CSD Dredging
Inshore - Berth & Wharf Pocket, Arrival & Departure Basins, Link Channel, Link Widening			
10	15	15	3
8	15	15	7
5	16	20	10
3	23	23	40
1	31	27	40
Offshore - Departure Channel			
15	15	12	3
10	15	20	7
7	20	22	10
5	20	22	40
1	30	24	40

Previous observations of sediment dumping from hopper vessels (e.g. Swanson *et al* 2004) have shown that there is an initial rapid descent of solids, with the heavy particles tending to entrain lighter particles, followed by a billowing of lighter components back into the water column after the sediments collide with the sea bed. A proportion of the lighter components will also remain suspended and may be trapped by density layers, if present. Because simulations in this study focussed on the far-field fate of particles due to transport and sinking after the initial dump phase, simulations were run with the initial vertical distribution specified to represent the post-collision phase for a case where a high proportion of the sediments are re-suspended after collision with the seabed, as summarised in Table 8-10.

Table 8-10 Initial vertical distribution of sediment from hopper disposal

TSHD Disposal	
Depth Above Seabed (m)	**% of Sediments**
10	5
6	10
2	15
1	30
0.5	40

8.3.5 Rates of Initial Suspension

Rates of suspension for the TSHD operations are expected to vary with the phase of the operation. A useful measure for calculating the mass flux of sediments into the water column generated by dredging is the suspension rate, R, which is calculated as the proportion of the production rate that is discharged, where the production rate is the mass of sediments removed over time. Published suspension rates from TSHD operations, with overflow, range from 0.003 to 2% of the production rate, with an 80th percentile of 1% (Anchor Environmental 2003). As a conservative approach, a rate of 1% was applied in this study for the overflow phase, and 0.03% for dredging with no overflow. Sediment suspension from the propeller wash was generated at a rate of 0.65 m^3/min (Herbich 2000).

As the CSD will discharge fractured material to the seabed using water pumps, all material dredged by the cutter was assumed to initially suspend, with highest concentrations toward the seabed, and the model allowed to calculate the separation of sediments, by particle size. The coarse sand particles would sink rapidly and force faster sinking rates and deposition of the finer components in this process.

8.4 Scenarios

Simulation scenarios were separated into four general operations:

1. dredging by TSHD of unconsolidated surface sediment;

2. dredging by CSD of rock strata, with direct discharge back to the seabed;

3. dredging by TSHD of the sediments deposited by CSD; and

4. TSHD disposal at the disposal site from operations 1 and 3. Due to the length and complexity of the proposed dredging program, it was necessary to separate the model scenarios into approximately 2 month blocks for quality control and security of the data.

The simulations were run using current and wave data spanning from May 1999 through to July 2004. The seasonal timing of the sample data reflected the proposed timing of the dredging programme, based on specifications from FAST JV which dictated that the dredging would commence in February. Potential inter-annual variability is captured within the dredge programme due to its length.

Simulations of the discharges for each particular operation (e.g. dredging by THSD) were run independently, as a time sequence with a span and seasonal timing defined by the timetable for that operation in the dredging plan. To account for the potential for ongoing resuspension and settlement of sediments contributed by these individual operations, simulations for each operation were continued for a further four months after discharges from that operation ceased. These simulations produced spatial distributions over time for individual operations.

The proposed dredging plan involves overlapping of individual operations, hence the potential for plumes and settlement patterns from individual operations to overlap and combine. This potential was accounted for by summing the sediment distributions predicted for individual operations at each hourly time-step for the duration of the operation plus the additional 4 months of post –operational investigation. This approach assumes that concentrations will be

additive and, therefore, that plumes do not interact in a manner that influences settlement or resuspension rates. Collectively, these simulations represented the cumulative outcomes of all dredging and disposal over the full operation, extending 4 months beyond the completion of operations. A summary of these simulations is presented in Table 8-11.
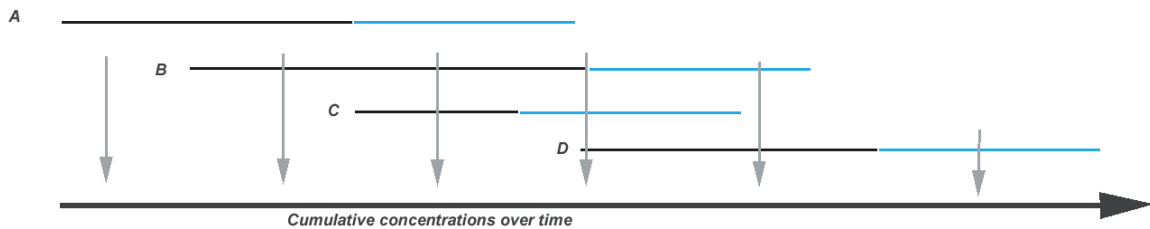
Figure 8-12: Schematic illustrating the approach used to represent the combined effect of individual operations (e.g. A, B, C, D) on the cumulative concentrations of TSS and sedimentation. Black bars represent simulations involving the discharge from a given piece of equipment. Blue bars represent on-going simulations without further new discharges to account for additional settlement and subsequent resuspension of sediments discharged from that equipment. Outcomes of overlapping simulations were subsequently summed to represent cumulative concentrations over space and time.

Table 8-11 Summary of the simulations representing the cumulative effects of dredging (TSHD and CSD) and hopper disposal.

Quantum 1			
Scenario	**Scenario Start/Finish**		**Number Days Covered**
Q1S1	1/02/2000	2/04/2000	61
Q1S2	2/04/2000	4/06/2000	63
Q1S3	4/06/2000	6/08/2000	63
Q1S4	6/08/2000	8/10/2000	63
Q1S5	8/10/2000	10/12/2000	63
Q1S6	10/12/2000	12/02/2001	64
Q1S7	12/02/2001	14/04/2001	61
Q1S8	14/04/2001	16/06/2001	63
Q1S9	16/06/2001	18/08/2001	63
Q1S10	18/08/2001	20/10/2001	63
Q1S11	20/10/2001	22/12/2001	63
Q1S12	22/12/2001	28/01/2002	37
Quantum 2			
Scenario	**Scenario Start/Finish**		**Number Days Covered**
Q2S1	28/01/2002	31/03/2002	65
Q2S2	31/03/2002	3/06/2002	64
Q2S3	3/06/2002	6/08/2002	64
Q2S4	3/08/2002	10/10/2002	68
Q2S5	10/10/2002	13/12/2002	64
Q2S6	13/12/2002	15/02/2003	64
Q2S7	15/02/2003	18/04/2003	62
Q2S8	18/04/2003	21/06/2003	64
Q2S9	21/06/2003	24/08/2003	64
Q2S10	24/08/2003	28/10/2003	65
Q2S11	28/10/2003	31/12/2003	64
Q2S12	31/12/2003	3/03/2004	63
Q2S12runon	3/03/2004	3/05/2004	61
Q2S12roro	3/05/2004	3/07/2004	61
Quantum 3			
Scenario	**Scenario Start/Finish**		**Number Days Covered**
Q3S1	1/05/1999	4/07/1999	64
Q3S2	4/07/1999	7/09/1999	65
Q3S3	7/09/1999	10/11/1999	64
Q3S4	10/11/1999	2/12/1999	22
Q3S4runon	2/12/1999	2/02/2000	62
Q3S4roro	2/02/2000	2/04/2000	59

8.5   Total Suspended Sediment Thresholds

Assessment for environmental influence and impact from suspended sediments was made by comparing the model estimates for TSS over time and space with thresholds for influence and impact developed from the field observations of TSS, turbidity and light attenuation within the study area. Full details of the field studies, data analysis and development of thresholds are provided in SKM 2009 and are only briefly summarised here.

Combined measurement of turbidity (correlated to TSS measurements) near seabed (~ 1m above seabed) and the light attenuation over the lower water column (between 2 m and 0.5 m above seabed) were made at 6 sites (Figure 8-13) off Port Hedland. These data, along with laboratory tests using local sediments, were used to calculate relationships between the attenuation of light at the seabed with TSS in the lower water column at each site. Three general environments were defined for the model domain based on variations in the observed light climate and patterns of turbidity (Figure 8-13):

1. Inshore environment (< 5 m chart datum): highly variable turbidity, highly variable light;

2. Midshore environment (5 to 10 m chart datum): less variable turbidity, but still occasional extremes of turbidity and low light;

3. Offshore environment (> 10 m chart datum): more stable and generally lower turbidity but with lower light reaching the lower water column.
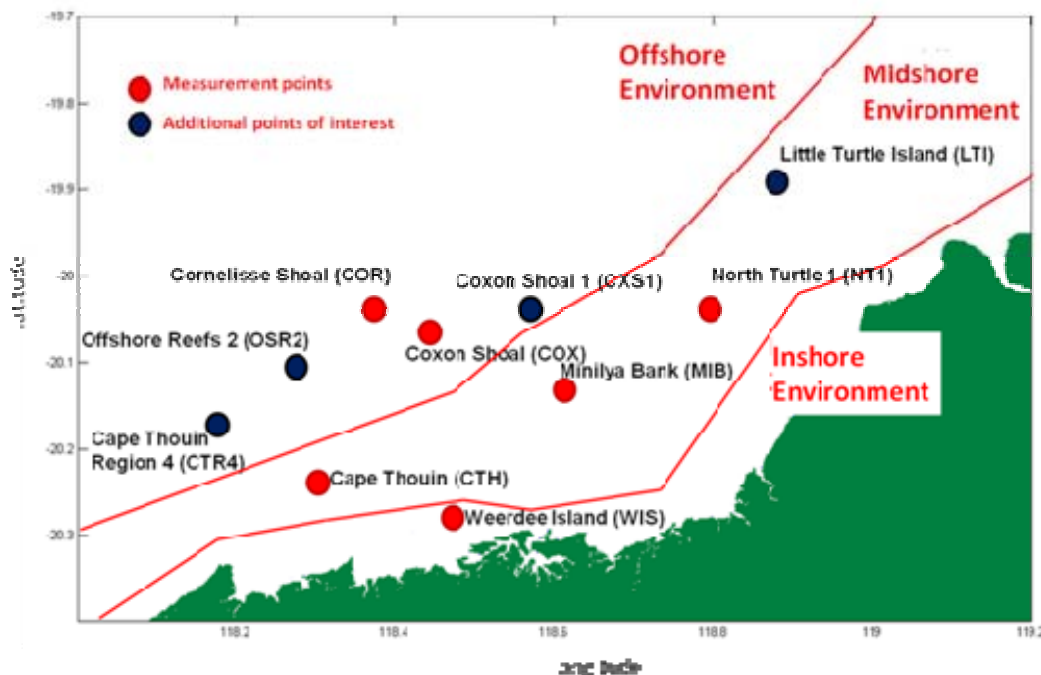
Figure 8-13 Threshold environments derived by SKM for both TSS and sedimentation thresholds. The environments are labelled Inshore/Midshore/Offshore as shown.

The field data also indicated seasonal patterns in the turbidity and light attenuation, which were related to the direction of prevailing winds and the potential for rainfall and cyclones.

These were used to define two major "seasons" for the turbidity and light attenuation affecting benthic primary producers.

1. Dry: June to November

2. Wet: December to May

It should be noted that the seasons defined for the threshold analysis are a simplification of the summer, autumn, winter and spring delineation considered elsewhere in this report.

Preliminary modelling interrogations used the value of the LAC in the lower water column as an estimation of the background LAC for the entire water column. Field investigations indicated that measurements of LAC in the bottom layer of the water column represented a gross overestimate of the depth averaged LAC because sediments tend not to be distributed evenly in the water column, occurring at highest concentrations close to the seabed. Consequently, it was necessary to develop more realistic estimates of the LAC due to background.

The alternative estimate that was derived was to analyse the 12 months of turbidity measurements from each monitoring site to calculate a background turbidity value for the entire study area, suitable for both summer and winter seasons. This turbidity value was converted to LAC via the laboratory-derived relationship between turbidity and LAC and used in the plume model interrogations as background LAC.

Estimates for the TSS (mg/l) that would attenuate 99% of the light reaching the benthic layer were then derived for each combination of environmental zone (Inshore, Midshore and Offshore) and season (Dry season and Wet season) and supplied to APASA to interrogate the model predictions for occurrences of 'total' light attenuation at hourly steps during the photosynthetically-productive daylight hours.

The analysis for the TSS thresholds was performed using the following conditions, following SKM 2009:

- TSS concentrations were derived from the model as depth-averaged values for the water-column. The depth-averaged model TSS concentration was converted to a light attenuation coefficient (LAC) using the TSS-LAC relationship derived in a tank by IMO using sediments from the Pt Hedland Geotech programme according to LAC = $TSS/64.599$ m^{-1}.

- A constant background LAC = 0.025 m^{-1} was added to the model calculated LAC.

- The analysis of model results was performed on daytime TSS estimates only (8 am to 5 pm), and durations were reset after 5 pm on each day (i.e. there was no carryover from one day to the next morning).

- Thresholds were analyzed based on discrete 14 day periods based on sampling statistics of the measured data being composed of 14 day periods.

To determine if there was a change in the areas of influence and impact over the different stages of the proposed operation, separate analyses were conducted for Stages, 1, 2 and 3. Cumulative areas of Influence and impact were then mapped for the end of each break in

operations, namely at the end of Stage 2 (cumulative of Stage 1 and 2) and the end of Stage 3 (cumulative of Stages 1, 2 and 3).

The Zone of Potential Influence was defined as follows:

- The surface light attenuation condition is defined when E*d > 1.6 (where d=depth in m and E is the light attenuation coefficient in m^{-1}).

- If the surface light attenuation condition (E*d > 1.6) is reached for >135 times in a 14 day period, then there is an exceedence for that 14 day period.

- If four or greater consecutive fortnights of exceedences this area is deemed to be influenced and goes into the zone of potential influence.

The Zone of Potential Impact was defined as follows:

- The surface light attenuation condition is defined when E*d > 2.0 (where d=depth in m and E is the light attenuation coefficient in m^{-1}).

- If the surface light attenuation condition (E*d > 2.0) is reached for >125 times in a 14 day period, then there is an exceedence for that 14 day period.

- If four or greater consecutive fortnights of exceedences this area is deemed to be impacted and goes into the zone of potential impact.

8.5.1 *Gross daily Sedimentation Rate Thresholds*

Statistics for the gross daily sediment deposition rates were calculated by SKM from field measurements within the study area (Table 8-12) and are based upon gross sedimentation rates.

Based on these statistics, SKM defined an exceedance as any estimate for the gross daily sedimentation rate calculated at a given location that exceeded the calculated values for any one of a range of statistics. The statistics that were calculated were the 1.1x, 1.5x and 2x the maximum values defined for each environment. Tests for the other statistics are based on statistics calculated over 14 day periods. Note also that sedimentation rates were calculated for data estimated for day and night (24 hrs per day for 14 days).

Table 8-12 Sedimentation estimates per 14 day period derived for the study zones by SKM. Values for the variables in bold were set as potential thresholds of exceedance.

Sedimentation (mg/cm2/day)	INNER (WIS)		MID (CTH/MIB/LTI)		OUTER (COX/COR)	
	DRY	WET	DRY	WET	DRY	WET
Mean	**93**	**482**	**13**	**95**	**7**	**26**
Median	78	188	10	40	5	12
80th	135	682	19	87	10	37
95th	169	1417	28	304	15	122
99th	209	2046	53	725	18	131
100 th	220	2203	57	726	20	133
1.1 times max	**242**	**2423**	**63**	**798**	**22**	**147**
1.5 times max	**331**	**3304**	**86**	**1088**	**29**	**200**
2 times max	**441**	**4406**	**114**	**1451**	**39**	**267**

Based on the estimated rates of background sedimentation, there is substantial variation in the thresholds that were applied for each season and zone combination. For example, the tolerances for sedimentation rates permissible within the outer zone were 15 to 20 times lower than those for the inner zone, depending on the season and statistic. The dry season tolerances were also substantially lower than those for wet season in all zones. In addition, the range between the maximum and median is substantially lower during the dry season.

8.6   Results of the main dredging and disposal study

8.6.1   General findings

There were a number of general observations derived from simulations of the dredging and disposal operations.

Simulations indicated that plumes of suspended sediments would mostly only affect near-surface waters immediately around individual operations because sediments suspended by the operations would tend to only mix to the surface close to the sources and would then sink to near seabed with distance. Figure 8-14 shows an example of the exponential decrease in surface concentrations and clear vertical bias in the predicted distribution of plumes generated by dredging operations. The example is for a point in time approximately 2 months after the operation commences (mid-April environmental sample). Near-surface concentrations around the operations at this time are predicted to decrease to < 5 mg l^{-1} above background within 1 km of the source locations through sinking and dispersal of the suspended sediments. However, concentrations are predicted to exceed 10 mg l^{-1} above background up to 10 km away in the near bottom layer. Due to the vertical stratification of the plumes that were predicted from dredging and disposal, the remainder of the analysis concentrated on concentrations expected in the lower water column (< 2 m above seabed), rather than depth-averaged concentrations. It should be noted that 1) the full distributions that are described will not be visible to observers viewing from above water level because of their vertical position in the lower water column and 2) concentration values that are presented will be substantially higher than the equivalent results quoted in a depth-averaged fashion. Depth-averaged values would be diluted by the lower concentrations in the upper water column.

Sinking rates will be exponentially higher for higher particle-sizes of sediment suspended by the operations. Consequently, the particle-size distribution of the plumes was predicted to change with distance from the release. Particles of the size of coarse sand and larger, which would be released by cutter suction operations, propeller wash and the action of the TSHD draghead, are predicted to settle rapidly and therefore close to the discharge sources. In contrast, finer particles initially suspended by all operations tended to drift over a relatively long distance (multiple kilometres) immediately above the seabed, undergoing short term sedimentation and resuspension due to the magnitude of the shear stress generated by the local tidal currents alone. The influence of the wave climate was also manifest in the results. The influence of shorter waved-length wind waves, which occur frequently with a daily rhythm (increasing in the afternoons), was mostly expressed in the resuspension of sediments that had settled in the shallower waters. In contrast, the influence of longer wave-length swell-waves on resuspension (hence suspended sediment concentrations in the lower water column) occurred less frequently, more randomly, and extended into deeper water. The collective outcome was that near-seabed plumes are predicted to extend over a substantially larger area than the obvious surface plumes.

It should be recalled at this point that predictions for the resuspension of fine sediments that have deposited to the seabed are based on 1) the levels of shear stress that are required to suspend particles of a given size from the surface layer and 2) assumptions in the model for how cohesive the dredged sediments will be and hence to what degree the fine sediments would bind to the seabed, hence limiting their resuspension. While the model does account for clumping and armouring of sediments among the interstitial spaces of the seabed, which is based on a dynamic calculation of the average particle-size distribution of deposits, a relatively low level of cohesion has been assumed for the sediments to be discharged by dredging and disposal in this study area. This assumption is applied as a conservative measure because the resuspension of the particular material in the area.

Plume distributions and migrations over the longer term were affected by two main processes: onshore-offshore migration and mixing by the tide and longshore migration due to seasonal drift. The relatively strong tidal currents were predicted to set up sufficient shear stress at the seabed to inhibit settlement of the finer sediments (clay and fine silt size classes) to the seafloor and to resuspend a proportion of fine sediments that had previously deposited. Resuspension of finer sediments was also predicted in the simulations to generate secondary surface plumes along the shallow coastal margin, which are illustrated in Figure 8-14.

Turbidity levels in this inshore area are naturally turbid, with patterns that indicate increased turbidity during spring tide periods, indicative of resuspension by tides. Tidal oscillations are predicted to maintain fine dredged sediment in suspension where they will undergo on-shore-offshore migration. Because shear-stresses decrease over the slack tides at the end of the ebb and flood, there is a resulting increase in the rate of settlement over the turning of the tides followed by an increased rate of suspension as the tidal current speeds increase. This process is illustrated for a time sequence in Figure 8-15. Note that the resuspending particles are restricted to the lower water column (see cross-sections), forming a turbid bottom layer and that concentrations fluctuate over relatively short time periods. One consequence is that turbidity layers will not be maintained for long durations (> hours) over a given location on the seabed. Elevated concentrations will occur as pulses.

Because deposition and suspension are competing processes, increases and decreases in suspended sediment concentrations were associated with decreases and increases in sediment deposition, respectively. One outcome of this was that both TSS concentrations and deposition concentrations outside of the immediate area of operations were predicted to be variable over time with a tidal frequency.

In contrast to tidal influences, the effect of waves tended to be less regular, dependent upon the study area experiencing long-period waves (swells) of sufficient magnitude to penetrate to the seabed. Return periods for these events are of the order of multiple days to multiple weeks. Although less frequent, levels of shear stress are predicted to last longer than a tidal cycle (one or more days) and reach sufficient magnitude to resuspend deposited sediments ranging up to the size of coarse sand. Hence, a proportion of the finer sediments was predicted to resuspend from the deposits generated within the dredging and disposal areas under these conditions. Thus, these periodic events tended to redistribute coarser sediment deposits, generate additional short-lived TSS concentrations and contribute to the mass of fine sediments available for subsequent tidal resuspension.

The variability of the TSS concentrations expected from tidal and wave forcing has consequences for the analysis of ecological risks due to such stressors as light reduction or smothering because influences will tend to be variable with time over a given part of the seabed.

Simulations indicate that there would be a net drift of finer sediments originating from the dredging and disposal operations over the long-shore axis. This net drift was set up by wind forcing during periods of sustained wind patterns and affected both the transport of fine sediments released directly from the dredging and disposal, and the sediments resuspended off the bottom after previously settling. The net drift tended to be persistent over time scales of multiple days to months.

The net drift was to the northeast for the majority of the time, predominantly during late spring, summer and early autumn but reversed to westward during mid to late winter, as expected from the analysis of the current data measured adjacent to the project area. The dredging operation would involve multiple sources of initial sediment suspension, extending up to 36 km in the inshore-offshore direction and this large spread of the initial plume sources had the effect of widening the sources of the initial suspension across the axis of the drift currents, thus widening the source of sediment available for resuspension and net drift.

Predictions for the spatial distribution of elevated TSS and sediment deposition with the influence of resuspension, under net drift, were also influenced by the timetable that was assumed for the operations. Simulations assumed that dredging would commence at the end of a summer season, limiting the time for material to drift northeast before the drift reversed towards the west over the first winter. Hence, significant net drift of fine dredged sediments towards the northeast was not predicted until the second summer. Above background TSS and sediment deposition loads that are predicted to affect locations to the north-east over this second summer were increased due to resuspension of sediments that had previously deposited. In general, there was a prediction for the TSS and sediment deposition rates to increase as the operation continued due to the increased availability of resuspendable sediments (i.e. the sediment mass associated with dredging and disposal increased at a greater rate than that of dispersal and stable deposition). Following cessation of Stage 2 and Stage 3, the TSS and sediment deposition rates decreased as the supply of new mass ceased.

.
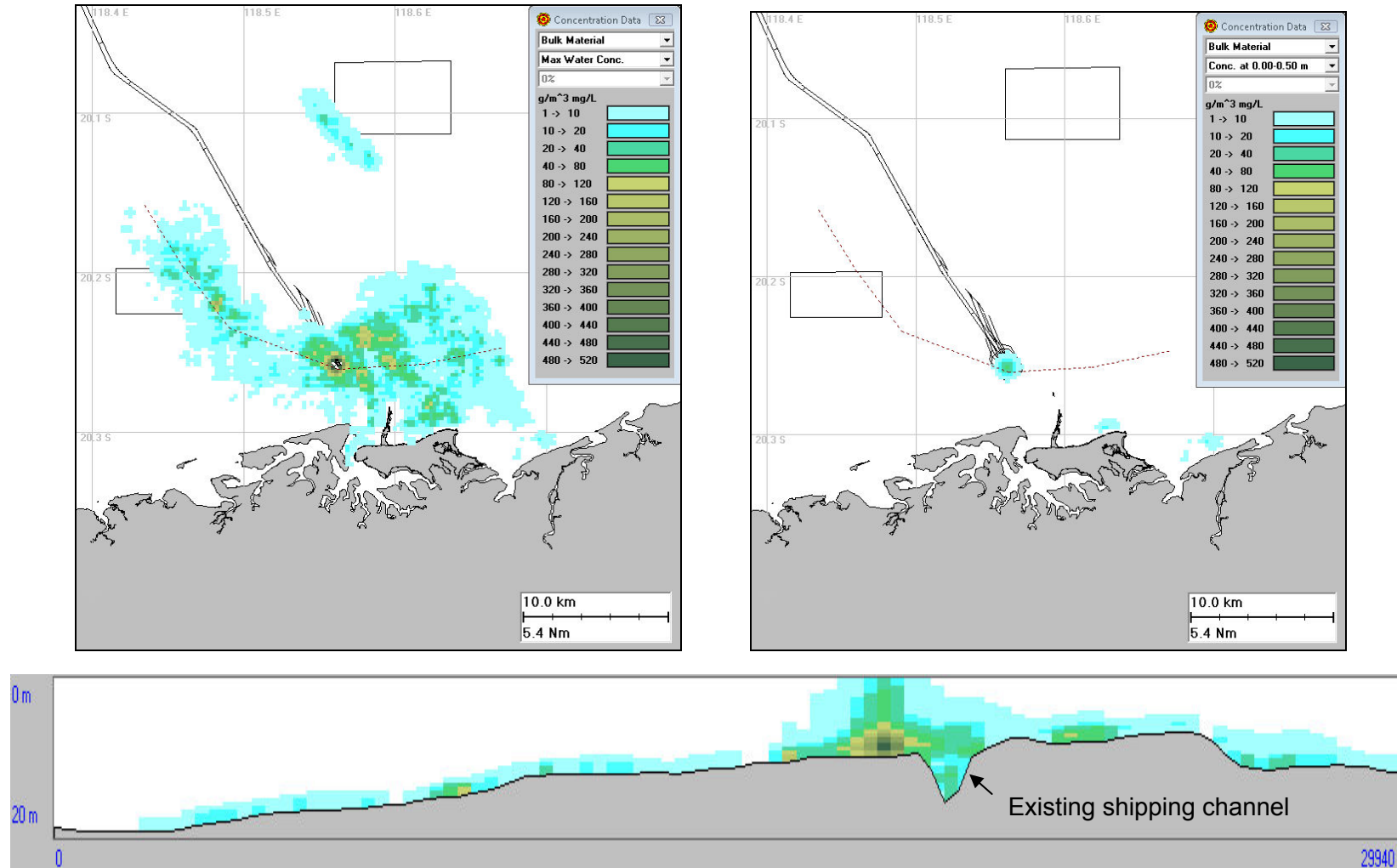
Figure 8-14: Example predictions for the above-background TSS generated by dredging operations in the berth and disposal into the disposal grounds illustrating the trend for plumes to sink and migrate near seabed. The upper images show the spatial distribution at one point in time for (left) the seabed layer (0-0.5 m above bottom) and (right) the surface layer (0-0.5 m below sea level). The lower image shows a cross-section along the dotted line shown in the upper images.
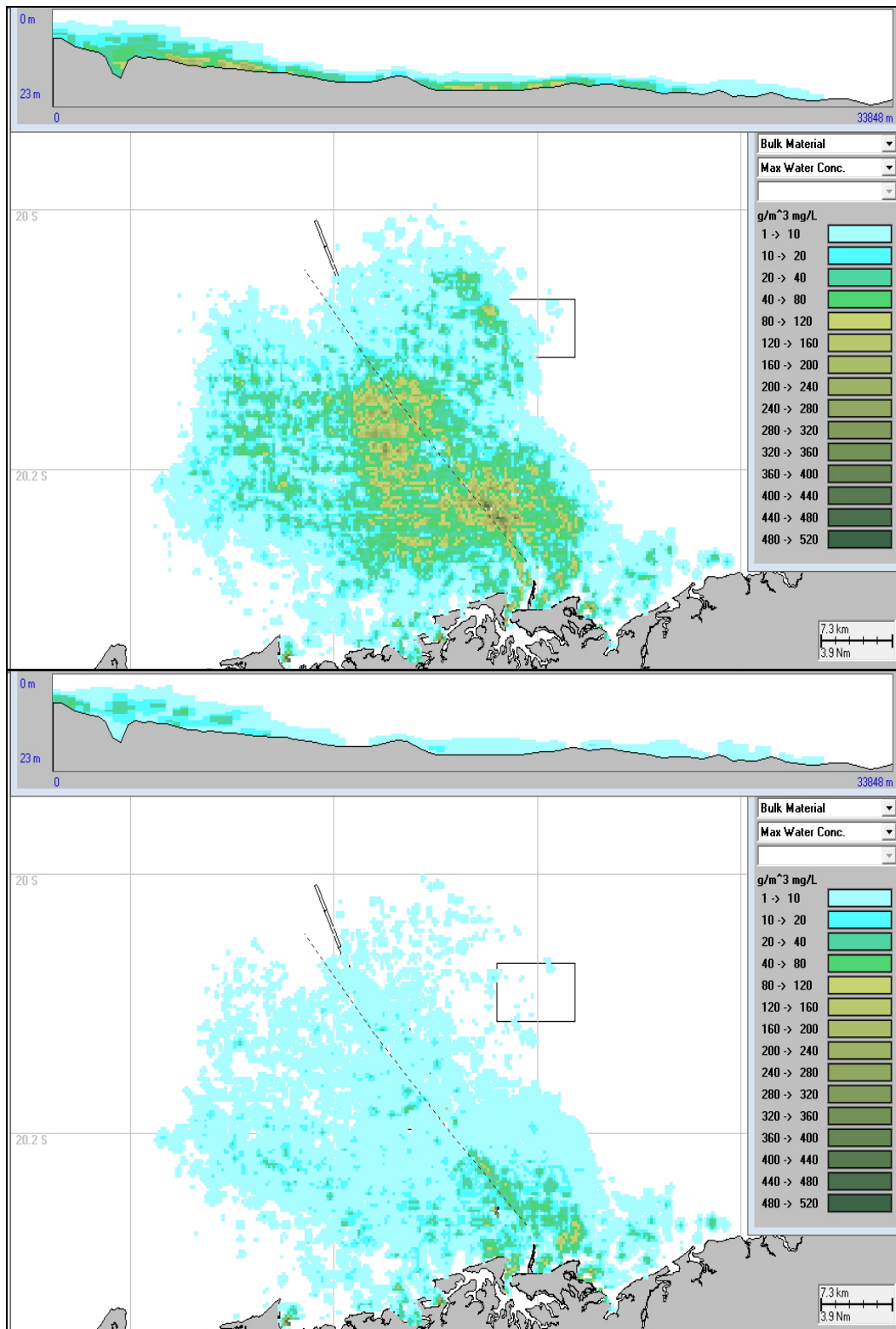
Figure 8-15: Examples of the TSS distributions predicted for points in time over a tidal cycle showing the influence of tidal resuspension and migration. The figures represent a time series at 3 hourly intervals and show (upper) mid-ebb flow (lower), slack tide after the ebb. The example is from 3 months after commencement of dredging.
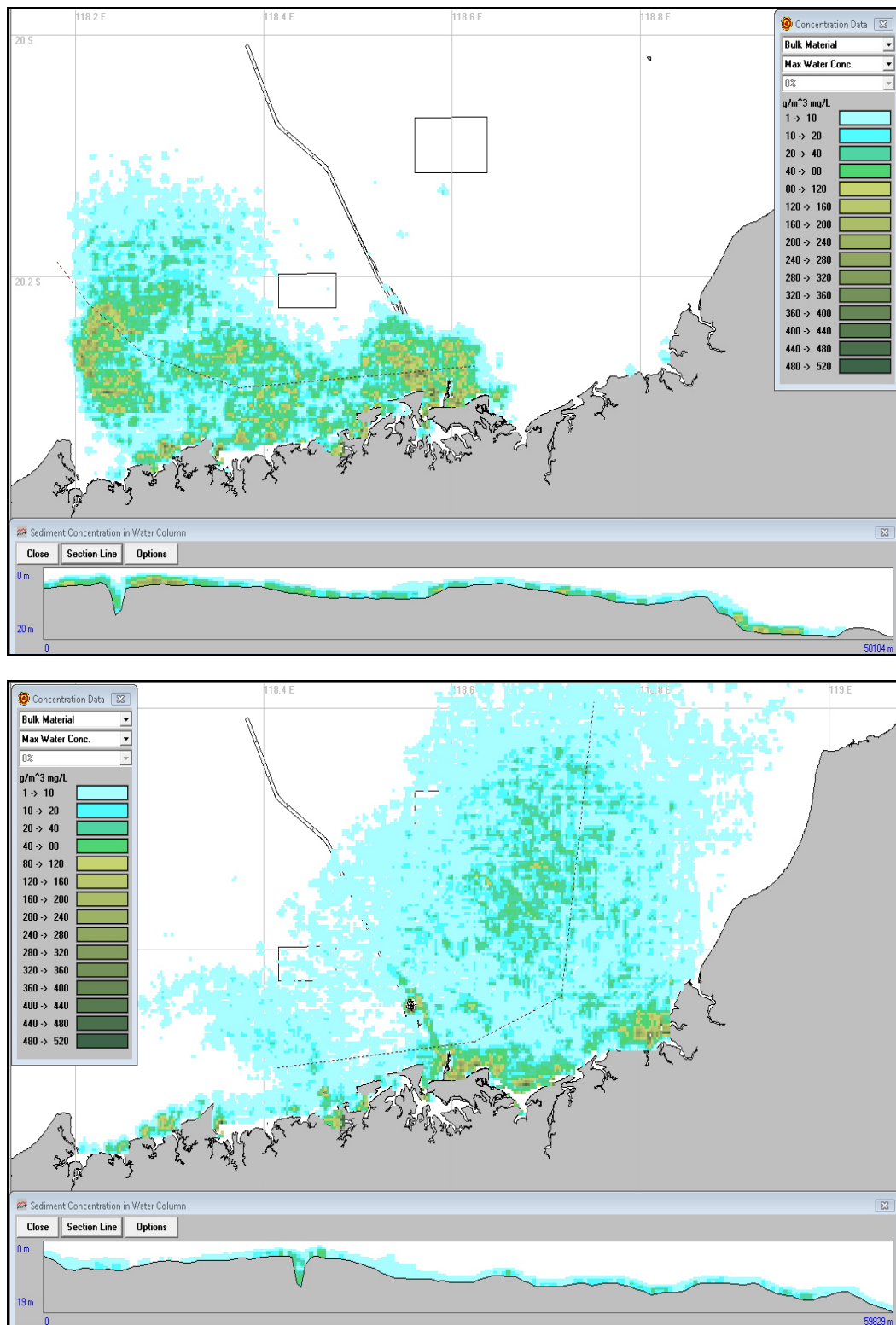
Figure 8-16: Examples of the TSS concentrations predicted at single points in time near the end of the first winter period (upper image) and the second summer period (lower image). The images show the concentrations near seabed in plan view and vertical cross-sections along the lines marked in the plan view.

8.6.2   Temporal summaries of predicted TSS concentrations

Outcomes of the dredge simulations have been summarised in Appendices D and E in terms of the median and 80th percentile of TSS concentrations and net sediment deposition predicted for each location over all three stages of the operation. Median concentrations are used to indicate the central tendency (i.e. more typical concentrations) because the data is distinctly skewed, with a small percentage of high values among a high percentage of low values. The 80th percentile concentrations (concentrations that are $\geq$ 80% of the concentration estimates over time) will be more indicative of unusually energetic combinations of tidal currents and wave conditions that are generating high resuspension of dredged sediment from the seabed. The approach of isolating individual stages of the dredging and disposal programme allows analysis of the evolution of the field of effect.

TSS concentrations that were used in the analysis were the concentrations predicted for the layer between 0.5 and 1.5 m above seabed, to correspond with the general depth of measurement of background turbidity conducted for the project by FAST JV. As previously noted, suspended sediments will not be evenly mixed among depth layers and are expected to concentrate near-bottom outside of the immediate dredging and disposal discharge. Hence, the highest concentrations will tend to be reported for the lower water column. It is important to note that these estimates will be considerably higher than depth-averaged estimates, which would be diluted by the lower concentrations expected in the higher water column. Statistics for sediment deposition are for measures of the mass per area at hourly steps.

Stage lengths over which the median and 80th percentiles were calculated were approximately 2 months in each case (Table 8-11) and the input values were at hourly steps.

Results indicate a trend for the TSS concentrations to generally rise over time around the dredging and disposal area during the first months. For example, simulations over the first 2 months (Q1S1) indicated median TSS concentrations up to 20 mg l^{-1} near bottom would be restricted around the dredging operations. Over the next 2 months (Q1S2), median concentrations > 20 mg l^{-1} near bottom was expected to cover a larger area. However, this trend was periodically broken, with concentrations falling between periods. As previously discussed, this prediction is attributed to a tendency for the finer sediments released from the operations to regularly resuspend with the tidal climate. The rate at which fines were released by the dredging and disposal was predicted to exceed the rate of dispersal from the area during some periods, hence there was a net increase in TSS expected. During other periods, there was reduced wave and current forcing, reduced dredging discharge, or both.

Seasonal changes in the current and wave conditions resulted in shifts in the general magnitude and distributions of elevated TSS in the simulations. Plumes were predicted to migrate inshore and offshore with the tide but with an alignment diverted alongshore due to the prevailing net drift. Under the more common south-westerly seabreeze pattern, the near-dredge and near-disposal plume that is visible at the surface will drift toward the east to northeast. The plume was indicated to sink and form a dense layer close to the seabed over distances of a few hundred meters to 1-2 km. Both the maintenance of these plumes as suspended sediment, and the generation of additional suspension concentrations (from previously settled sediments), was enhanced during spring tides and when swells were

affecting the seabed. Highest suspension loads were generated when spring tides corresponded with swells. These observations indicate that resuspension of previously handled sediment will enhance background concentrations, which will also respond to similar forces. Locally generated plumes resulting directly from dredging and disposal operations would add to the background loads and local turbidity could be managed with consideration to variations in these background concentrations. Simulations described in this study did not adjust rates of dredging and disposal for the sea conditions. Hence the area of impact that is predicted immediately around the operations might be reduced by an operation that reduced new discharges when swells were anticipated. Noting that sediments that have deposited for short time periods (hours to days) require much reduced bed stress to be resuspended, management would need to consider forecasts for a number of days ahead.

The dredging and disposal sites are in relatively shallow water (5-13 m) and the measured wave data for this area indicates that long period swell waves (wave period of 12-20 seconds) occur up to 35% of the time. Although waves rarely (< 10% of the time) have a significant height >1 m, the simulations indicated that these waves would set up sufficient bed shear in the water depth to force resuspension of both the natural seabed sediments and fine sediments that have deposited after release from dredging and disposal. Significant reworking and mobilisation of the sediment piles is predicted to occur frequently, adding to the fine sediments loads over the seabed downstream of these sources. Given the working environment, reactive adjustments to dredging operations would not affect resuspension from the bed of this material.

Further from the sources, finer sediments are predicted to migrate near seabed towards the east then north-east (with the northward divergence of the coast) over a series of resuspension and settlement cycles during the summer and transitional seasons. Under the winter winds, a net westward drift was indicated both by the hydrodynamic model and the measured current data, which is attributed to the more persistent easterly winds. This change in the net drift is expected to result in the shunting of fine dredged/disposed sediments westward. The migration distance was indicated to be smaller than the case under summer winds. This result is attributed to the reduced wave action in the modelled area (due to the reduced fetch) represented in the winter samples, due to the prevailing wind approaching from the land. Summer winds and associated swell waves are predicted to cause increased resuspension rates and a net drift to the north-east over a relatively wide area extending parallel with the depth contour, as far as Larrey Point in the simulations (e.g. Figure D-11 to D-14; D-21 to D-26; D-38 to D-48). Elevated TSS concentrations up to 50 mg l^{-1} are predicted to occur along the axis of the drift and over patches as far as North Turtle Island. Larrey Point was at the easternmost margin of the model and while the model indicated that concentrations would be decreasing by this distance, results indicate that some sediment might be migrated further beyond Larrey Point over summer seasons.

Elevated TSS concentrations were also predicted for pockets along the coastal margin under both summer and winter conditions due to the net transport of this material through tidal shunting. Trapping and build up of the sediments was indicated to result in turbidity due to repeated resuspension under wave action. Concentrations > 100 mg l^{-1} are indicated over these sections (e.g. D-36).

Simulations in the post-dredging periods, following Stages 2 and 3, represented TSS and sedimentation rates resulting from resuspension only, with no new discharge sources. Results indicate that elevated TSS concentrations will continue to generate for some time (a number of months as a minimum), but with a more restricted distribution. These distributions were closer to the dredge and disposal areas where sediment loads from dredge and disposal discharges are predicted to remain at higher concentrations.

8.6.3 Estimates for the zones of Potential Influence due to suspended sediments

The Zone of Potential Influence due to light attenuation resulting from suspended sediment concentrations are plotted below, delineated for the wet and dry seasons during each stage of the operation. The figures show the locations of exceedance of the TSS threshold for potential influence. The TSS thresholds for potential influence were calculated for TSS expected to occlude 40% of light reaching the seabed, based on persisting for defined durations and frequencies, respectively (See SKM 2009 for full details).
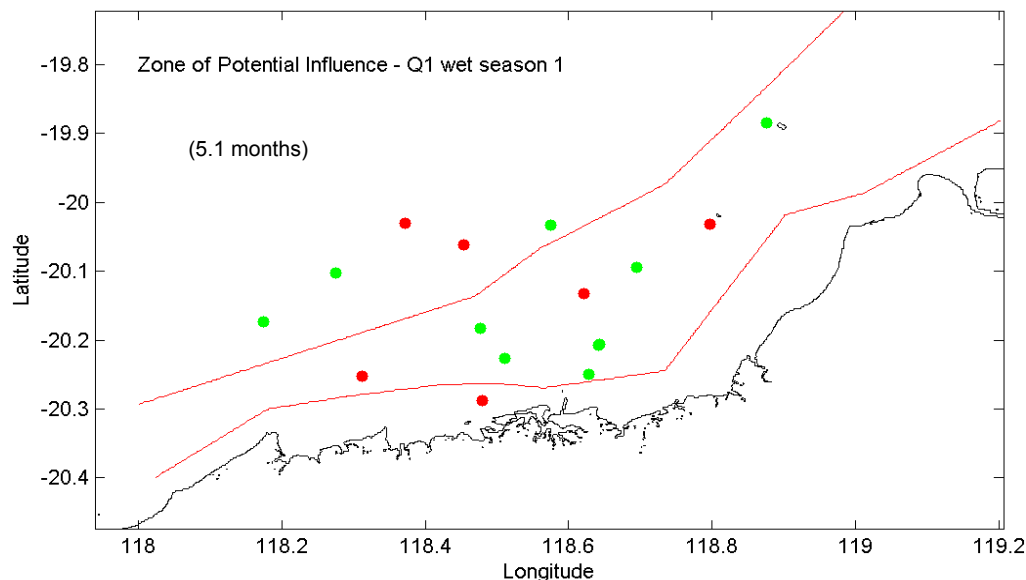
Figure 8-17 Zone of Potential Influence for the first wet season of Quantum Stage 1, which is 5.1 months long. The red lines mark defined zone boundaries, where different threshold criteria were applied. The red dots are the monitoring sites; the green dots are additional sites of interest.
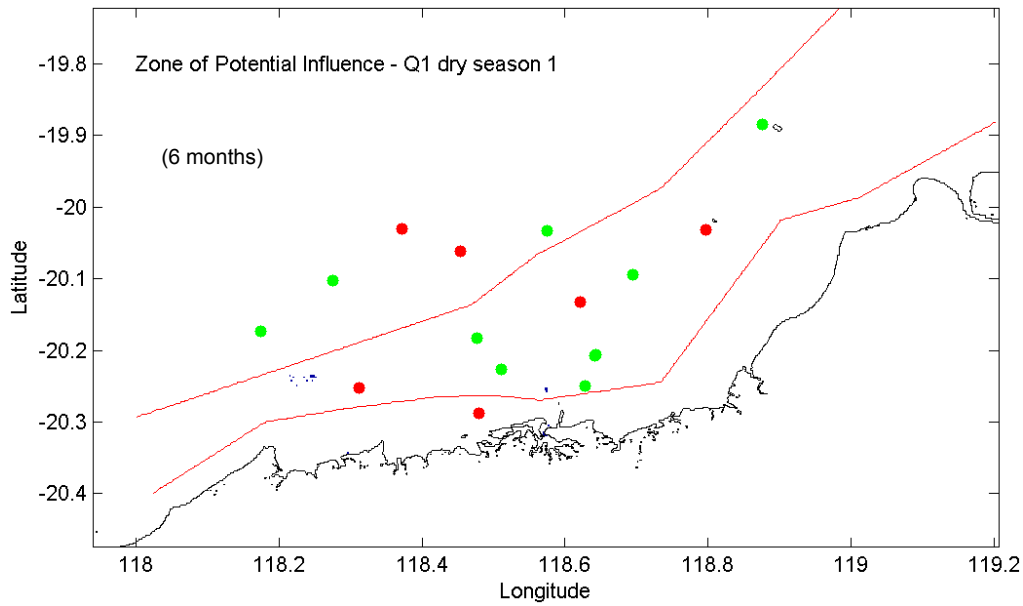
Figure 8-18 Zone of Potential Influence for the first dry season of Quantum Stage 1, which is 6 months long. The red lines mark defined zone boundaries, where different threshold criteria were applied. The red dots are the monitoring sites; the green dots are additional sites of interest.
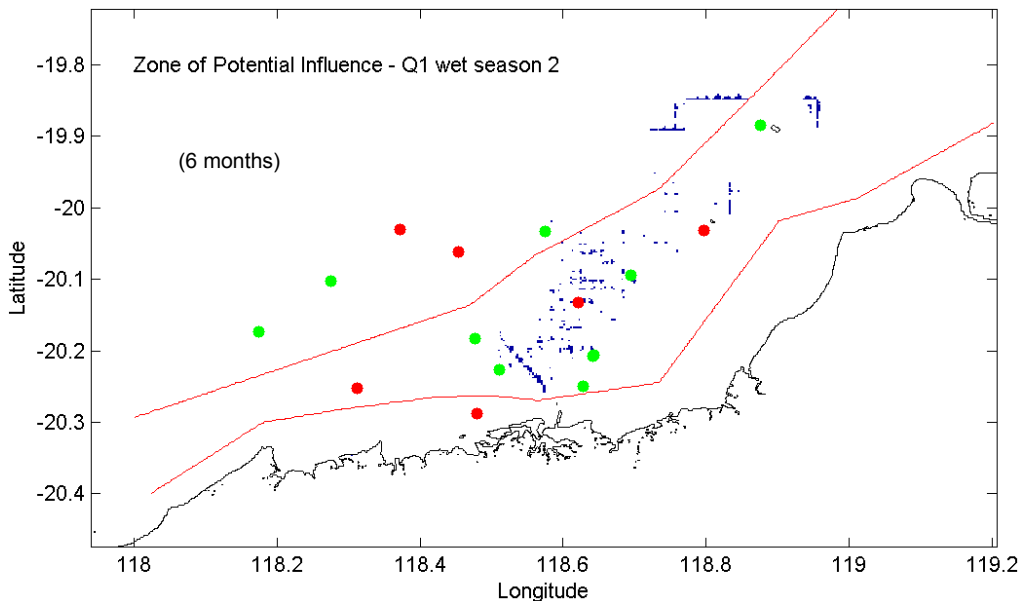
Figure 8-19 Zone of Potential Influence for the second wet season of Quantum Stage 1, which is 6 months long. The red lines mark defined zone boundaries, where different threshold criteria were applied. The red dots are the monitoring sites; the green dots are additional sites of interest.
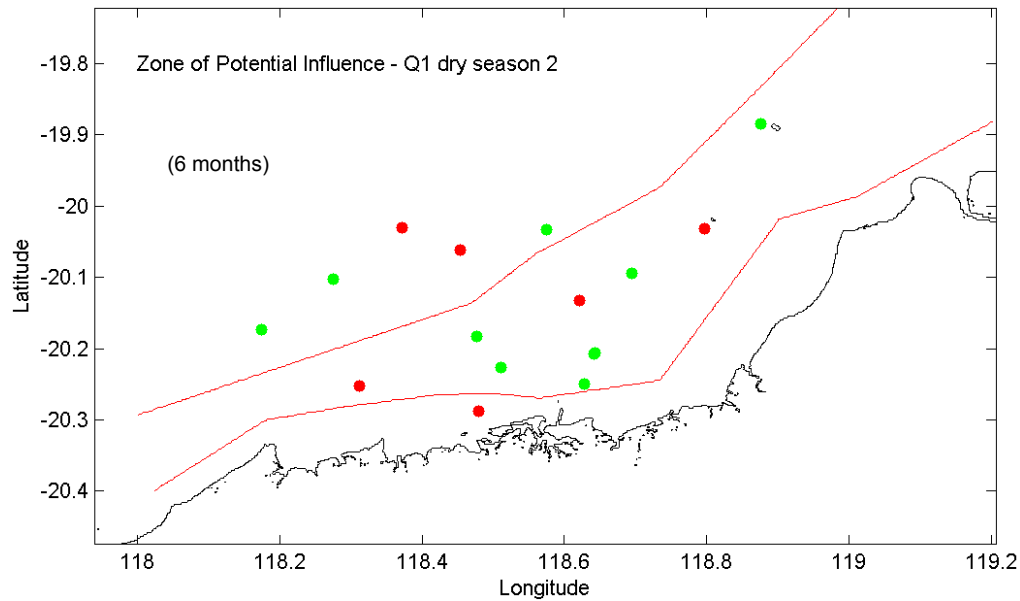
Figure 8-20 Zone of Potential Influence for the second dry season of Quantum Stage 1, which is 6 months long. The red lines mark defined zone boundaries, where different threshold criteria were applied. The red dots are the monitoring sites; the green dots are additional sites of interest.
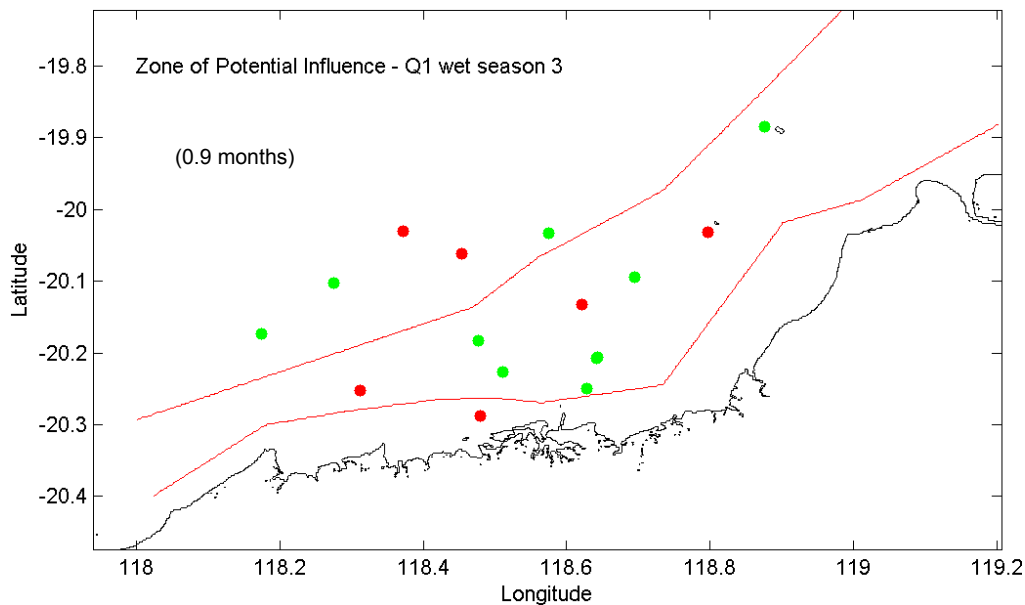
Figure 8-21 Zone of Potential Influence for the third wet season of Quantum Stage 1, which is 0.9 months long. The red lines mark defined zone boundaries, where different threshold criteria were applied. The red dots are the monitoring sites; the green dots are additional sites of interest.
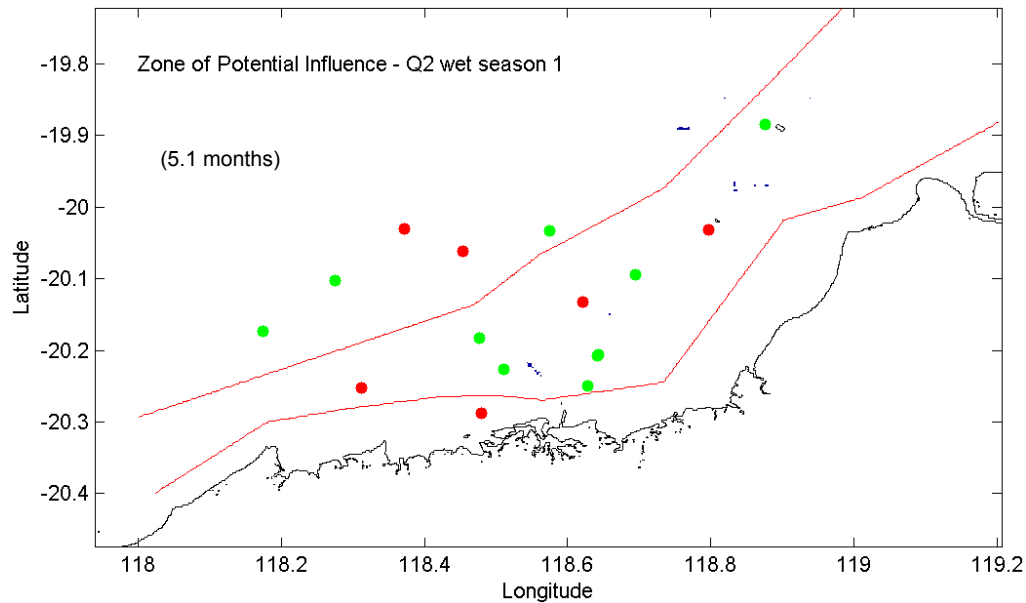
Figure 8-22 Zone of Potential Influence for the first wet season of Quantum Stage 2, which is 5.1 months long. The red lines mark defined zone boundaries, where different threshold criteria were applied. The red dots are the monitoring sites; the green dots are additional sites of interest.
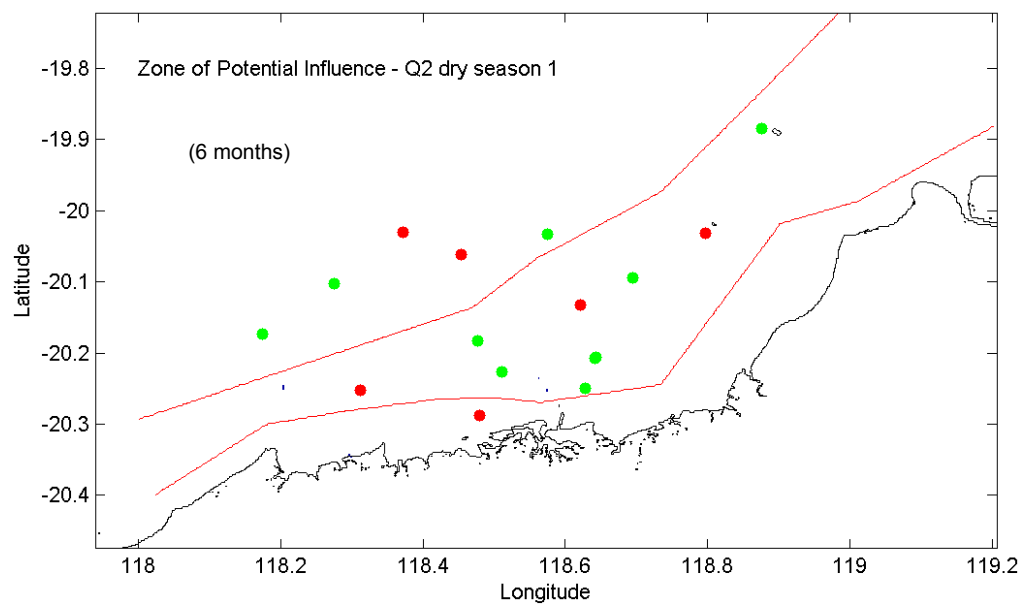
Figure 8-23 Zone of Potential Influence for the first dry season of Quantum Stage 2, which is 6 months long. The red lines mark defined zone boundaries, where different threshold criteria were applied. The red dots are the monitoring sites; the green dots are additional sites of interest.
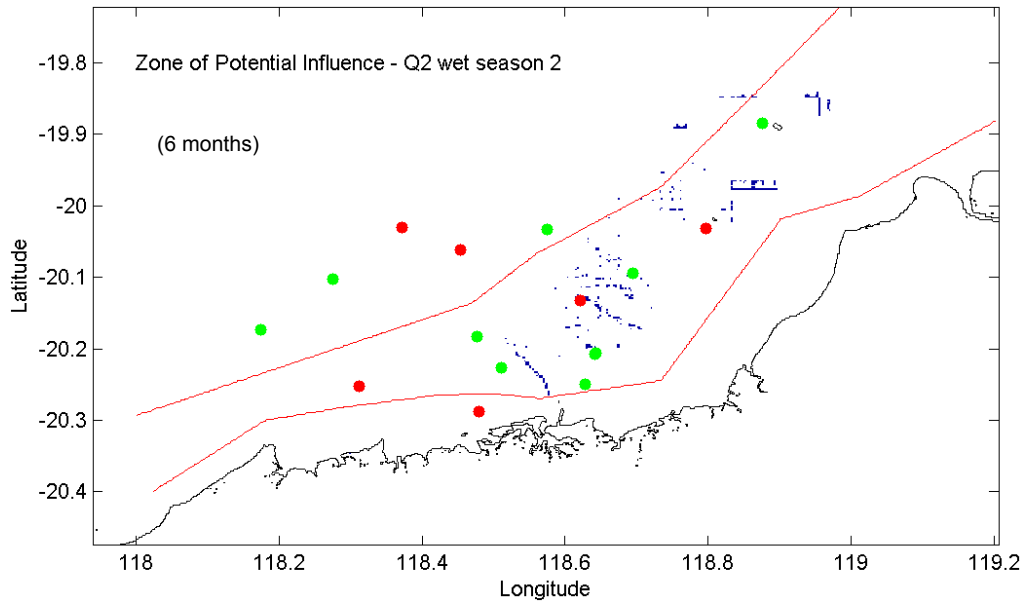
Figure 8-24 Zone of Potential Influence for the second wet season of Quantum Stage 2, which is 6 months long. The red lines mark defined zone boundaries, where different threshold criteria were applied. The red dots are the monitoring sites; the green dots are additional sites of interest.
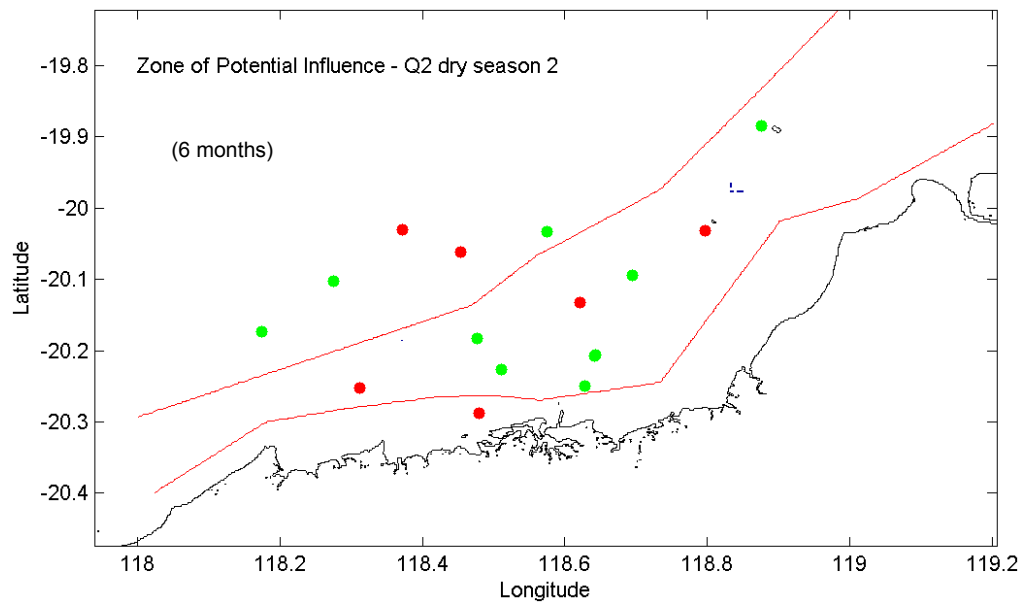
Figure 8-25 Zone of Potential Influence for the second dry season of Quantum Stage 2, which is 6 months long. The red lines mark defined zone boundaries, where different threshold criteria were applied. The red dots are the monitoring sites; the green dots are additional sites of interest.
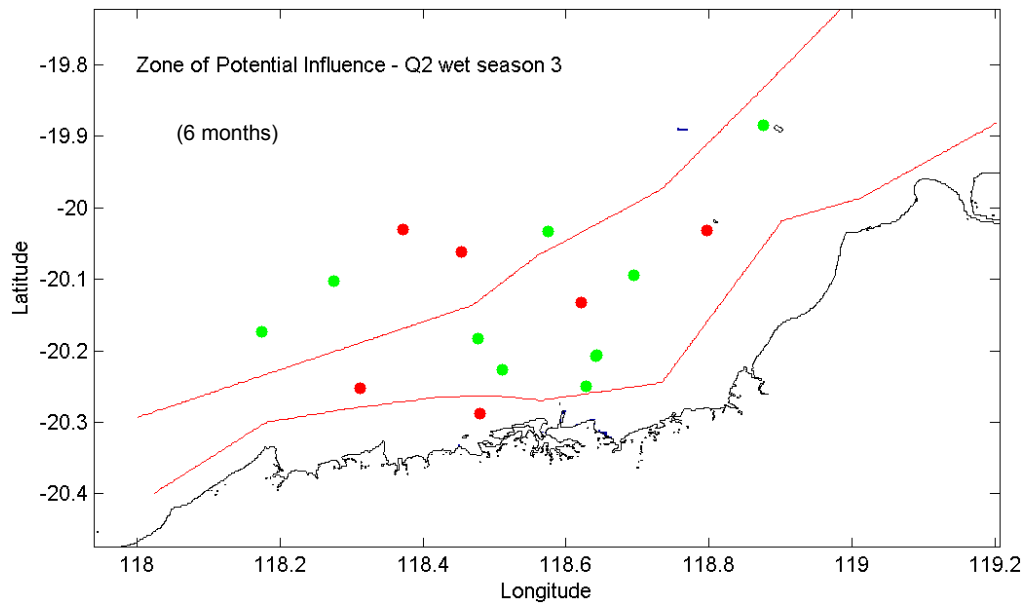
Figure 8-26 Zone of Potential Influence for the third wet season of Quantum Stage 2, which is 6 months long. The red lines mark defined zone boundaries, where different threshold criteria were applied. The red dots are the monitoring sites; the green dots are additional sites of interest.
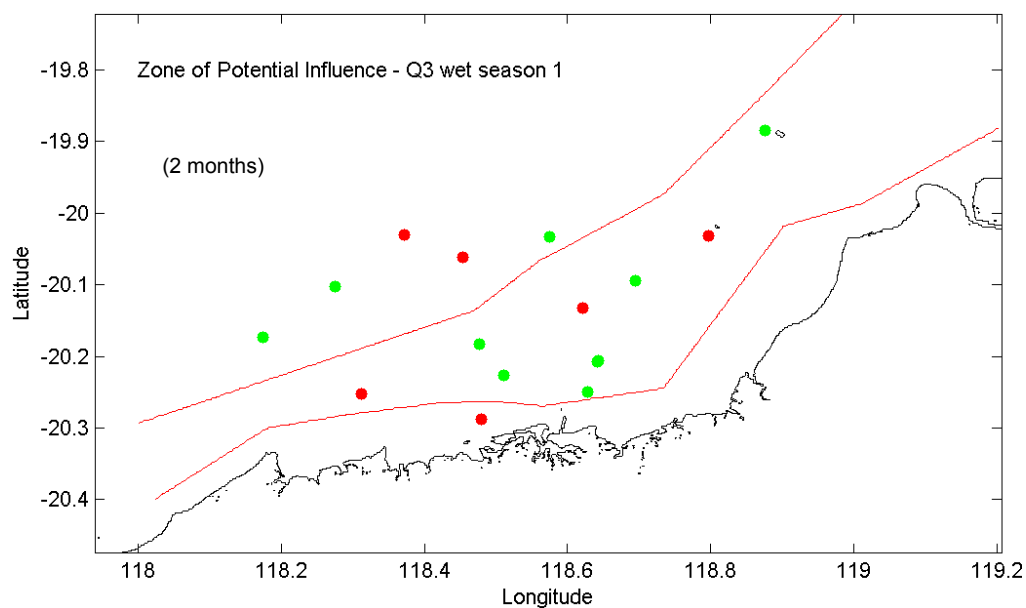
Figure 8-27 Zone of Potential Influence for the first wet season of Quantum Stage 3, which is 2 months long. The red lines mark defined zone boundaries, where different threshold criteria were applied. The red dots are the monitoring sites; the green dots are additional sites of interest.
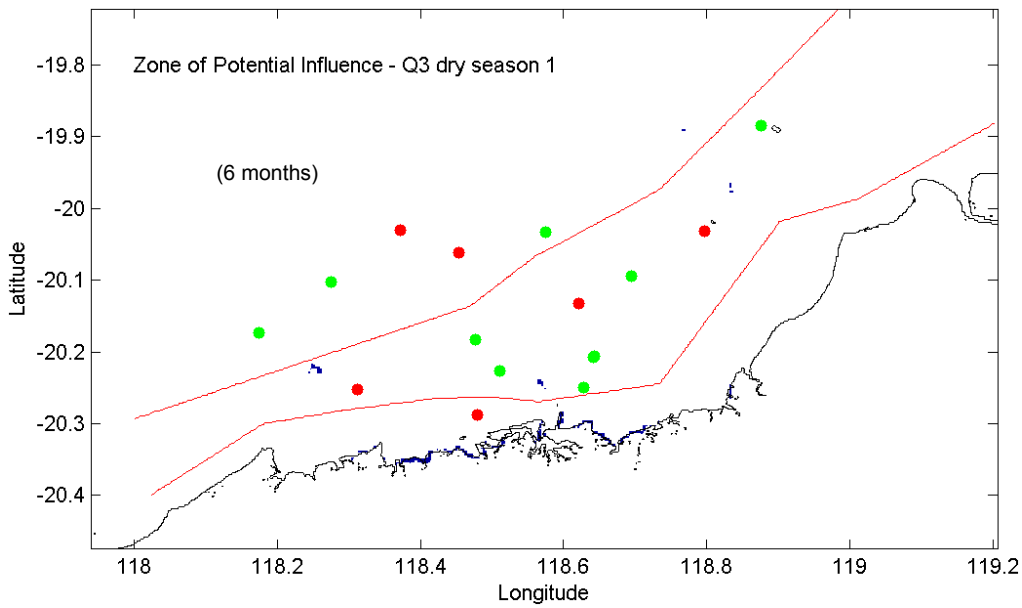
Figure 8-28 Zone of Potential Influence for the first dry season of Quantum Stage 3, which is 6 months long. The red lines mark defined zone boundaries, where different threshold criteria were applied. The red dots are the monitoring sites; the green dots are additional sites of interest.
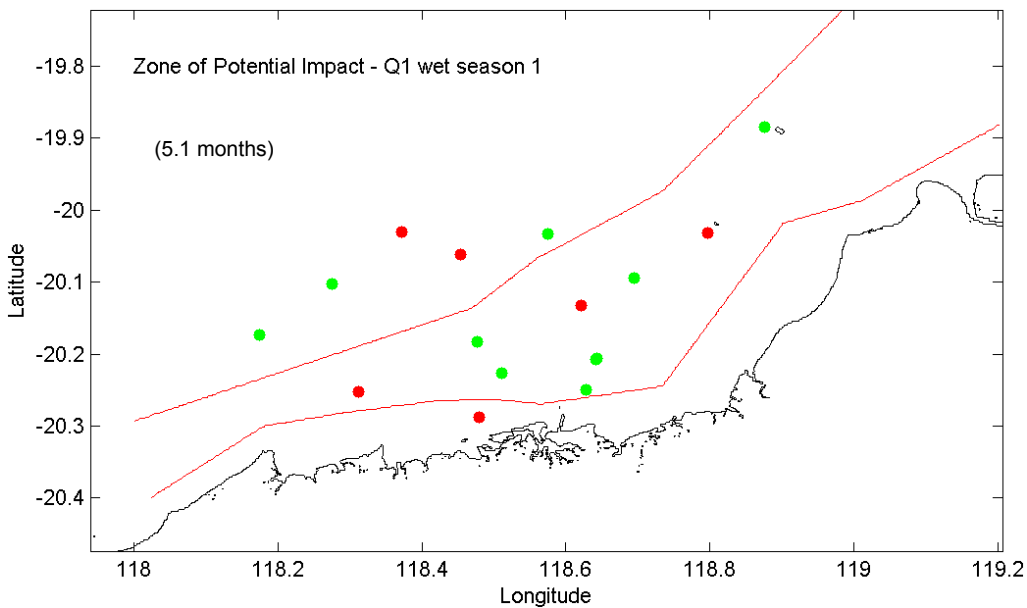
Figure 8-29 Zone of Potential Impact for the first wet season of Quantum Stage 1, which is 5.1 months long. The red lines mark defined zone boundaries, where different threshold criteria were applied. The red dots are the monitoring sites; the green dots are additional sites of interest.
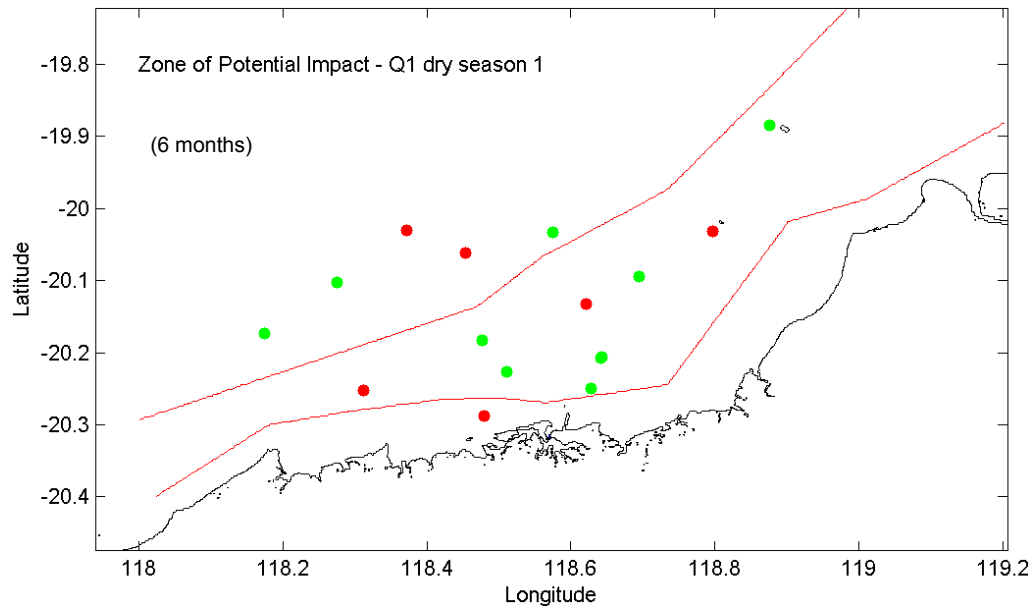
Figure 8-30 Zone of Potential Impact for the first dry season of Quantum Stage 1, which is 6 months long. The red lines mark defined zone boundaries, where different threshold criteria were applied. The red dots are the monitoring sites; the green dots are additional sites of interest.
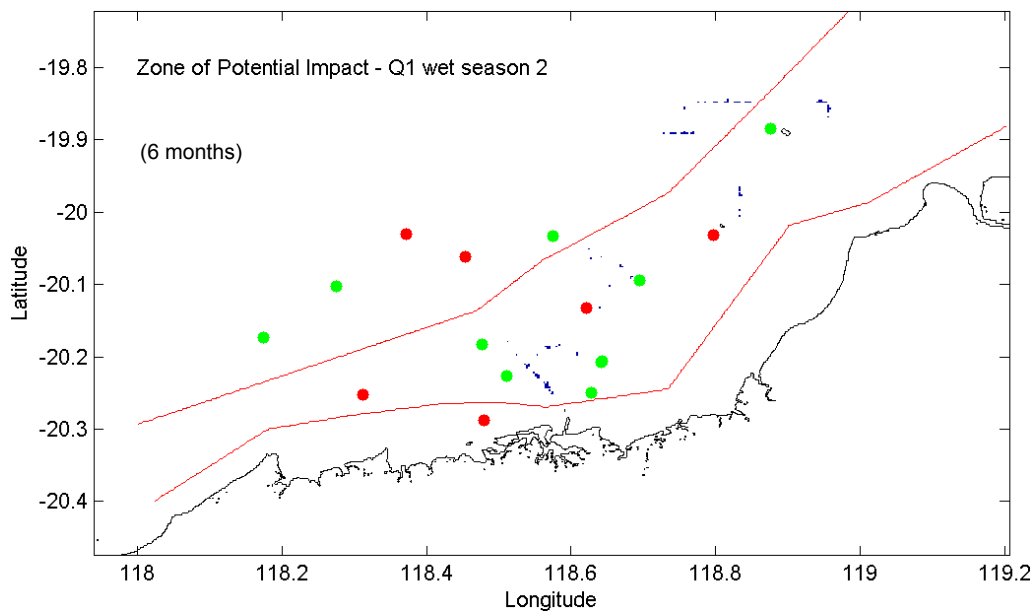
Figure 8-31 Zone of Potential Impact for the second wet season of Quantum Stage 1, which is 6 months long. The red lines mark defined zone boundaries, where different threshold criteria were applied. The red dots are the monitoring sites; the green dots are additional sites of interest.
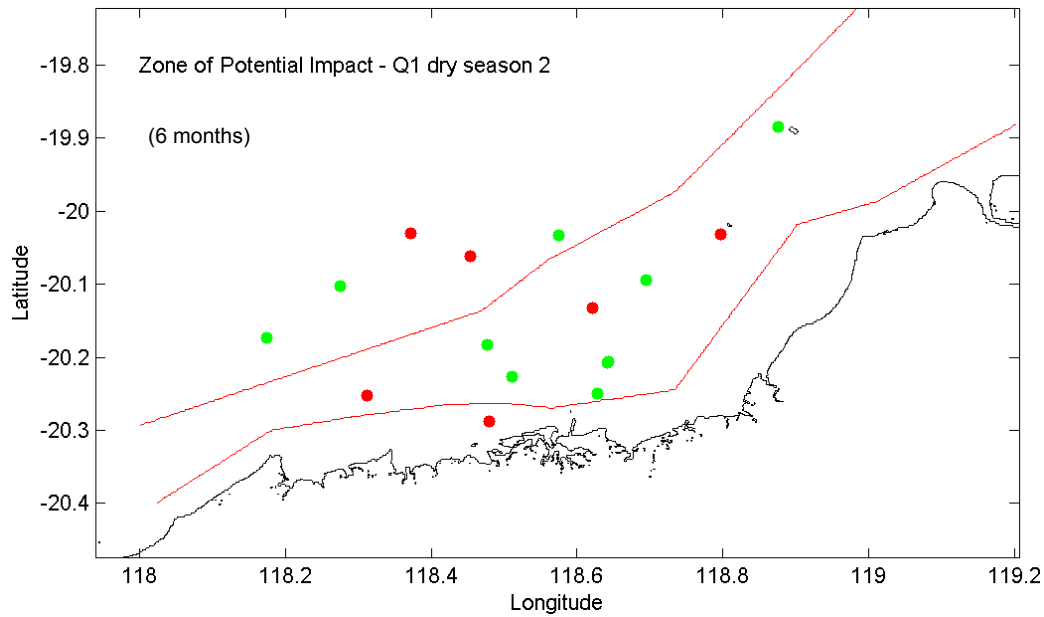
Figure 8-32 Zone of Potential Impact for the second dry season of Quantum Stage 1, which is 6 months long. The red lines mark defined zone boundaries, where different threshold criteria were applied. The red dots are the monitoring sites; the green dots are additional sites of interest.
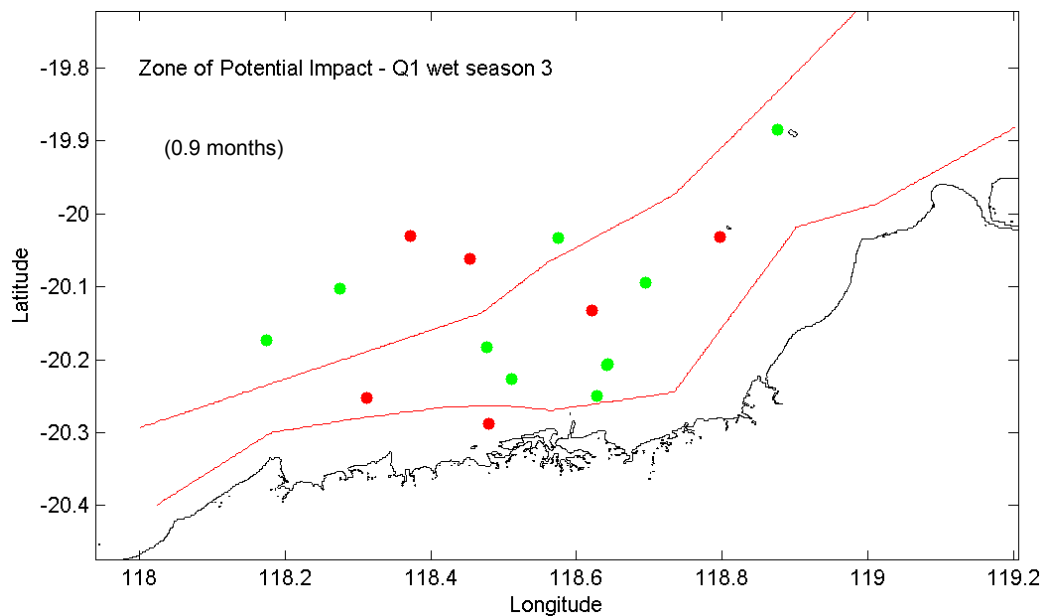
Figure 8-33 Zone of Potential Impact for the third wet season of Quantum Stage 1, which is 0.9 months long. The red lines mark defined zone boundaries, where different threshold criteria were applied. The red dots are the monitoring sites; the green dots are additional sites of interest.
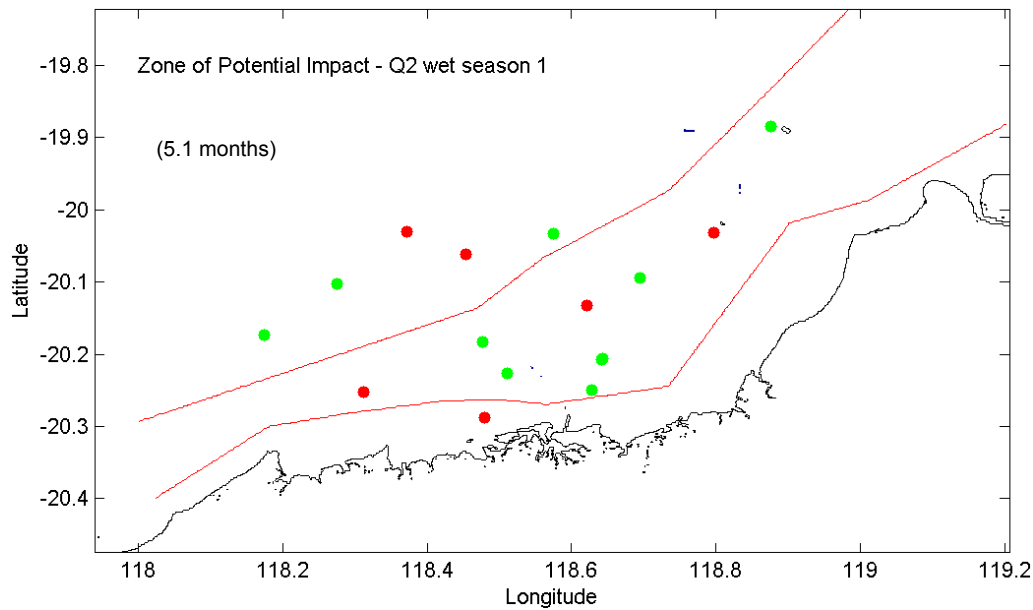
Figure 8-34 Zone of Potential Impact for the first wet season of Quantum Stage 2, which is 5.1 months long. The red lines mark defined zone boundaries, where different threshold criteria were applied. The red dots are the monitoring sites; the green dots are additional sites of interest.
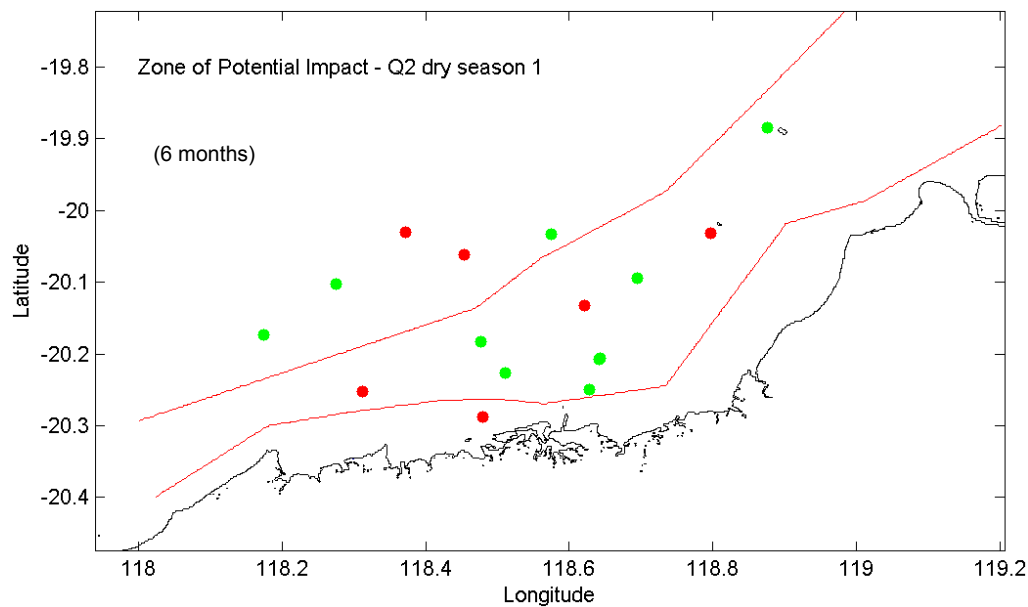
Figure 8-35 Zone of Potential Impact for the first dry season of Quantum Stage 2, which is 6 months long. The red lines mark defined zone boundaries, where different threshold criteria were applied. The red dots are the monitoring sites; the green dots are additional sites of interest.
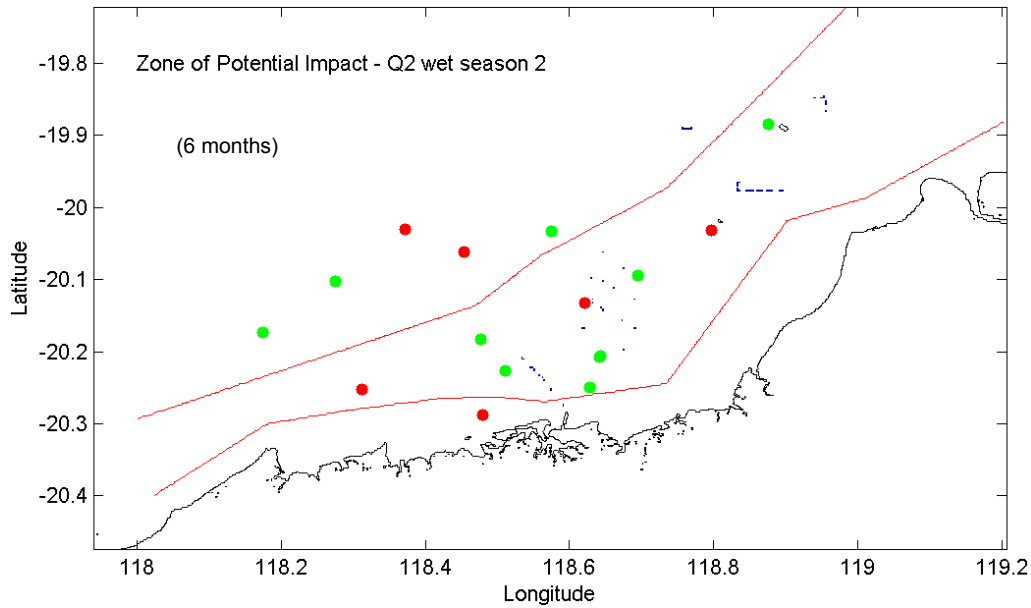
Figure 8-36 Zone of Potential Impact for the second wet season of Quantum Stage 2, which is 6 months long. The red lines mark defined zone boundaries, where different threshold criteria were applied. The red dots are the monitoring sites; the green dots are additional sites of interest.
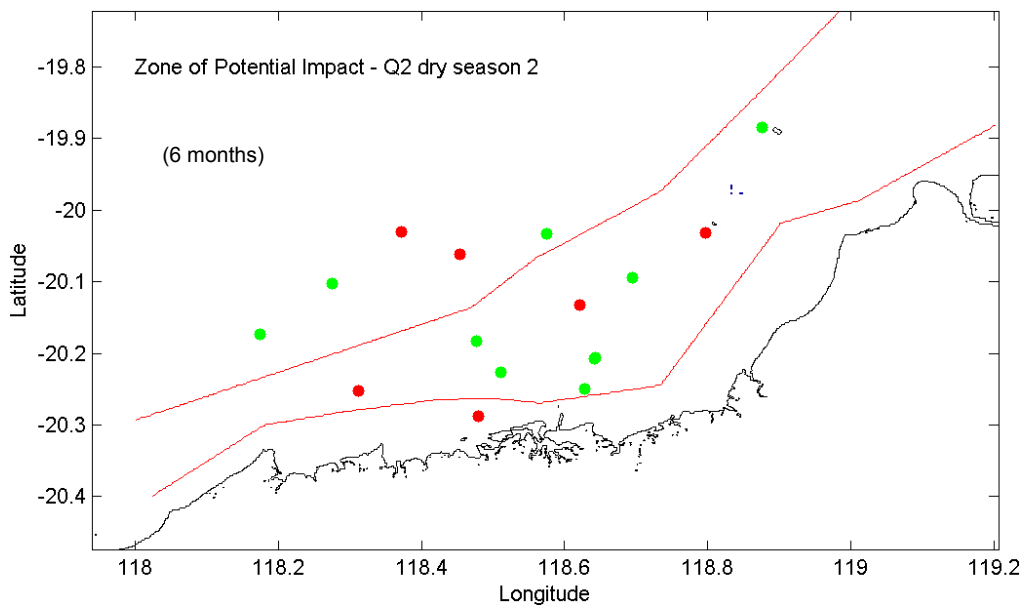
Figure 8-37 Zone of Potential Impact for the second dry season of Quantum Stage 2, which is 6 months long. The red lines mark defined zone boundaries, where different threshold criteria were applied. The red dots are the monitoring sites; the green dots are additional sites of interest.
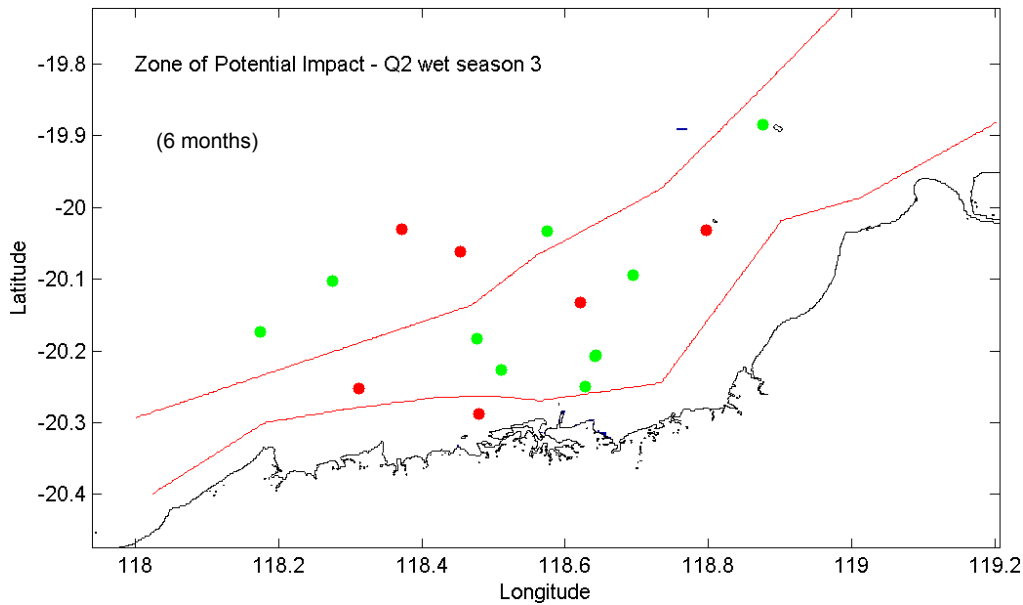
Figure 8-38 Zone of Potential Impact for the third wet season of Quantum Stage 2, which is 6 months long. The red lines mark defined zone boundaries, where different threshold criteria were applied. The red dots are the monitoring sites; the green dots are additional sites of interest.
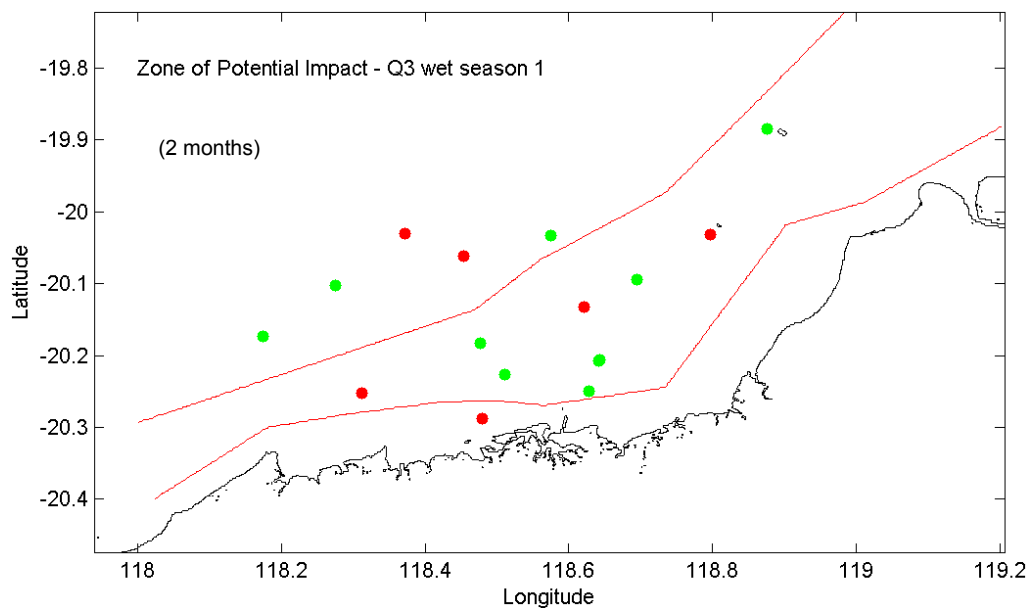
Figure 8-39 Zone of Potential Impact for the first wet season of Quantum Stage 3, which is 2 months long. The red lines mark defined zone boundaries, where different threshold criteria were applied. The red dots are the monitoring sites; the green dots are additional sites of interest.
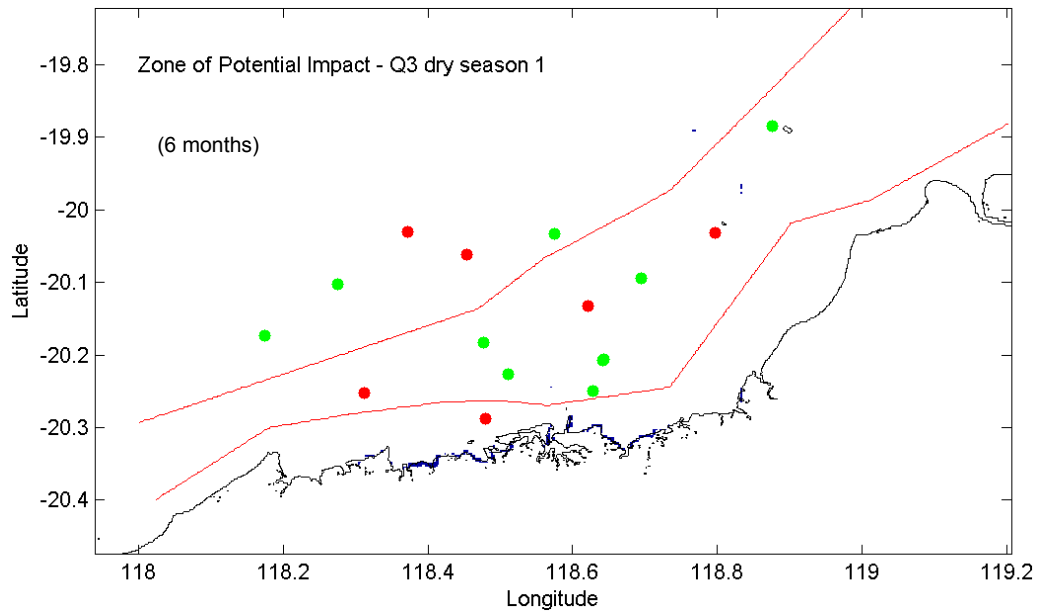
Figure 8-40 Zone of Potential Impact for the first dry season of Quantum Stage 3, which is 6 months long. The red lines mark defined zone boundaries, where different threshold criteria were applied. The red dots are the monitoring sites; the green dots are additional sites of interest.

The maps indicate that the Zone of Potential Influence thresholds would be exceeded over an area around the dredging and disposal during both the wet and dry seasons during Quantum Stage 1 and 2. The Zone of Potential Influence for the dry season is biased towards the coastal fringe and is predicted to not be triggered offshore. The Zone of Potential Influence for the wet season over Stages 1 and 2 is both larger in extent than the dry season results and biased to the west, due to a shift in the net transport. The maps indicate that the Zone of Potential Influence thresholds would be exceeded over a relatively wide area during the 2nd wet season of Quantum Stage 2 (see figures).

Quantum Stage 3 results indicate that the Zone of Potential Influence during the dry season will be larger than during the wet season zone.

The Zones of Potential Impact calculated for TSS for both the dry and wet seasons are plotted below in Figure 8-29 to Figure 8-40. These maps indicate that the thresholds would be exceeded over a small part of the Zones of Potential Influence, in both the wet and dry seasons. The threshold results in the NE corner in Figure 8-41 are likely the result of the grid resolution around Little Turtle Island.
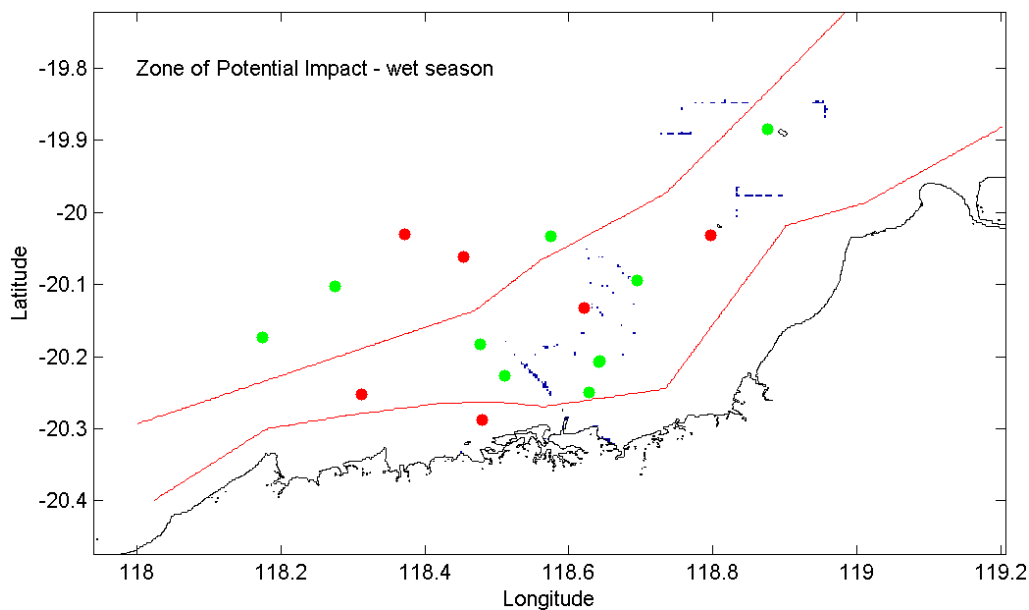
Figure 8-41 Composite wet season Zone of Potential Impact for the total Quantum programme. The red lines mark defined zone boundaries, where different threshold criteria were applied. The red dots are the monitoring sites; the green dots are additional sites of interest.
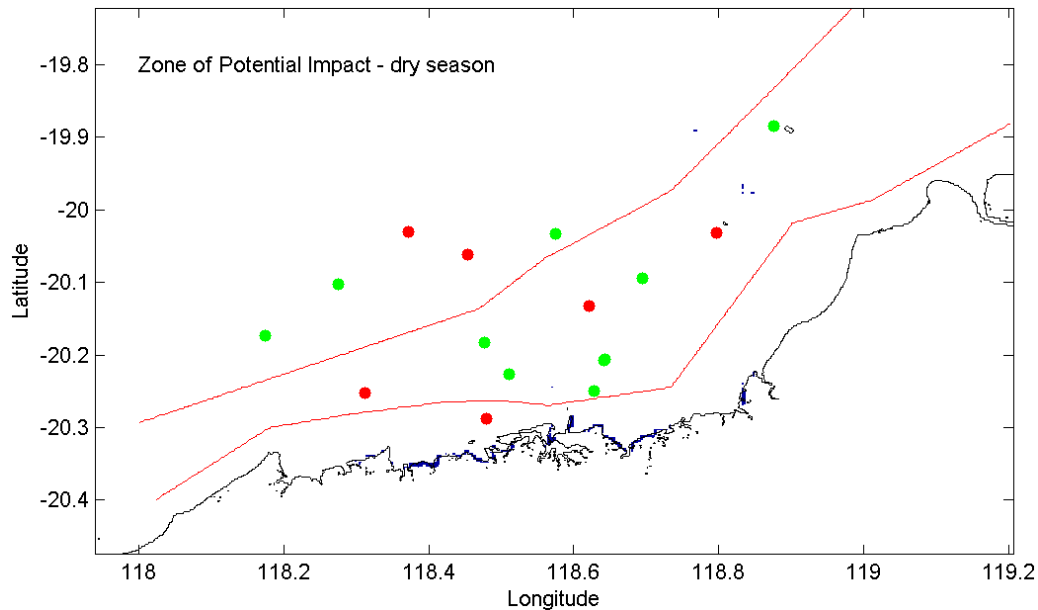
Figure 8-42 Composite dry season Zone of Potential Impact for the total Quantum programme. The red lines mark defined zone boundaries, where different threshold criteria were applied. The red dots are the monitoring sites; the green dots are additional sites of interest.

The composite Zone of Potential Impact for the cumulative Quantum stages 1-3 for both the wet and dry seasons are shown in Figure 8-41 and Figure 8-42, respectively. The Zone of Potential Impact for the wet season is sporadic and to the north of the dredging site, while the dry season impact is restricted to the coastal fringes. Cross-comparisons of these outcomes with the percentile analysis plots (Appendix E) indicates that the zones of Influence has a similar distribution to the more extreme TSS concentrations revealed in the 80th percentile plots. Thus, the threshold events can be attributed to individual stages of the dredge programme that may have relatively short durations at a given location, which are triggered by resuspension of deposited material.

Variations in TSS concentrations (1m above the seafloor) over time at the six monitoring sites and the four 'sites of interest' within the model domain are summarized in box and whisker plots below to provide an insight into the temporal and spatial variability of TSS concentrations predicted by the modelling. The location of the time series points are shown in Figure 8-13 and correspond to the turbidity measurement points used to derive background turbidity and light statistics.

The box and whisker plots show the 25th and 75th percentile values as a box marked with a red horizontal line indicating the median. The whiskers are lines extending from each end of the boxes to show range of values falling within 1.5 times the range between the 25th and 75th percentile. Outliers exceeding the upper inter-quartile value are shown by red crosses. The outliers were predicted < 1% of the time during the full simulations and, hence, can be considered as rare extremes. Analysis of the data also indicated that these extreme values were represented in the data as fluctuations lasting no more than one hour. For influences of

TSS on light penetration, which require longer durations, these fluctuations are not indicative of impacts, but have been included to show the potential short term concentrations.

The box and whisker plots show that the TSS estimates are strongly skewed, with generally low medians and upper quartile ranges compared to the rarer outliers. The medians at all sites are relatively low, indicating that above background concentrations will be at or near zero for most of the time. Outliers at many of the sites exceed 100 mg l^{-1}, with some sites estimated to occasionally experience higher concentrations.
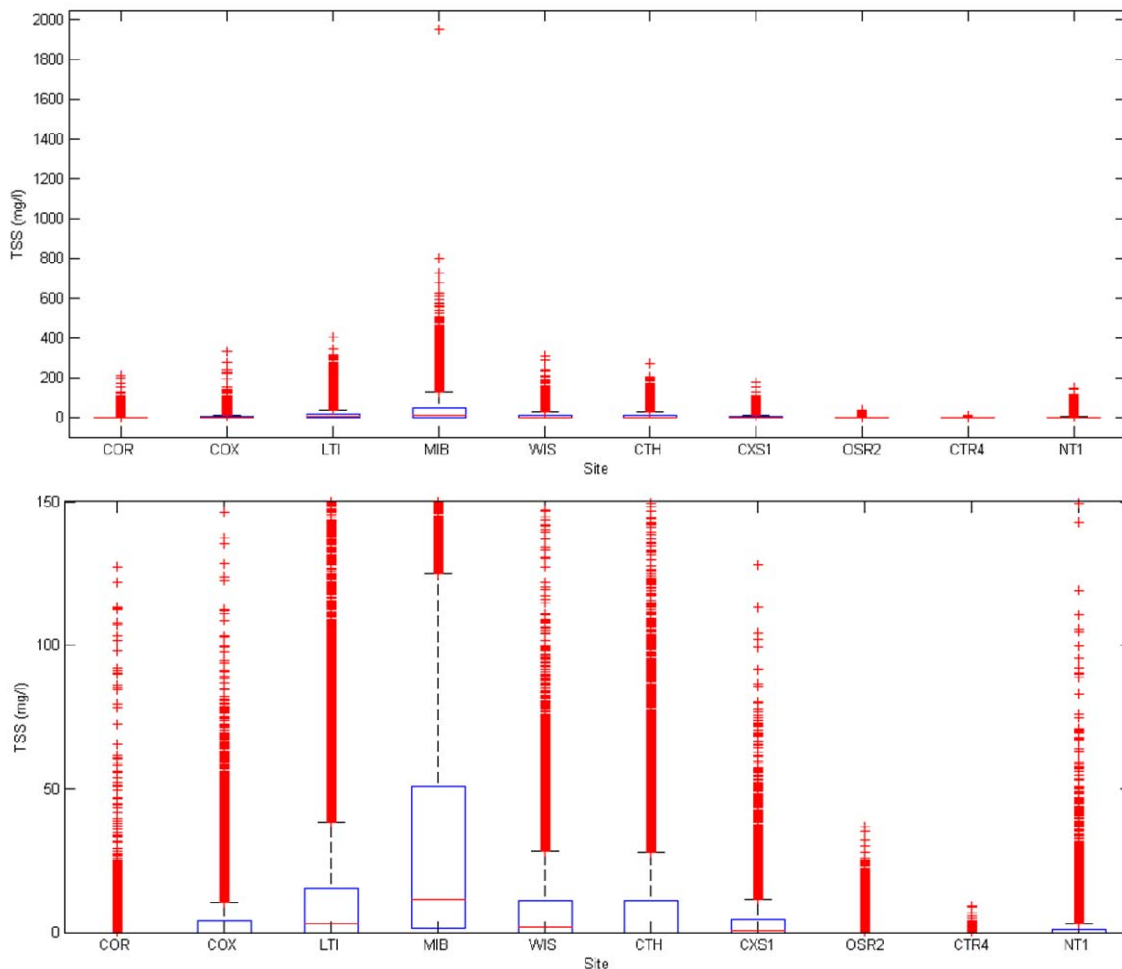
Figure 8-43 Box and Whisker plots summarising the TSS estimates for 1 m off bottom at ten output sites over Stages 1 and 2. Values are. for 1 m off bottom. The top panel shows the full range of values, the bottom panel shows the range of TSS from 0 to 150 mg/L.
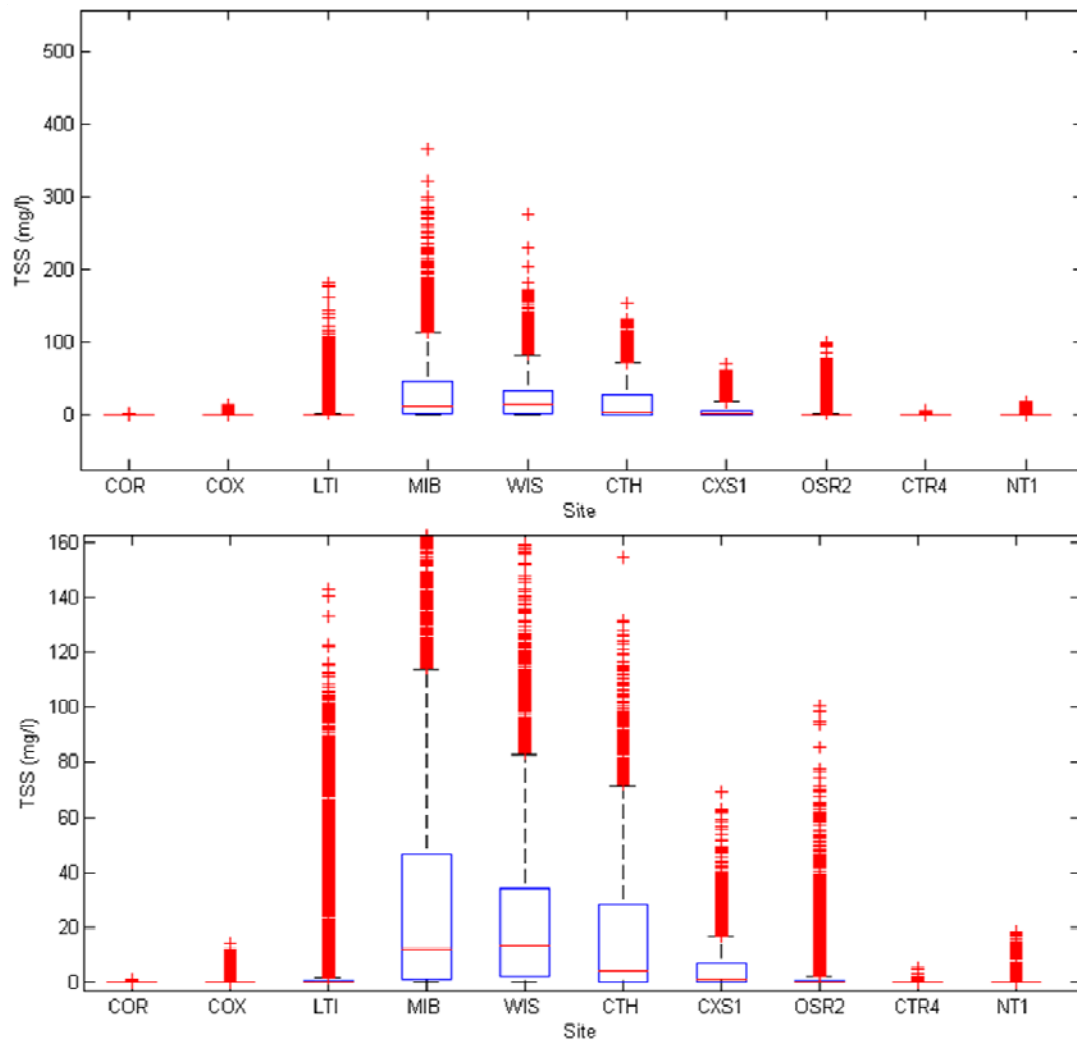
Figure 8-44 Box and Whisker plots summarising the TSS estimates at ten output sites over Stage 3. Values are for 1 m off bottom. The top panel shows the full range of values, the bottom panel shows the range of TSS from 0 to 160 mg/L.

8.6.4   Temporal summaries of predicted sediment deposition

The 50th and 80th percentile plots for sediment deposition over time (Appendix E) indicated a progressive build up of the seafloor area that would receive elevated deposition of sediment derived from dredging and disposal at times during the operations. Deposition loads were initially predicted to elevate in the disposal areas and around the dredging. However, with increasing inputs and spreading of the discharged sediments, the deposits were predicted to extend laterally in the longshore and, to a lesser extent, in the onshore-offshore directions. However, this trend was not always consistent over the longer duration of the dredging, with the median deposition reverting to lower concentrations and areal coverage at irregular intervals. For example, compare the concentrations of deposited sediment in Figure E-48, for an autumn period after 2 years of dredging with an earlier prediction during the preceding summer (Figure E-46). This result indicates that there will be respreading and dispersion of the sediment deposits over time, due to periods of increased wave activity.

The sediment deposition zones are plotted in Figure 8-45 and Figure 8-47 for the dry season and Figure 8-48 and Figure 8-50 for the wet season for Quantum Stages 1, 2 and Quantum 3 combined, respectively. Zones where the model predicted sedimentation rates would exceed the allowances based on background estimates were mostly concentrated around the dredge and dredge disposal sites and extending offshore from these areas of operation.

The areas indicated for the wet season were generally smaller than those for the dry season and increasingly restricted distribution around the immediate dredging and disposal areas for the extreme estimates. This outcome can be attributed to the greater tolerances allowed for during the wet season.

The central tendency and variability of sedimentation rates over time at different spatial locations is summarized as box and whisker plots shown in Figure 8-51. The box and whisker plots illustrate that the upper inter-quartile estimate for these locations were < 3 mg cm^2 d^{-1} and < 0.1 mg cm^2 d^{-1} for MIB and COX, respectively, which is lower than any of the thresholds defined for sedimentation rates. None of the monitoring sites were indicated to fall within the sedimentation exceedance zones.
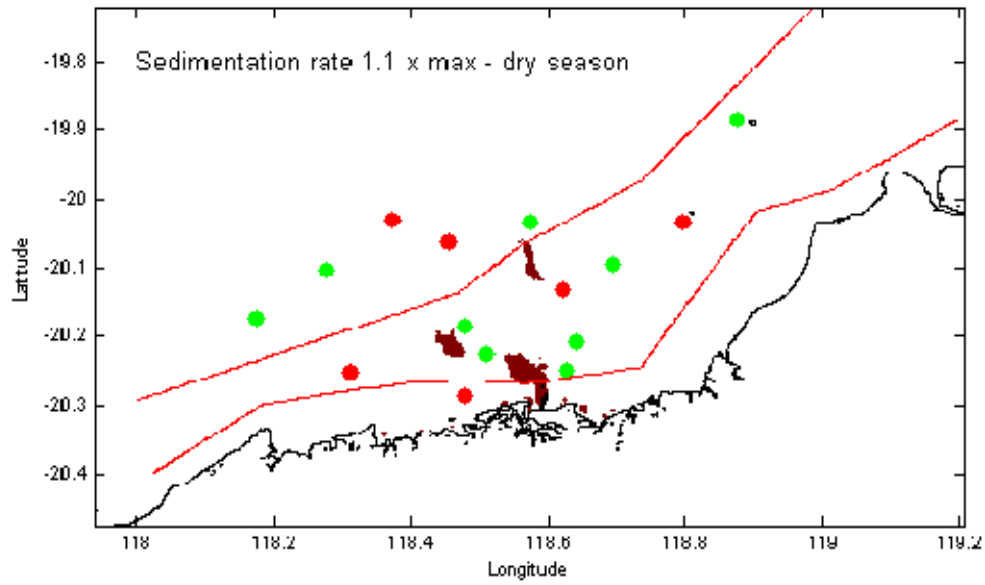
Figure 8-45 Dry season sedimentation rate thresholds for 1.1x maximum.
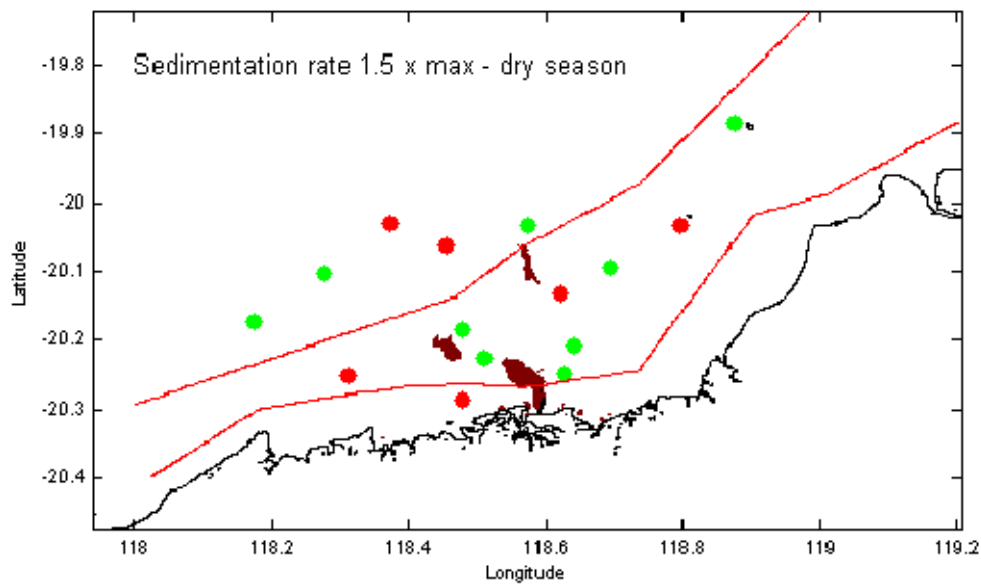
Figure 8-46 Dry season sedimentation rate thresholds for 1.5x maximum.
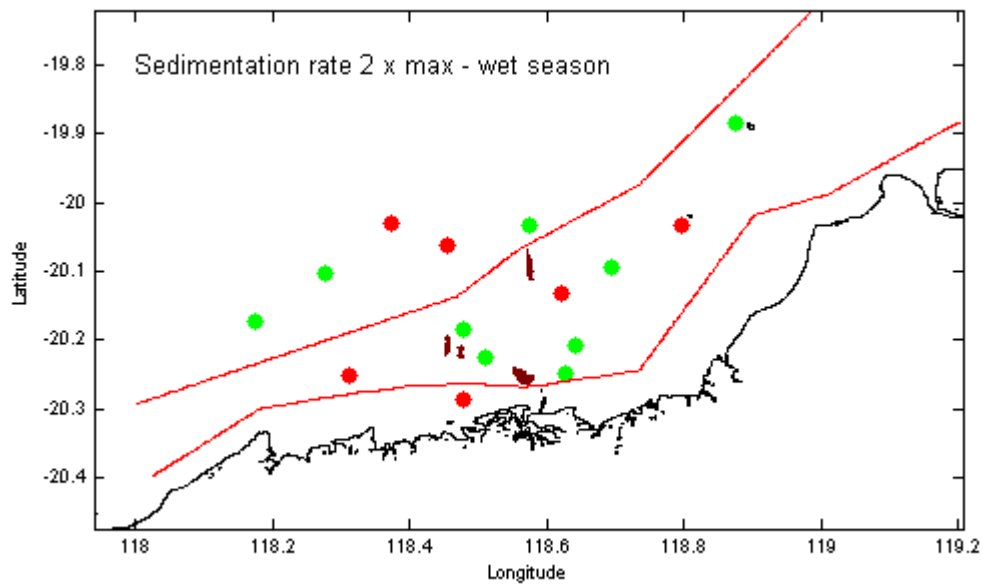
Figure 8-47 Dry season sedimentation rate thresholds for 2x maximum.
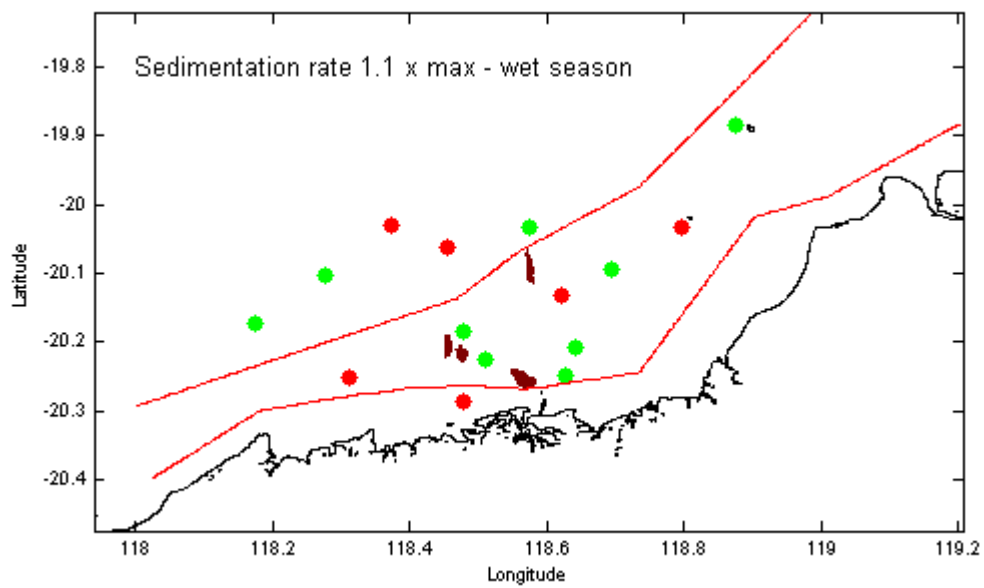
Figure 8-48 Wet season sedimentation rate thresholds for 1.1x maximum.
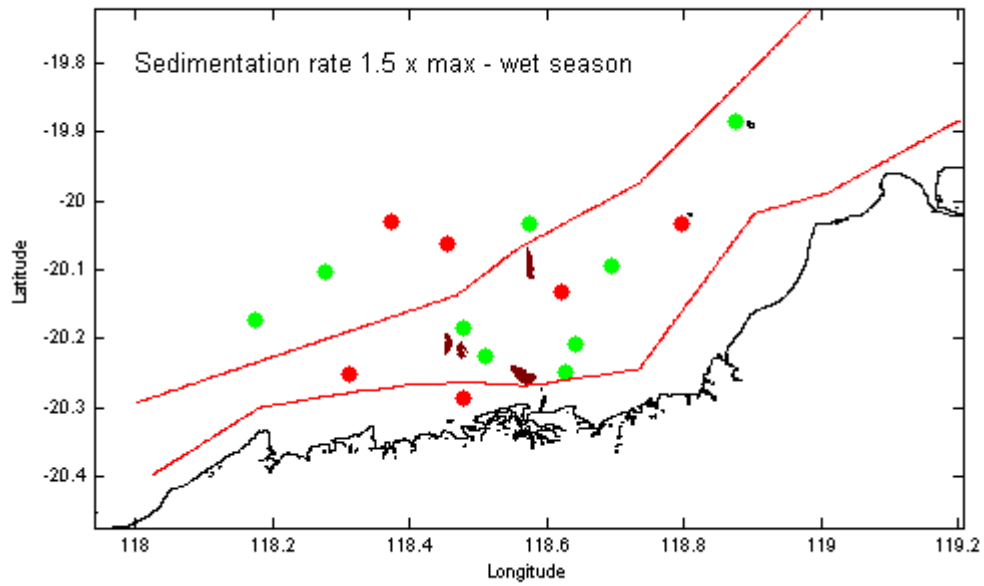
Figure 8-49 Dry season sedimentation rate thresholds for 1.5x maximum.
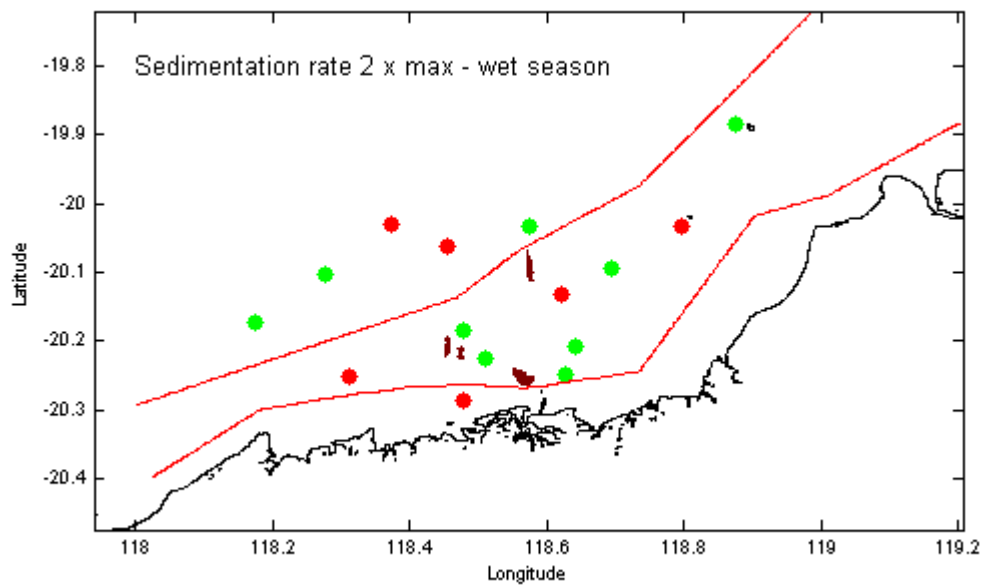
Figure 8-50 Wet season sedimentation rate thresholds for 2x maximum.
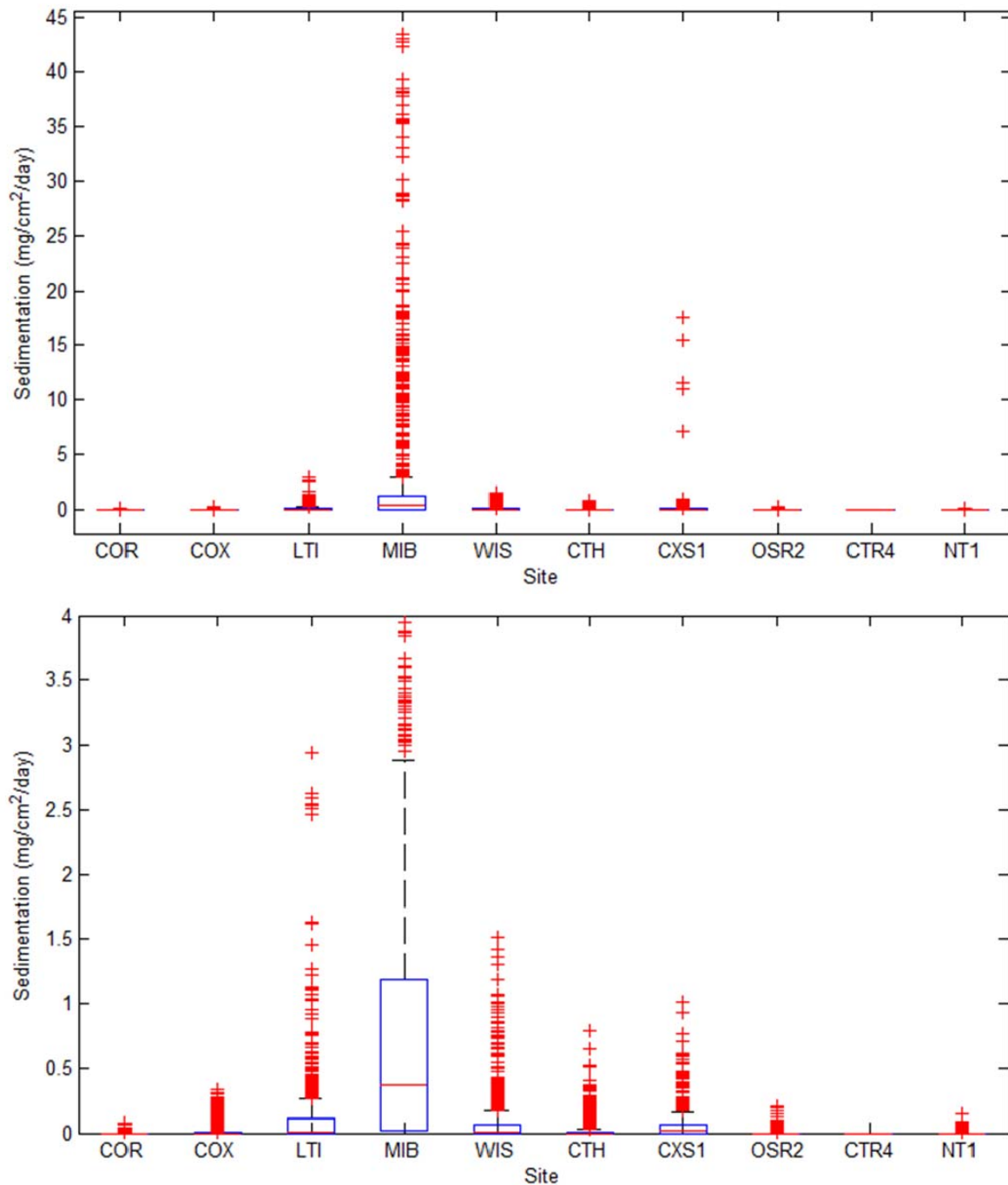
Figure 8-51 Box and whisker plot of sedimentation rates over the combined operations of Stages 1 and 2. The blue rectangle encloses the 25th to 75th percentile values over time. The red line dissecting the blue box indicated the median over time. The upper ranger bar indicates 1.5 times the interquartile range, which will encompass > 99% of the range of values. The red crosses indicate values that are larger than the upper range bar value, hence are represented < 1% of the time in the data and are referred to as 'outliers'.

9   REFERENCES

Anderson, E., B. Johnson, T. Isaji and E. Howlett. 2001. SSFATE (Suspended Sediment FATE), a model of sediment movement from dredging operations. Presented at WODCON XVI World Dredging Congress, 2-5 April 2001, Kuala Lumpur, Malaysia.

Anchor Environmental (2003). Literature review of effects of resuspended sediments due to dredging operations. Prepared for Los Angeles Contaminated Sediments Task Force, Los Angeles, California. June 2003.

ANTT (2008), Australian National Tide Tables 2008, Australian Hydrographic Service, Commonwealth of Australia.

ANZECC (2000), Australian and New Zealand Guide lines for Fresh and Marine Water Quality, Australian and New Zealand Environment and Conservation Council, National Water Quality Management Strategy Paper No. 4.

BOM (2008), Tropical Cyclones Affecting Port Hedland, Bureau of Meteorology, http://www.bom.gov.au/weather/wa/cyclone/about/pthed/index.shtml

Davies, A. M., (1977a), The numerical solutions of the three-dimensional hydrodynamical equations using a B-spline representation of the vertical current profile. Proc. 8th liege colloquium on Ocean hydrodynamics, J. C. J. Nihoul, Ed., Elsevier, 49-68.

Eldeberky, Y. and J.A. Battjes, (1996), Spectral modelling of wave breaking: Application to Boussinesq equations, J. Geophys. Res., 101, No. C1, 1253-1264.

GEMS (2003). Geraldton Port Redevelopment- Further Dredge Plume Turbidity Modelling. Report 13/03 to URS

Godfrey, J.S. and Ridgway, K.R. (1985) The large-scale environment of the poleward-flowing Leeuwin Current, Western Australia: Longshore steric height gradients, wind stresses and geostrophic flow. J Phys. Oceanogr. 15:481–495.

Gordon. R., (1982), Wind driven circulation in Narragansett Bay. Ph. D. Thesis. Department of Ocean Engineering, University of Rhode Island, Kingston, RI, 161 pp.

Hasselmann, K., (1974), On the spectral dissipation of ocean waves due to whitecapping, Bound.-layer Meteor., 6, 1-2, 107-127.

Hays, D. & Wu, P. (2001). Simple approach to TSS source strength estimates, Western Dredging Association Proceedings. WEDA XXI, Houston, TX, June 25027, 2001.

Herbich, J. B. 2000 Handbook of Dredging Engineering. 2nd Edition. Mcgraw Hill Professional. 922 pp. http://books.google.com.au/books?id=YD43sagFy_AC&pg=RA2-PA92&lpg=RA2-PA92&dq=%22propeller+wash%22+dredging&source=bl&ots=k_ZrwPXmZG&sig=ns8hYM3z xFApvTIA1LI0m69lsi4&hl=en&ei=r2i4ScbVMYHasAPboNRB&sa=X&oi=book_result&resnum =1&ct=result

Holthuijsen, L.H., N. Booij, R. Ris, J.H. Andorka Gal and J.C.M. de Jong, (1997), A verification of the third-generation wave model "SWAN" along the southern North Sea coast, Proceedings 3rd International Symposium on Ocean Wave Measurement and Analysis, WAVES '97, ASCE, 49-63.

Isaji, T. and M. Spaulding., (1984), Notes and Correspondence. A Model of the Tidally Induced Residual Circulation in the Gulf of Maine and Georges Bank. Published in: Journal of Phys. Ocean., June. pp. 1119-1126.

Isaji, T. Howlett, E. Dalton C. and Anderson E. (2001), Stepwise-Continuous-Variable-Rectangular Grid, Proc. 24th Arctic and Marine Oilspill Program Technical Seminar, pp 597-610.Zigic *et al*, 2003.

Johnson, B.H., E. Anderson, T. Isaji, and D.G. Clarke. 2000. Description of the SSFATE numerical modelling system. DOER Technical Notes Collection (TN DOER-E10). U.S. Army Engineer Research and Development Center, Vicksburg, MS. http: //www.wes.army.mil/el/dots/doer/pdf/doere10.pdf.

Komen, G.J., S. Hasselmann, and K. Hasselmann, (1984), On the existence of a fully developed wind-sea spectrum, J. Phys. Oceanogr., 14, 1271-1285.

Madsen, O.S., Y.-K. Poon and H.C. Graber, (1988), Spectral wave attenuation by bottom friction: Theory, Proc. 21 th Int. Conf. Coastal Engineering, ASCE, 492-504.

Madsen, P.A. and O.R. Sørensen, (1993), Bound waves and triad interactions in shallow water, Ocean Engineering, 20, 4, 359-388.

Owen, A., (1980), A three-dimensional model of the Bristol Channel. J. Phys. Oceanography., 10, 1290-1302.

SKM (2009), Port Hedland Outer Harbour Development – Water Quality thresholds. Report number WV03716-MV-RP-0029.

Soulsby, R. (2007) Dynamics Of Marine Sands. Thomas Telford Publishers, 272 pgs.

Swanson, J., Isaji, T., Clarke, D. & Dickerson, C. (2004). Simulations of dredging and dredged material disposal operations in Chesapeake Bay, Maryland and Saint Andrew Bay, Florida, *Proceedings* of the 36th TAMU Dredging Seminar, WEDA XXIV, 6-9 July 2004, Orlando Fl.

Swanson J.C., Isaji T., Galagan C., 2007, Modelling the Ultimate Transport and Fate of Dredge-Induced Suspended Sediment Transport and Deposition. Proceedings of Wodcon 2007, Lake Buena Vista, Florida.

Swanson, J.C., T. Isaji, M. Ward, B.H. Johnson, A. Teeter, and D.G. Clarke. 2000. Demonstration of the SSFATE numerical modelling system. DOER Technical Notes Collection (TN DOER-E12). U.S. Army Engineer Research and Development Center, Vicksburg, MS. http: //www.wes.army.mil/el/dots/doer/pdf/doere12.pdf.

UKHO (UK Hydrographic Office) (2005), Admiralty Sailing Directions, Australia Pilot Volume 1 NP13, Somerset, England.

USACE (US Army Corps of Engineers) (2001), Coastal Engineering Manual, Circular No. 1110-2-1110, Washington DC

HR Wallingford (2003). Protocol for the field measurement of sediment release from dredgers. Issue 1, August 2003.

Wilmott, C.J., (1981), On the Validation of Models, J. Phys. Oceanogr., 2, 184-194.

Zigic, S, Zapata, M, Isaji, T, King, B and Lemckert, C, MODELLING OF MORETON BAY USING AN OCEAN/COASTAL CIRCULATION MODEL, Proceedings of Coasts & Ports Australasian Conference 2003